KAPITAŁ LUDZKI
NARODOWA STRATEGIA SPÓJNOŚCI

Politechnika Wrocławska

UNIA EUROPEJSKA
EUROPEJSKI
FUNDUSZ SPOŁECZNY

ROZWÓJ POTENCJAŁU I OFERTY DYDAKTYCZNEJ POLITECHNIKI WROCŁAWSKIEJ

Wrocław University of Technology

Nanoengineering

A. Ciżman, R. Poprawski, A. Sieradzki

DIELECTRIC PHYSICS

Introduction to Selected Problems of Dielectric Physics

Wrocław 2011

Projekt współfinansowany ze środków Unii Europejskiej w ramach
Europejskiego Funduszu Społecznego

Wrocław University of Technology

Nanoengineering

A.Ciżman, R. Poprawski, A. Sieradzki

DIELECTRIC PHYSICS

Introduction to Selected Problems of Dielectric Physics

Wrocław 2011

Reviewer: J. Misiewicz

ISBN 978-83-62098-54-5

Published by PRINTPAP Łódź, www.printpap.pl

Reviewer: J. Misiewicz

ISBN 978-83-62098-54-5

Published by PRINTPAP Łódź, www.printpap.pl

Contents

BASIC CONCEPTS OF DIELECTRIC PHYSICS

Chapter 1

CONTENTS

1.1 Classification of materials depending on electric conductance

Electric conductivity of natural and artificial materials can differ by many ranges. Materials conducting electric current are called electricity conductors. The **conductors** are **metals** and **electrolytes**. Electric conductance of metals exceeds $10^5 \Omega^{-1}cm^{-1}$. Materials which do not conduct electric current, or those in which the conductivity is very low, are called **dielectrics or insulators** and their electric conductance is lower than $10^{-10}\ \Omega^{-1}cm^{-1}$. Materials with intermediate conductance are called **semiconductors**. There are also materials, known as **superconductors**, in which the electrical resistance in specific conditions is zero (it is not measurable). Fig.1. 1 presents the division of materials depending on the electric conductivity, as well as examples of conductivity values of some groups of materials (metals, semiconductors and insulators).

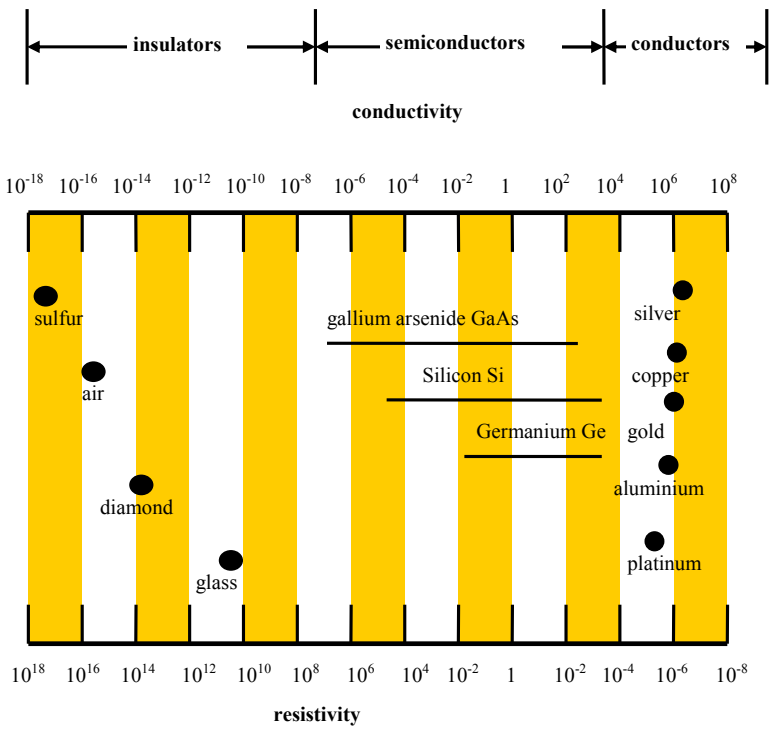

Fig.1. 1 Division of materials, depending on electric conductivity and examples of conductivity values of dielectrics, semiconductors, metals and electrolytes.

It is worth noting that the value of conductivity is not the deciding factor in classifying the material as a dielectric, semiconductor or conductor. There are no definite values of

conductivity which determine the type of material; the important point is the mechanism of conductance, which is the result of the band structure of the considered material. Before starting a description of the conductivity mechanism, it is important to recall basic information related to electric current conductivity.

1.2 Basic information related to conductivity of electric current

The **current intensity** I is defined as a quotient of electric charge Q which is flowing through the conductor cross-section to the time of the flow t.

$$I = \frac{dQ}{dt}. \tag{1. 1}$$

The unit of the current intensity is 1A=1C/1s. The Ampere is a basic SI unit.

The **current density** is equal to:

$$j = \frac{dJ}{dS}, \tag{1. 2}$$

where dS is the field of cross-section of the conductor. If the current is uniform across the cross-section, then

$$j = \frac{J}{S}. \tag{1. 3}$$

The unit of current density is 1A/m.

The electric charges can be transmitted with the positively and negatively charged carriers, so the current density can be described:

$$j = \sum_i n_{i+} q_{i+} v_{i+} + \sum_j n_{j-} q_{j-} v_{j-}, \tag{1. 4}$$

where n_{i+}, (n_{i+}) is the **concentration** of the positive (negative) carriers – the number of carriers in the unit volume, q_{i+}, q_{i+} positive (negative) electric charge of the carriers, and v_{i+}, v_{i-} is the velocity of corresponding carriers. The carriers velocity depends on their **mobility** μ and the intensity of electric field E.

$$v_+ = \mu_+ E, \qquad v_- = \mu_- E \tag{1. 5}$$

Mobility of the electric carriers is the average value of velocity of the carriers in the unit intensity of electric field (1V/m):

$$\mu = \frac{v}{E} \qquad \textbf{(1. 6)}$$

Taking equation (4), the mobility of the positive and negative carriers and assuming that there is only one type of positive and negative carriers we obtain:

$$j = (n_+ q_+ \mu_+ + n_- q_- \mu_-)E \,. \qquad \textbf{(1. 7)}$$

Designating the part in the bracket in equation (1.7 $j = (n_+ q_+ \mu_+ + n_- q_- \mu_-)E$.

(1. 7) as σ (σ – **specific conductivity** of material) gives:

$$j = \sigma E = \frac{E}{\rho} \,. \qquad \textbf{(1. 8)}$$

It is a differential form of Ohm's law (ρ=1/σ is called **specific resistivity**).

Specific conductivity of material consisting of only one type of positive and negative carriers:

$$\sigma = n_+ q_+ \mu_+ + n_- q_- \mu_- \,. \qquad \textbf{(1. 9)}$$

Equation (1.9) presents the conductivity dependence of material upon concentration and mobility of the carriers. Using this equation and the band model for the basic mechanism of electric current flow, conductivity in various types of materials will be presented .

1.3 Mechanism of electric current conductivity in various type of materials

1.3.1 Electric conductivity of gases

In standard conditions, gases do not conduct electric current, because of high value of ionisation energy. Gases can be ionised by ionising radiation (ultraviolet, Roentgen or γ-radiation), streams of charged particles (electrons or protons), strong electric fields or high temperatures. The current carrying particles in gases are electrons and ions. The concentration of charges depends on many external factors, such as temperature, pressure, intensity of electric field or radiation. Detailed description of current conductance in gases is very wide area, which is beyond the scope of this work. It is worth noting that electric current conductivity in gases plays important role in many sources of light such as fluorescent lamps, neons, gas lasers, electron lamps, plasma displays; it is also used in ionic radiation counters and various other types of sensors and transducers.

1.3.2 Electric conductivity of electrolytes

a) Liquid electrolytes

During dissolving of acids, bases or salts in certain solutions (mostly in water) **electrolytic dissociation** occurs, meaning that there is a decomposition into ions, positive - cations and negative - anions. Electrolytic dissociation also occurs during melting of the above mentioned materials. The carriers (particles) in liquid electrolytes are both **cations** and **anions**. In the presence of current conduction, ion transportation occurs and there is a deposition of electrolysis products on the electrodes.

The electrolytes can be divided into strong, for which the **level of dissociation** (ratio of dissociated particles to particle concentration in the solution) is large (almost equal to 1) and weak – where the level of dissociation is less than 1. The level of dissociation of electrolytes also depends on the temperature and strength of the solution. The electrolytes specific conductivity is described by the following equation:

$$\sigma = \kappa c w e(\mu_+ + \mu_-), \qquad \textbf{(1. 10)}$$

where κ – the level of dissociation, c – the concentration of solution, w – the valency, e – the elementary charge.

In **strong electrolytes** the concentration of the particles does not depend on the temperature. An increase of temperature causes reduction of viscosity of the solution; that is why the electric conductivity increases with the temperature. In strong electrolytes the ratio of conductivity and viscosity within a wide temperature range is constant (**Walden's rule**). The level of dissociation of **weak electrolytes** increases with the temperature. Such an increase is caused by an increase in the concentration of particles in the solution (increase of level of dissociation) and decrease of viscosity.

Conductivity of liquids find applications in electrolysis processes: obtaining various materials such as chlorine, sodium hydroxide, copper; coating of protective layers – electroplating – e.g. nickel plating, and is also used in batteries, chemical analysis (conductometry) and lithography.

b) Solid electrolytes

A separate group of ionic conductors are the solid electrolytes (**super-ionic conductors**). Such materials are solids having ionic conductivity with similar values to liquid electrolytes

(solutions of electrolytes or molten salts). Concentration and mobility of ions in super-ionic conductors is similar to the values in liquid electrolytes.

The transition from insulator to ionic conductor phase can be continuous (conductivity grows exponentially with the temperature); there are also materials that with a certain temperature one can observe rapid decrease of energy of activation in it or a step change of electrical conductivity (many ranges) and change of its activation energy. The temperature at which a change of activation energy or a change of conductivity occurs is called the temperature of **super-ionic phase transition**. The carriers are usually light, positive ions (e.g. protons, Li^+, K^+, Na^+, Ag^+, Cu^{2+}), but there are also known some super-ionic conductors with negative carriers, such as F^-, O^{2-}.

The occurrence of high ionic conductivity in solid electrolytes can be explained in a simple way as the melt down of crystal sub-lattice. It is worth noting that the specific heat of super-ionic phase transition is similar to the specific heat of melting of that material. Ions of the so-called "*melting sub-lattice*" are able to move in relation to the stationary matrix created by the other sub-lattices during reconfiguration of the crystal structure (vibration of the atoms of non moving sub-lattice around their position of equilibrium has not been considered).

The charge transport in solid electrolytes is related to mass transport materials of particular scientific interest are those with hydrogen bonding. Such materials are called **super-protonic conductors**. An area of interest in super-ionic conductors is related to the possibility of application such materials in batteries and fuel cells. More information about solid electrolytes can be found in the monography [1].

1.3.3 Electric conductivity of metals

Typical metals are the elements of from first and second group of periodic table, e.g. lithium, sodium, potassium, copper, silver, gold, mercury, platinum. In metals, the carriers of the current are free electrons, which partially filled the conduction band. Electric conductivity can be expressed:

$$\sigma = n_e e \mu_e , \tag{1. 11}$$

where: n_e – the concentration of free electrons, e – the electric charge of electron and μ_e – the mobility of free electrons. Concentration of electrons does not depend on a temperature. During movement in an external electric field free electrons are dispersed in a non-uniform crystal lattice (defects and vibration of crystal lattice called **phonons**). The vibrational energy

of the crystal lattice increases with temperature. This phenomena yields to electrons scattering and thus decreases their mobility and as a result to a decrease in electrical conductivity.

It is worth noting that alloys can be considered as strongly defected crystals. Because of the high concentration of defects the conductivity is smaller than the conductivity of pure metals. In the case of alloys the dominant factor of electron dissipation is defects of crystal lattice (not phonons). That is why thermal resistance coefficients in alloys are smaller than in pure metals. **Thermal resistance coefficient** α is defined as

$$\alpha = \frac{1}{R}\frac{dR}{dT}, \qquad \textbf{(1. 12)}$$

In Table 1 there are several examples of specific resistance and thermal resistance coefficients of some metals and alloys.

Table 1. Specific resistance and thermal resistance coefficients of some metals and alloys.

Material	ρ [Ωm]	α [1/K]*10^{-3}	temperature range [^{O}C]	
			from	to
Platinium	0.107	3.92	-250	600
Copper	0.0175	4.25	-50	150
Nickel	0.12	6.4	-50	200
Aluminium	0.0278	3.8		
Silver	0.016	3.8		
Tungsten	0.055	4.1		
Konstantan	0.50	0.0005		
Manganin	0.43	0.004		
Cupro-nickel	0.043	0.23		
Nickel chrome steel	1.0	0.25		

Thermal dependence resistivity is used for temperature measurement. Metallic temperature sensors are mainly made of platinum or thin layers of gold. Those materials are resistant to the environment, ensuring stability of parameters over time. From Table 1, one can notice that the resistivity of platinum is linear over a wide temperature range (from -250 to 600 °C). Platinum temperature sensors with a resistance of 100 Ω at 0 °C are commercially produced and their parameters meet international standards.

1.3.4 Semiconductors

In semiconductors the width of energy gap is in the range from 0.1 to 2eV. Treating electrons as an ideal gas and using energy equipartition rule it is possible to calculate the average kinetic energy of thermal movement at room temperature

$$E_{śr} = \frac{3}{2} k_B T = 6.2 \cdot 10^{-21} J = 3.8 \cdot 10^{-2} eV \,, \qquad \textbf{(1. 13)}$$

where k_B – Boltzmann constant. The vast majority of electrons have higher energy than average energy of thermal movement or the width of gap energy. Electrons concentration in the conduction band increases with temperature, resulting in the increase of conductivity semiconductors with temperature, according to following relationship:

$$\sigma = \sigma_0 e^{-\frac{\Delta E}{2k_B T}}, \qquad \textbf{(1. 14)}$$

where ΔE is the width of energy gap. In doped semiconductors there are energy levels located close to the **conduction band** (**acceptor levels**) or **valence band** (**donor levels**). In p-type semiconductors, electrons from valence band move to acceptor levels creating "**holes**" in the valence band, which in presence of electric field behave as positive charges. In n-type semiconductors, carriers having negative charge move from the donor level to conduction band. Scheme of a silicon crystal lattice doped with impurities to produce *n*-type (arsenic) and *p*-type semiconductor (gallium) material is presented in Fig.1.2.

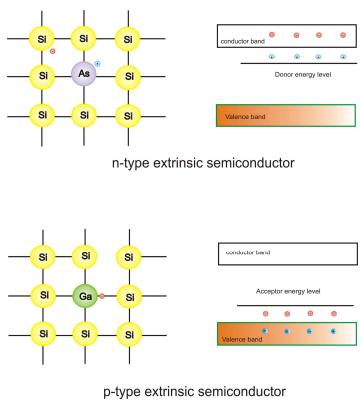

Fig.1. 2 Band structure of an n-type and p-type semiconductor

In materials, there are both types of impurities, but one of them called majority carriers plays a dominant role in conductivity. The temperature dependence of conductivity in both types of

semiconductors is described by an equation similar to (1.14), while ΔE is the energy difference between localized acceptor levels and valence band or donor levels and conduction band. Semiconductors find their application in many areas of modern technology, e.g. electronic circuits, processors, computer memories or in optoelectronics.

1.3.5 Insulators (dielectrics)

In insulators the width of the energy gap between the valence band and the empty conduction band is usually higher then few 3eV, that the probability of electrons moving from the valence level into the conduction band is very small under normal conditions (lack of current carriers). Thus the conductivity of dielectric is very small.

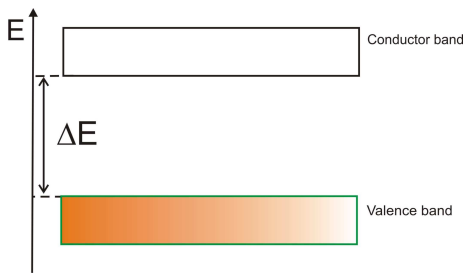

Fig.1. 3 Schematic representation of insulator

An electric field applied to dielectrics can induce dipole moments of atoms or particles and in case of polar dielectrics (built of dipole particles) creates ordering of chaotic oriented dipoles. The main feature of dielectrics is the almost complete lack of electric conductivity, and that in an electric field polarization is induced. It is worth noting that there are some dielectrics with non-zero polarization in the absence of electric field.

1.4 Basic information about dielectrics

Electric dipole is a system of two electric charges q with opposite signs which are located at a distance d between each other. **Dipole momentum** μ of such system is given:

$$\vec{\mu} = q\vec{d} \qquad \textbf{(1. 15)}$$

Distance ***d*** is measured from negative to positive charge. It is worth noting, that in nature there are lots of dipole molecules, e.g. molecule of water. The water molecule is composed of oxygen O^{-2} and two protons and which are located in a distance of 1.015Å. The angle

between the oxygen and protons bonds is $104^{o}45'$. Such structure causes the centre of positive and negative charges to be moved from each other followed by dipole creation. The dipole momentum of the water molecule determines its extraordinary physical properties, which are so crucial to life on Earth.

1.4.1 Electrical polarisation

The electrical polarization P – is a dipole momentum of a volume unit

$$\vec{P} = \frac{1}{V}\sum_i \vec{\mu_i}\,. \qquad \textbf{(1. 16)}$$

A polarization unit is C/m², so it is a measure of charge surface density (polarization can be treated as a surface density of bonded (charges). In the majority of dielectrics when electric field is E=0 the polarization is also P=0. Materials with $P \neq 0$ at E=0 are called **piroelectrics** and specially interesting as sub-group one **ferroelectrics**. The polarization value of the materials at E=0 is called **spontaneous polarization**. In ferroelectrics the direction of spontaneous polarization can be changed with the help of an external electric field. The dependence of spontaneous polarization on the electric field shows a **hysteresis loop** similar to hysteresis in ferromagnetic materials. Ferroelectrics are very interesting thanks to their electromechanical and optical properties and their application.

There are four basic mechanisms of polarization: **electronic, atomic, orientational** polarization and **polarization of the space charges**.

Electron polarization is present in all of dielectrics and is related to the displacement of electron clouds in relation to the nucleons, which is caused by external electric fields (see Fig.1. 4). Relative displacement of electron clouds and the nucleus:

$$\vec{r} = \frac{q\vec{E}}{k} = \alpha_e \vec{E}\,, \qquad \textbf{(1. 17)}$$

where: k is the force constant, q is the electric charge of the nucleus, E is the intensity of the **local electric field**. The intensity of the field acting on the particles inside the dielectric is generally different than a field which is acting from outside. The term α_e is called an **electronic polarizability**.

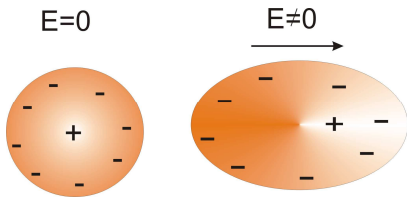

Fig.1. 4 Schematic representation of electronic polarizability

The principle of atomic polarization is connected with relative displacement of atoms (ions) forming molecules of dielectrics and is described by an equation similar to (1.17). However the proportional coefficient in (1.17) is denoted by α_a and is called **atomic (ionic) polarizability** (Fig.1. 5).

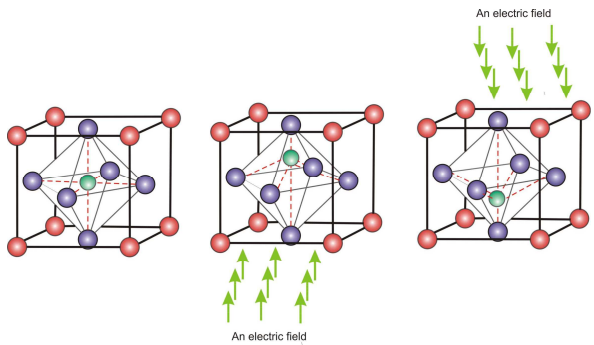

Fig.1. 5 Schematic representation of atomic polarizability

As it was mentioned before, in certain dielectrics there are dipole molecules. Usually dipole moments are oriented in random directions due to thermal movement which is causing the polarization of such material to be zero. The electric field, which is acting on the dipole, is creating momentum of force which is causing the orientation of the dipole in the parallel direction to the field.

$$\vec{M} = \vec{\mu} \times \vec{E} \qquad \textbf{(1. 18)}$$

The thermal movements are acting against the ordering possibilities of the electric field, but there is still resultant polarization which depends on the electric field intensity. Such polarization is called **orientational polarization**. Characteristic feature of the molecules after removing the electric field fades with a relaxation time. The coefficient, which is connecting orientational polarization and the electric field intensity (for not very strong fields) is denoted by α_d and is called dipole or **orientational polarizability** (Fig.1. 6).

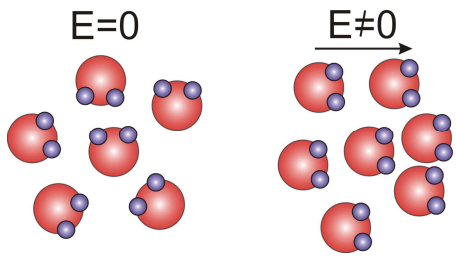

Fig.1. 6 Schematic representation of orientational polarizability

An introduction of non-uniform distribution of charge (e.g. by injection of electrons) causes the creation of a resultant polarization P_p, called **polarization of space charges**. This type of polarization plays an important role in special types of material, called **electrets**. The lifetime of spatial charges can be long (tens or hundreds of years). Such materials are used for manufacturing microphones and electromechanical transducers.

Total polarization is:

$$P = P_e + P_a + P_d + P_p. \tag{1. 19}$$

The sum of electronic and atomic polarization is called **spring polarization**, as after removing the electric field the polarization rapidly fades away.

1.4.2 Electric permittivity

Electric permittivity ε is defined by the relation between electrical induction D and intensity of electric field E.

$$\vec{D} = \varepsilon \vec{E}. \tag{1. 20}$$

In various handbooks and scientific publications the dielectric constant term is used. It is worth noting that the value of electrical permittivity depends on frequency, temperature, pressure, intensity of electric field and many other external factors, so the use of the term 'constant' is not strictly correct. **Relative electric permittivity** ε_r is a ratio of the electric permittivity of the medium to the **electric permittivity of a vacuum** ε_0=8.854187818 F/m,

$$\varepsilon_r = \frac{\varepsilon}{\varepsilon_0}. \tag{1. 21}$$

The electric permittivity of a vacuum is one of the basic constants in nature.

Dependence of electric permittivity upon frequency is called dispersion (relative permittivity of water measured at low frequencies is around 80 while at optical frequencies is around 1.77). Electric permittivity can be regarded as a **scalar quantity** only for isotropic

media (**isotropic** means that physical properties do not depend on the orientation). In **anisotropic** media some of the physical properties measured in different directions can be different. The relationship between electrical induction and intensity of the electric field for anisotropic media can be expressed (using summation convention)

$$D_i = \varepsilon_{ij} E_j \text{, where } i, j = 1, 2, 3. \quad \textbf{(1. 22)}$$

Electrical permittivity is a **second range symmetrical tensor**. Electrical permittivity as a tensor can be expressed as a 3x3 matrix:

$$\begin{matrix} \varepsilon_{11}\ \varepsilon_{11}\ \varepsilon_{13} \\ \varepsilon_{21}\ \varepsilon_{22}\ \varepsilon_{23} \\ \varepsilon_{31}\ \varepsilon_{32}\ \varepsilon_{33}, \end{matrix} \quad \textbf{(1. 23)}$$

where $\varepsilon_{ij} = \varepsilon_{ji}$. The number of components of the tensor of electrical permittivity depends on the **media symmetry**. Using the **von Neuman rule** it is possible to find non-zero components of the tensor, which describe physical properties of the medium and relationships between them. In Table 2 the components of the symmetrical second range tensor in various crystallographic systems (e.g. electrical permittivity and thermal deformation) are presented.

Table 2. Components of symmetrical tensor of second range in seven crystallographic systems and polarized ceramics or films.

Crystallographic system	linearly independent components of symmetrical second rank tensor
triclinic	$\boldsymbol{\varepsilon_{11}}$ $\boldsymbol{\varepsilon_{12}}$ $\boldsymbol{\varepsilon_{13}}$ $\boldsymbol{\varepsilon_{21}}$ $\boldsymbol{\varepsilon_{22}}$ $\boldsymbol{\varepsilon_{23}}$ $\boldsymbol{\varepsilon_{31}}$ $\boldsymbol{\varepsilon_{32}}$ $\boldsymbol{\varepsilon_{33}}$
monoclinic	$\boldsymbol{\varepsilon_{11}}$ **0** $\boldsymbol{\varepsilon_{13}}$ **0** $\boldsymbol{\varepsilon_{22}}$ **0** $\boldsymbol{\varepsilon_{31}}$ **0** $\boldsymbol{\varepsilon_{33}}$
rhombic	$\boldsymbol{\varepsilon_{11}}$ **0** **0** **0** $\boldsymbol{\varepsilon_{22}}$ **0** **0** **0** $\boldsymbol{\varepsilon_{33}}$
tetrahedral, trigonal, hexagonal	$\boldsymbol{\varepsilon_{11}}$ **0** **0** **0** $\boldsymbol{\varepsilon_{11}}$ **0** **0** **0** $\boldsymbol{\varepsilon_{33}}$
cubic	$\boldsymbol{\varepsilon_{11}}$ **0** **0** **0** $\boldsymbol{\varepsilon_{11}}$ **0** **0** **0** $\boldsymbol{\varepsilon_{11}}$
polarized ceramics and films	$\boldsymbol{\varepsilon_{11}}$ **0** **0** **0** $\boldsymbol{\varepsilon_{11}}$ **0** **0** **0** $\boldsymbol{\varepsilon_{33}}$

It is worth mentioning that it is always possible to choose the coordinate system in such way that non-diagonal components of the tensor of electric permittivity are equal to zero (ε_{ij}=0, for $i \neq j$). For the triclinic system, monoclinic and rhombic $\varepsilon_{11} \neq \varepsilon_{22} \neq \varepsilon_{33}$, for tetrahedral, triagonal and hexagonal $\varepsilon_{11} = \varepsilon_{22} \neq \varepsilon_{33}$ and for regular and isotropic media $\varepsilon_{11} = \varepsilon_{22} = \varepsilon_{33}$.

It should be noted the relationship between electric permittivity and optical properties of media. Speed of light in vacuum:

$$c = \frac{1}{\sqrt{\mu_0 \varepsilon_0}}, \qquad \textbf{(1. 24)}$$

while in the medium with electrical permittivity $\varepsilon_o\varepsilon_r$ (for optical frequencies) is:

$$c_o = \frac{1}{\sqrt{\mu_0 \varepsilon_0 \varepsilon_r}}, \qquad \textbf{(1. 25)}$$

where μ_0 is magnetic permittivity of vacuum. Absolute value of refraction coefficient (index) is equal to the ratio of the speed of light in vacuum to the speed of light in the media

$$n = \frac{c}{c_o} = \sqrt{\varepsilon_r}. \qquad \textbf{(1. 26)}$$

From equation (1.26) one can notice that anisotropy of electrical permittivity is related to the anisotropy of optical properties (in anisotropic media there is birefringence phenomena). The quantity ε_r in equation($n = \frac{c}{c_o} = \sqrt{\varepsilon_r}$. (1. 26) is measured at optical frequencies.

The relationship between electrical induction and intensity of the electric field is linear only for linear dielectrics and weak electric fields. If the relationship is non-linear, then the electrical permittivity can be defined as dD/dE. Another frequently used approach is to develop the relationship between induction and field intensity as a power series (e.g. to describe the generation of second harmonic of the light).

$$D = \varepsilon_1 E + \varepsilon_2 E^2 + \varepsilon_3 E^3 + \ldots, \qquad \textbf{(1. 27)}$$

where ε_2, ε_3 are nonlinear permittivity.

The values of electrical permittivity in the frequency range from 10^{-6} to 10^7 Hz are evaluated by measuring of electrical capacitance C of a capacitors. Knowing dimensions of the capacitor with dielectric. We may calculate its capacity C as:

$$C = \varepsilon_r C_0, \qquad \textbf{(1. 28)}$$

where C_0 is the capacitance of the vacuum capacitor with the same dimensions as the capacitor with the dielectric. In order to evaluate the electrical permittivity at higher frequencies the microwave or optical methods are used.

Electrical induction of the media can be described:

$$D = \varepsilon E = \varepsilon_0 \varepsilon_r E = D_0 + P = \varepsilon_0 E + \chi \varepsilon_0 E = (1+\chi)\varepsilon_0 E . \quad \textbf{(1. 29)}$$

The χ coefficient is called **electric susceptibility**. From the equation

(1.29 $D = \varepsilon E = \varepsilon_0 \varepsilon_r E = D_0 + P = \varepsilon_0 E + \chi \varepsilon_0 E = (1+\chi)\varepsilon_0 E .$ (1. 29)

$$\varepsilon_r = 1 + \chi . \quad \textbf{(1. 30)}$$

In some materials, e.g. ferroelectrics at a temperature in the neighbourhood of the phase transition temperature the electric permittivity can reach very high values (10^3-10^6). In such cases it is possible to assume, that $\varepsilon \approx \chi$.

1.4.3 Complex form of electric permittivity

Assuming that the system consists of the source of alternating current with the amplitude U_0 and frequency ω and flat vacuum capacitor with the capacitance C_0 (see Fig.1. 7).

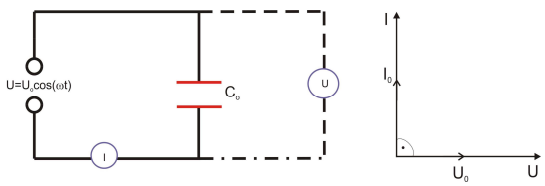

Fig.1. 7 Vacuum capacitor in the alternating current circuit and vector representation of the current and voltage

The current in the circuit is given by:

$$I = \frac{dQ}{dt}, \quad \textbf{(1. 31)}$$

The charge on the plates of the capacitor is

$$Q = C_0 U . \quad \textbf{(1. 32)}$$

where $C_0 = \frac{\varepsilon_0 S}{d}$.

In equation (1.32) S is the surface of capacitor and d is the distance between the plates. The voltage on the plates of the capacitor changes according to the equation:

$$U = U_o \cos(\omega t) = \mathrm{Re} U_0 e^{i\omega t} \quad \textbf{(1. 33)}$$

The current in the circuit:

$$I = \frac{d}{dt}\left(\frac{\varepsilon_0 S}{d} U_0 \cos(\omega t)\right) = -\frac{\varepsilon_0 \omega S U_0}{d} \sin(\omega t) = -\varepsilon_0 \omega S E_0 \sin(\omega t), \qquad \textbf{(1. 34)}$$

where $E_0 = \frac{U_0}{d}$ is the intensity of electric field between the plates of the capacitor.

The current density is:

$$j = \frac{I}{S} = -\varepsilon_0 \omega E_0 \sin(\omega t). \qquad \textbf{(1. 35)}$$

In this circuit the phase of the current 'overtakes' the phase of the voltage with the factor π/2 (see figure 1.7)

To describe the real capacitor filled with dielectric it is necessary to use the complex form of the capacitance

$$C^* = \varepsilon^* \frac{S}{d}, \qquad \textbf{(1. 36)}$$

where

$$\varepsilon^* = \varepsilon' - i\varepsilon''. \qquad \textbf{(1. 37)}$$

In equations (1.36) and (1.37) the term ε^* is the complex form of electrical permittivity, ε' – is a real part of the electrical permittivity, ε'' is the imaginary part. From the equations (1.36) and (1.37) the capacitance of the capacitor can be computed as:

$$C^* = \left(\varepsilon' - i\varepsilon''\right)\frac{S}{d}. \qquad \textbf{(1. 38)}$$

The charge on the plates of the capacitor can be calculated as $Q = C^* U$, and the current in the circuit is:

$$I = \frac{d}{dt}\left(\left(\varepsilon' - i\varepsilon''\right)\frac{S}{d} U_0 e^{i\omega t}\right) = i\omega\left(\varepsilon' - i\varepsilon''\right)\frac{S}{d} U_0 e^{i\omega t} = i\omega\left(\varepsilon' - i\varepsilon''\right) S \frac{U}{d}. \qquad \textbf{(1. 39)}$$

The current density

$$j = \frac{I}{S} = \left(i\omega\varepsilon' + \omega\varepsilon''\right)E = \sigma_a^* E. \qquad \textbf{(1. 40)}$$

The term σ_a^* is the complex conductivity. The factor in the brackets in equation (1.40) $i\omega\varepsilon' + \omega\varepsilon'' = \sigma_a^*$ describes total electrical conductivity (admittance), the product $\omega\varepsilon'' = \sigma$ – real electric conductivity, and $\omega\varepsilon' = \sigma_s$ imaginary part of electric conductivity (susceptance). The real term of conductance describes losses of electrical energy in the dielectric (conversion of energy into heat), while the imaginary part describes the current of the 'shift' related to induction of polarization. The equation $j_k = \omega\varepsilon'' E$ and $j_s = i\omega\varepsilon' E$ describes real part and imaginary part of the current density. The Fig.1. 8 presents the relationships between total

current density j and its real and imaginary parts for real dielectric. It is worth noting that the real part of the current is in phase with voltage and total current density creates the phase angle δ with the current direction.

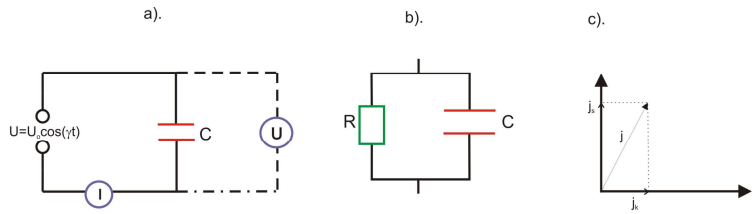

Fig.1. 8 Real capacitor in the circuit of alternating current a), substitute circuit diagram of a real capacitor b) and relationships between total current density and its real and imaginary parts for real dielectrics c).

From the figure 1.8 one can notice that the tangents of δ (δ is called the angle of dielectric losses) is:

$$tg\delta = \frac{j_k}{j_s} = \frac{\varepsilon''}{\varepsilon'}. \qquad \textbf{(1. 41)}$$

Writing relationship between electrical permittivity and susceptibility in complex form:

$$\varepsilon^* = \varepsilon' - i\varepsilon'' = \chi^* + 1 = 1 + \chi' - i\chi'' \qquad \textbf{(1. 42)}$$

and comparing the real and imaginary parts one obtains

$$\varepsilon' = 1 + \chi' \text{ and } \varepsilon'' = \chi''. \qquad \textbf{(1. 43)}$$

In some cases instead of imaginary electrical permittivity it is more comfortable to use the electric modulus defined as the inverse of complex electrical permittivity

$$M^* = \frac{1}{\varepsilon^*} = \frac{1}{\varepsilon' - i\varepsilon''} = \frac{\varepsilon'}{\varepsilon'^2 + \varepsilon''^2} + \frac{i\varepsilon''}{\varepsilon'^2 + \varepsilon''^2} \qquad \textbf{(1. 44)}$$

In order to describe behaviour of real dielectrics in the alternating electric field the components ε' and ε'', ε' and $tg\delta$, $\sigma = \omega\varepsilon''$ or χ' and χ'' are often used.

As a conclusion of the description of the behaviour of dielectrics in alternating electric fields it is necessary to define impedance Z. The relationship between the voltage and current in the circuit of alternating current is described:

$$I_{(\omega,t)} = \frac{U_{(\omega,t)}}{Z(\omega)} \qquad \textbf{(1. 45)}$$

Impedance

$$Z^* = R + iX. \qquad \textbf{(1. 46)}$$

In equation (1.46) R is the resistance and X is called reactance. Modulus of the impedance is denoted as Z. Impedance of loss-less capacitor:

$$Z^* = X_C = \frac{1}{i\omega C}. \qquad \textbf{(1. 47)}$$

Quantity X_c is called capacitance (capacity impedance). Inductive impedance

$$X_L = i\omega L \qquad \textbf{(1. 48)}$$

is called inductance. The total impedance of series or parallel connected elements is calculated in a similar way as the total resistance of resistors connected in series or parallel. Very often the loss capacitor is described as a parallel connection of resistor R and capacity impedance X_c.

1.5 Electrical capacity, energy of electric field

Electric capacity C of the set of two electrodes (conductors) is called the ratio of the charge Q on the surface to the voltage U between them:

$$C \equiv \frac{Q}{U}. \qquad \textbf{(1. 49)}$$

In the SI system the capacity unit is Farad $1F = \frac{1C}{1V}$. It is very large unit comparing to practice where capacity is in the range of μF, nF, pF and fF.

To derive the equation describing the electrical capacity of the set of electrodes (plates of the capacitor) it is necessary to calculate distribution of the electric field between the plates of the capacitor (using Gaussian Law), then integrate the obtained equation, calculate the difference of potential between the plates and introduce the obtained relationship in equation (1.49).

1.5.1 Parallel plate capacitor

Flat capacitor consist of two parallel conducting plates separated by the free space or a dielectric medium. The capacitance depends on the geometry of capacitor but the charge Q and potential different U does not affect the capacitance value (Fig.1.9) .

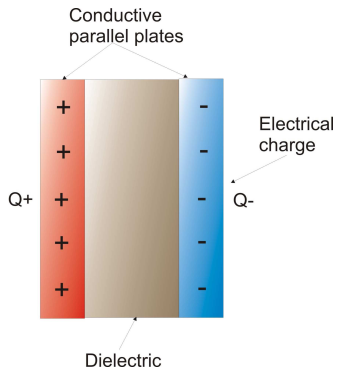

Fig.1. 9 Parallel plate capacitor

Electrical capacity C_0 of flat capacitor with vacuum with the surface S and distance between plates d is equal:

$$C_0 = \frac{\varepsilon_0 S}{d}, \tag{1. 50}$$

while the capacity of such capacitor filled with dielectric with relative electric permittivity ε_r

$$C = \frac{\varepsilon_0 \varepsilon_r S}{d} = \frac{\varepsilon S}{d} = \varepsilon_r C_0. \tag{1. 51}$$

The capacitance is independent of charge and the potential difference across the plates but only of the geometrical dimensions of the capacitor.

It is worth noting, that eq. (1.50) and (1.51) are approximate, because they have been derived for two infinite parallel planes (electric field 'leaving' the capacitor has not been considered), so it can be used for large surface of electrodes which are located at small distance. Equation (1.50) and (1.51) are frequently used to derive electric permittivity of various types of materials. On a sample of tested material with known dimensions: thickness d and surface area S, the electrodes are installed and the electric capacity is measured. Relative dielectric permittivity of the sample is calculated by dividing the electric capacity C by the capacity of the vacuum capacitor C_0 with the same dimensions

$$\varepsilon_r = \frac{C}{C_0}. \tag{1. 52}$$

It is important to add that capacitance measurement is very often used for liquid level measurement, to measure the ingredients of the liquids and gases, small deformations (thermal expansion, piezoelectric deformation, electrostriction, magnetostriction or

measurement of the dielectric layers thickness on the conductive bases, for example to measure the distribution of the thickness of the paint on the cars elements). Capacity measurement is also used in nanoactuators (actuators with actuating ranges of nm). For small distances between the plates of the capacitor the sensitivity of measurement is more sensitive by a couple of orders than interference measurement!.

1.5.2 Capacity of cylindrical capacitor

Cylindrical capacitor is created by two coaxial cylinders with the length l and radius of inner plate r_1 and outer plate r_2, charged with the two opposite signs $+Q$ and $-Q$ (Fig.1. 10).

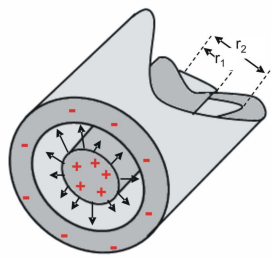

Fig.1. 10 Cylindrical capacitor

Using Gauss Law, it is possible to derive the intensity of electric field between the cylinders and then electric capacity:

$$C = \frac{2\pi\varepsilon l}{\ln(r_2 / r_1)}. \qquad \textbf{(1. 53)}$$

From the equation (1.53) one way to conclude that the capacitance of the cylindrical capacitor depends on the length of the cylinder and the ratio of the radii of the cylinders. One can also notice that coaxial cables, made of conductive core and conductive screen, are forming a cylindrical capacitor. In electrical capacity measurement it is important to minimize the capacity of the cables. During very accurate measurement of capacitance (especially small values) it is necessary to compensate the capacitance of the cables, or to take it into account capacitance of cables during measurement.

1.5.3 Capacity of spherical capacitors

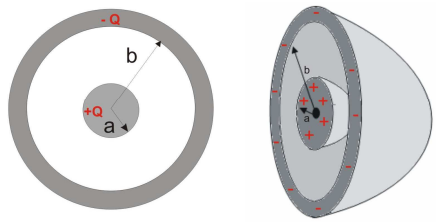

Fig.1. 11 Spherical capacitor with two spherical concentric shells of radii a and b.

A spherical capacitor consists of two concentric spherical conductors, the inner one of radius *a* and outer of radius *b* (Fig.1. 11). The capacitance for spherical conductors can be obtained from Gauss Law and is given as:

$$C = \frac{Q}{\Delta V} = 4\pi\varepsilon_0\left[\frac{1}{a} - \frac{1}{b}\right] \qquad \textbf{(1. 54)}$$

1.5.4 Energy of charged capacitor

The capacitor energy change (energy stored inside of the capacitor)

$$W_E = \int_0^U QdU = \int_0^U CUdU = \frac{1}{2}CU^2 . \qquad \textbf{(1. 55)}$$

For the flat capacitor with the surface of plates *S* and the distance between them *d* filled with dielectric with the permittivity ε

$$W_E = \frac{\varepsilon SU^2}{2d} = \frac{\varepsilon U^2 Sd}{2d^2} = \frac{1}{2}\varepsilon E^2 V = \frac{1}{2}DEV . \qquad \textbf{(1. 56)}$$

where: the intensity of electric field $E = \frac{U}{d}$, $Sd = V$ – the volume of the capacitor and $\varepsilon E = D$ is the electric inductivity.

Energy density of electric field is:

$$w_E = \frac{W_E}{V} = \frac{1}{2}\varepsilon E^2 = \frac{1}{2}\varepsilon_0(1+\chi)E^2 = \frac{1}{2}\varepsilon_0 E^2 + \frac{1}{2}\varepsilon_0\chi E^2 = \frac{1}{2}\varepsilon_0 E^2 + \frac{1}{2}PE . \qquad \textbf{(1. 57)}$$

From equation (1.57) one can notice that the energy of electric field is proportional to the square of its intensity. Factor $\frac{1}{2}PE$ describes energy of the interaction of dielectric with external electric field.

1.6 Methods of capacity (permittivity) measurement

1.6.1 Static methods

There are two methods, which are considered as static methods: the method of "pick up electrode" and the method of "ballistic galvanometer". Above methods principle is related to measurement of charges on the surface of the dielectric and can be used for the measurement of the dielectrics with small losses. In the method of "pick up electrode" the charge flowing from the electrode during the disconnection from the surface of the dielectric is determined. The schematic of the method of ballistic galvanometer is presented in Fig. 1.12.

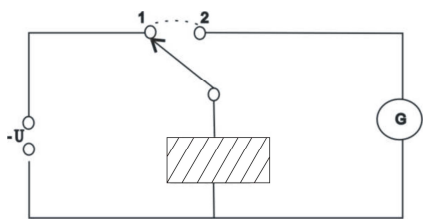

Fig.1. 12 The schema of the method of ballistic galvanometer method of measurement of capacitance

Setting the switch in position 1 charge the capacitor filled with tested dielectric from the source of direct current to the voltage *U*. After charging the capacitor the switch is set to position 2. The capacitor is discharged through the ballistic galvanometer, which is used to measure the charge (ballistic galvanometer is a device which does not have a return torque – the displacement of such a galvanometer is proportional to the charge which flows through the coils of the device). Measuring the charge flowing through the coils of galvanometer during discharging the capacitor without the dielectric, it is possible to derive the relative dielectric permittivity of measured dielectric according to the equation:

$$\varepsilon_r = \frac{Q}{Q_0}. \qquad \textbf{(1. 58)}$$

Currently to measure electric charge, very sensitive and accurate electrometers are used.

1.6.2 Quasi-static methods

In quasi-static methods an alternating current is used. The frequency $f<<f_r$, where f_r is the resonant frequency of that circuit. Capacitance of the capacitor can be derived by **measuring the impedance of the circuit**, which contains a series at connected resistances with known value *R* and the capacitor to be tested.

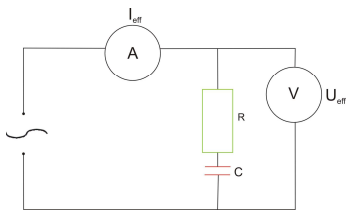

Fig.1. 13 Scheme of measurement of capacitance by measuring the impedance modulus.

Current in the circuit is measured using the ammeter A

$$I_{RMS} = \frac{U_{RMS}}{Z}. \qquad \textbf{(1. 59)}$$

Using the equation to calculate the impedance and deriving the RMS of voltage and the RMS of current it is possible to derive the impedance of the circuit, and thus capacitance of tested capacitor.

$$Z = \sqrt{R^2 + \left(\frac{1}{\omega C}\right)^2} \qquad \textbf{(1. 60)}$$

Between quasi-static methods is the integration method of capacitance measurement. The schematic of the method is presented in Fig.1. 14. The set up of the system consists of the test capacitor C_x, the switch, two resistances, a source of direct current with known voltage U, rectifying bridge and ammeter.

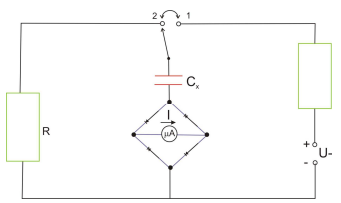

Fig.1. 14 Diagram of the measurement of capacitance by integration method.

When the switch is in position 1 the capacitor is charged to the voltage V, charge $Q=CU$ flows through the ammeter. After switching the switch to position 2 discharge occurs and charge Q flows through the ammeter in the same direction. If the switch is switched with

frequency f (most often 50Hz) then the average current which flows through ammeter is given by:

$$I = 2fUC_x \qquad \textbf{(1. 61)}$$

From equation (1.61), the mean value of the current is proportional to the tested capacitance, so the ammeter can be scaled in units of capacitance. The integration method is often used in multimeters and cheap capacitance meters.

1.6.3 Bridge method

Bridge methods are used to derive complex values of electric permittivity in a very wide frequency range (from 10^{-6} to 10^{7}Hz). The principles of the method are described by the example of Schering's bridge, the schematic of which is presented in Fig.1.15.

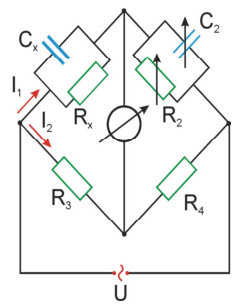

Fig.1. 15 Schering bridge diagram

The test capacitor with losses C^* is presented as a parallel connection of the resistance R_x and ideal capacitor C_x, R_2 is an adjustable resistance, R_3 and R_4 are the resistances of lower branches of the bridge. The bridge is supplied with a source of alternating current with frequency ω. A voltmeter measuring alternating voltage is used as an indicator of the balance of the bridge.

The inversion of the impedance of the upper branches of the bridge is:

$$\frac{1}{Z_1} = \frac{1}{R_x} + \frac{1}{\frac{1}{i\omega C_x}} = \frac{1}{R_x} + i\omega C_x, \qquad \frac{1}{Z_2} = \frac{1}{R_2} + i\omega C_2. \qquad \textbf{(1. 62)}$$

The bridge is balanced (in the diagonal used for measurement the current is equal to zero) when

$$I_1 Z_1 = I_2 Z_3 \text{ and } I_1 Z_2 = I_2 Z_4. \qquad \textbf{(1. 63)}$$

Dividing the equations one obtains:

$$\frac{Z_1}{Z_2}=\frac{Z_3}{Z_4}\Rightarrow\frac{1}{Z_1}=\frac{Z_4}{Z_3}\frac{1}{Z_2}. \quad \textbf{(1. 64)}$$

Replacing the inversion of impedance (Eq.1.62) yields:

$$\frac{1}{R_x}+i\omega C_x=\frac{R_4}{R_3}\left(\frac{1}{R_2}+i\omega C_2\right). \quad \textbf{(1. 65)}$$

Comparing the real parts and imaginary parts are obtains:

$$\frac{1}{R_x}=\frac{R_4}{R_3}\frac{1}{R_2} \qquad \text{and} \qquad C_x=C_2. \quad \textbf{(1. 66)}$$

Most often $R_4=R_3$, so $\frac{1}{R_x}=\frac{1}{R_2}=\Sigma$, where Σ is the electric conductance of the capacitor. The bridge can be scaled in the units of conductivity (siemens S) or (as it will be described below) showing the tangents of the angle of dielectric losses and the capacitance units. Knowing the geometric dimensions of the capacitor one can derive the specific conductivity σ of the test material using the equation $\Sigma=\frac{\sigma S}{d}$.

Electric permittivity is derived by dividing capacitance of the capacitor with the dielectric by capacitance of the vacuum capacitor with the same dimensions. It is worth noting that measured capacity C_x is the sum of capacitance of the connections and tested capacitance. In some bridges it is possible to compensate capacitance of the connections. If it is not possible it is necessary to measure the capacitance of the set up C_d without the tested capacitor and subtract it from measured capacitance C_x. Using the expression to calculate complex electric permittivity of the dielectric it is possible to write it in a form:

$$\frac{1}{Z_1}=i\omega\varepsilon^{*}C_0=i\omega\varepsilon'C_0+\omega\varepsilon''C_0=\frac{R_4}{R_3}\left(\frac{1}{R_2}+i\omega C_2\right) \quad \textbf{(1. 67)}$$

Comparing real parts and imaginary parts we obtain:

$$\omega\varepsilon''C_0=\frac{R_4}{R_3}\frac{1}{R_2}\ , \quad \textbf{(1. 68)}$$

If $R_4=R_3$ then

$$\varepsilon''=\frac{1}{\omega R_2C_0}, \quad \textbf{(1. 69)}$$

From equation (1.69) one concludes that to derive ε" it is necessary to know value of C_0, and so the geometrical dimensions of tested capacitor. Please notice that:

$$tg\delta = \frac{\varepsilon''}{\varepsilon'} = \frac{\frac{1}{\omega R_2 C_0}}{\frac{C_2}{C_0}} = \frac{1}{\omega R_2 C_2}. \qquad \textbf{(1. 70)}$$

Expression (1.70) contains quantities measured using the bridge, so the bridge can be used to measure capacitance of the capacitor and the value of tgδ or electric conductivity. Description of other types of bridges and the details of their operation is very wide area of research and it exceeds the content of this paper.

There are other bridges commercially available, they work with various frequencies (most often 1kHz, 100kHz or 1MHz) or in wide range of frequencies (from 10^{-6} to 10^{7}Hz) and measurement fields – variable amplitude of measurement field, measurement on the background or slow variable electric field). Suppliers are attaching specialized software, which enables computerized recording of measurement data and specialized result data processing.

1.6.4 Resonance methods of capacity measurement.

Resonance methods enable measurement of complex electric permittivity in the frequency range from 10^4 to 10^9Hz. A schematic of the method is presented in Fig.1. 16. It is worth mentioning that frequency measurement is very accurate (measurement of frequencies in the range of MHz with an accuracy of 1Hz is not problematic), so the resonance methods are used to measure very small changes of capacitance. There are various methods to derive resonance curves and measure electric capacitance.

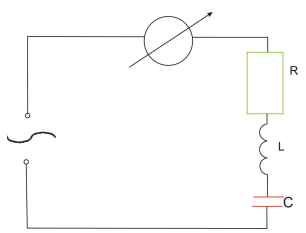

Fig.1. 16 Diagram of the resonance method

In the simplest case the current dependence in the circuit at constant supply voltage at the supplied frequency is derived. The current in the circuit is maximal when the inductive impedance is equal the capacity impedance so $\omega L = \frac{1}{\omega C}$. Knowing L of the resonance circuit

and the resonance frequency it is possible to derive measured capacitance C. Knowing the resonance curve it is possible to measure the quality factor of the circuit (goodness) Q_r. The goodness of the resonance circuit is defined as a ratio of energy stored in the system to energy dissipated during one period. It is possible to prove that the goodness of the system is equal to the ratio of resonant frequency to the width of the half maximum of the resonance curve (difference of the frequencies for which the amplitude is equal to half of the amplitude at the resonance frequency). Quality factor (goodness) of the LC system is equal to the inverse of the tangent of the angle of dielectric losses:

$$Q_r = \frac{1}{tg\delta}. \qquad \textbf{(1. 71)}$$

The resonance curve can be obtained also at the given supplied frequency ω and the induction L of the circuit by varying the capacitance of the model (known) capacitor C_n. First it is necessary to derive the frequency of the circuit which contains known capacity C_{n1}. After installation of the test capacitance C in the system the resonance will appear at lower value of known capacity C_{n2}.

Real part of the electric permittivity of the tested dielectric which fills the capacitor can be derived from:

$$\varepsilon' = \frac{C_{n1} - C_{n2}}{C_0} \qquad tg\delta = \frac{1}{Q_{r2}} - \frac{1}{Q_{r1}} \qquad \textbf{(1. 72)}$$

The resonance curve can be obtained using the Q-meter. In such a case the current dependence on the capacity is derived. The resonance curve is obtained for known model of capacitor and for the test capacitor.

When describing resonance methods it is worth mentioning the 'substitution method'. In this method the test capacitor is connected parallel to the adjustable capacity (Fig.1. 17). It is also possible to connect the loss-less capacitor and in parallel the resistor.

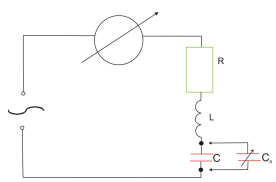

Fig.1. 17 Scheme of measurement of capacitance by substituting method.

Changing the adjustable capacitor and the resistor it is possible to tune the system in such way, that the resonance curve parameters (amplitude and resonance frequency) are not changed during switching the position of the switch.

1.6.5 Beat method

The schematic of the beat method is presented in Fig.1. 18. The test set up is made of two generators and the mixer in which the beat occurs, the filter which cuts off the high frequencies and the frequency meter. The capacitor to be tested C_x is connected to the resonance circuit of one of the generators (on the figure ω_2)

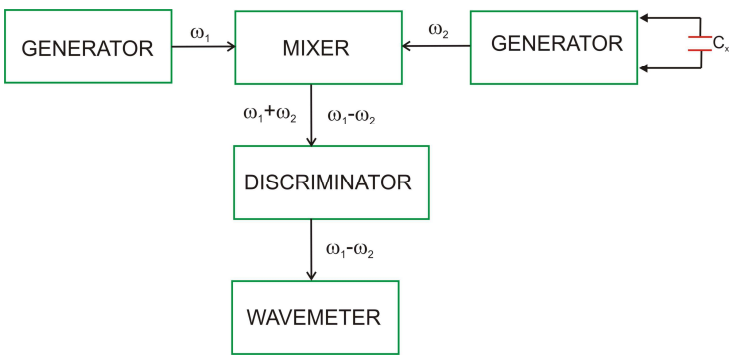

Fig.1. 18 Scheme of measurement of capacitance by beat method

To simplify we assume that the amplitude of the voltages on the outputs of both of the generators are equal $U_{01} = U_{02} = U_0$. The resultant voltage (after mixing both signals)

$$U_{12} = U_{01}\sin(\omega_1 t) + U_{02}\sin(\omega_2 t) = 2U_0 \sin\frac{\omega_1+\omega_2}{2}t\cos\frac{\omega_1-\omega_2}{2}t \qquad \textbf{(1. 73)}$$

The output signal of the mixer contains the sum part $\frac{\omega_1+\omega_2}{2}$ and difference part $\frac{\omega_1-\omega_2}{2}$. The filter cuts off the high frequency. The frequency meter is used to measure the difference frequency. The resonance frequency of the generator ω_2 depends on the capacitance connected to the resonance circuit, so the measurement of the difference frequency enables accurate derivation of the capacitance changes in the circuit of that generator.

It is worth noting that beat frequencies are used in many areas of science and technology, for example modulation of radio frequencies, optical mixing of frequencies, second harmonic generation of light (SHG), Raman and Brillouin scatering.

1.7 Thermodynamics of dielectrics – linear expansion and thermodynamic identities.

Phenomenological descriptions concerning the macroscopic scale (bulk materials) are not generally considered as being due to microscopic mechanisms of the particular phenomena in question. This fact enables us to make a description of macroscopic system response to external factors such as the electric field E, hydrostatic pressure p or mechanical stress σ

$$E \rightarrow P,$$
$$p \rightarrow V,$$
$$\sigma \rightarrow \eta,$$

where: P – the polarization, V – the volume, η – the deformation,

Macroscopic properties can however be linked with microscopic phenomena; for example polarization microscopy is related to the dipole moment. Usually external factors (generalized forces) to be considered are:

mechanical stress	$-\sigma$,
electric field	$-E$,
temperature	$-T$,
pressure	$-p$,
magnetic field	$-H$.

System response to external factors is manifested in the form of changes in such parameters (generalized coordinates) as:

deformation	$-\eta$,
polarization	$-P$,
entropy	$-S$,
volume	$-V$,
magnetization	$-M$.

The choice of variables depends on the type of phenomena under investigation; considering the dielectric properties, generalized forces are usually σ, E, T and p and the

generalized coordinates are: η, P, S and V, the variables being chosen to suit the appropriate thermodynamic function. The most frequently used functions, witch are describing dielectric properties are free energy or Gibbs function. The definitions of those functions are given in Table 3.

Table 3. Thermodynamic potentials used to describe the physical properties of dielectrics.

The name of the potential	Definition of potential	Independent variables	Proposed by
Free energy	$F = A = U - TS$	T, η, P	Helmholtz in 1882
Gibbs function	$G + U + x \cdot X - TS$	T, σ, p, E	Gibbs in 1930

U – internal energy.

Let us recall definition of entropy $dS = dQ / T$ and generalized work $dW = Xdx$. Examples of generalized work are: $dW = pdV$, $dW = EdP$ and $dW = \sigma d\eta$. Thermodynamic potentials are the functions of the state.

Consider the Gibbs Function:

$$G = U - TS + \sigma\eta + pV + EP. \tag{1.74}$$

If we would like to take into account the magnetic and magnetoelectric phenomena to the thermodynamic potential the MH term should be added.

Derivatives of the Gibbs function have a definite physical meaning:

$$\frac{\partial G}{\partial T} = -S \qquad \frac{\partial G}{\partial \sigma} = \eta \qquad \frac{\partial G}{\partial p} = V \quad \text{and} \quad \frac{\partial G}{\partial E} = P \tag{1.75}$$

Each of these physical quantities (derivatives) depends on all independent variables:

$$\begin{aligned} S &= S_{(T,\sigma,p,E)}, \\ \eta &= \eta_{(T,\sigma,p,E)}, \\ V &= V_{(T,\sigma,p,E)}, \\ P &= P_{(T,\sigma,p,E)}. \end{aligned} \tag{1.76}$$

Developing a linear function of the first derivatives of Gibbs functions and limiting the expansion to the linear terms we obtain:

$$dS = \frac{\partial S}{\partial T}dT + \frac{\partial S}{\partial \sigma}d\sigma + \frac{\partial S}{\partial p}dp + \frac{\partial S}{\partial E}dE,$$

$$d\eta = \frac{\partial \eta}{\partial T}dT + \frac{\partial \eta}{\partial \sigma}d\sigma + \frac{\partial \eta}{\partial p}dp + \frac{\partial \eta}{\partial E}dE\,, \tag{1.77}$$

$$dV = \frac{\partial V}{\partial T}dT + \frac{\partial V}{\partial \sigma}d\sigma + \frac{\partial V}{\partial p}dp + \frac{\partial V}{\partial E}dE\,,$$

$$dP = \frac{\partial P}{\partial T}dT + \frac{\partial P}{\partial \sigma}d\sigma + \frac{\partial P}{\partial p}dp + \frac{\partial P}{\partial E}dE\,.$$

In some cases components of the second row should be taken into account, for example, electrostriction or Kerr effect.

The last line includes terms describing the phenomena that allow conversion of non-electric properties into electrical ones, the last column describes the phenomena that control non-electrical quantities by means of an electric field.

Materials exhibiting piezoelectric and pyroelectric properties are classified as smart materials. An element made of such material can be used simultaneously as a detector and actuator; an example of an element made of a smart material is a piezoelectric transducer which can be used to detect elastic waves (acoustic or ultrasonic) and also to generate these types of waves.

The second derivatives of thermodynamic potential (the first in line expansions) have the following physical meaning:

$\frac{\partial S}{\partial T} = -\frac{\partial^2 G}{\partial T^2} = \frac{c}{T}$, c – specific heat,

$\frac{\partial S}{\partial \sigma_{ij}} = -\frac{\partial^2 G}{\partial T \partial \sigma_{ij}} = \alpha_{ij}$, piezocaloric effect,

$\frac{\partial S}{\partial p} = -\frac{\partial^2 G}{\partial T \partial p} = \beta$, volume piezocaloric effect (pressurecaloric effect),

$\frac{\partial S}{\partial E_i} = -\frac{\partial^2 G}{\partial T \partial E_i} = \gamma_i$ electrocaloric effect,

$\frac{\partial \eta_{ij}}{\partial \sigma_{kl}} = \frac{\partial^2 G}{\partial \sigma_{ij} \partial \sigma_{kl}} = c_{ijkl}$, elastic modulus,

$\frac{\partial \eta_{ij}}{\partial T} = \frac{\partial^2 G}{\partial \sigma_{ij} \partial T} = \alpha_{ij}$, thermal expansions,

$\frac{\partial \eta_{ij}}{\partial p} = \frac{\partial^2 G}{\partial \sigma_{ij} \partial p} = \delta_{ij}$, pressure deformation,

$$\frac{\partial \eta_{jk}}{\partial Ei} = \frac{\partial^2 G}{\partial \sigma_{jk} \partial E_i} = d_{ijk},$$ reversal piezoelectric effect,

$$\frac{\partial V}{\partial p} = \frac{\partial^2 G}{\partial p^2} = \chi,$$ volume compressibility,

$$\frac{\partial V}{\partial \sigma_{ij}} = \frac{\partial^2 G}{\partial p \partial \sigma_{ij}} = \delta ij,$$ stress compressibility,

$$\frac{\partial V}{\partial T} = \frac{\partial^2 G}{\partial p \partial T} = \beta,$$ volume thermal expansion,

$$\frac{\partial V}{\partial E_i} = \frac{\partial^2 G}{\partial p \partial E_i} = \theta_i,$$ reversal volume piezoelectric effect,

$$\frac{\partial P_i}{\partial E_j} = \frac{\partial^2 G}{\partial E_i \partial E_j} = \kappa_{ij},$$ electric susceptibility,

$$\frac{\partial P_i}{\partial p} = \frac{\partial^2 G}{\partial E_i \partial p} = \theta_i,$$ volume piezoelectric effect,

$$\frac{\partial P_i}{\partial T} = \frac{\partial^2 G}{\partial E_i \partial T} = \gamma_i,$$ pyroelectric effect,

$$\frac{\partial P_i}{\partial \sigma_{jk}} = \frac{\partial^2 G}{\partial E_i \partial \sigma_{jk}} = d_{ijl},$$ piezoelectric effect.

The number of non-zero components of tensors describing the physical properties of materials and the relationships between these components is determined by the symmetry of the material. It should be noted that the physical properties are described by the even-order tensors in all materials.

Since the thermodynamic potential is a function of the state then the mixed derivatives do not depend on the order of differentiation. With this condition, we get six equations – the thermodynamic identities:

$$\frac{\partial S}{\partial \sigma_{ij}} = \frac{\partial \eta_{ij}}{\partial T}, \qquad \frac{\partial S}{\partial p} = \frac{\partial V}{\partial T}, \quad \frac{\partial S}{\partial E_i} = \frac{\partial P_i}{\partial T}, \qquad \frac{\partial \eta_{ij}}{\partial p} = \frac{\partial V}{\partial \sigma_{ij}} \qquad \frac{\partial \eta_{jk}}{\partial E_i} = \frac{\partial P_i}{\partial \sigma_{jk}}$$

and $$\frac{\partial V}{\partial E_i} = \frac{\partial P_i}{\partial p}$$ **(1.78)**

Pyroelectric coefficient is equal to the coefficient describing the electrocaloric effect,

$$\gamma_i = \frac{\partial P_i}{\partial T} = \frac{\partial}{\partial T}\left(\frac{\partial G}{\partial E_i}\right) = \frac{\partial^2 G}{\partial T \partial E_i} = \frac{\partial^2 G}{\partial E_i \partial T} = -\frac{\partial S}{\partial E_i}.$$ **(1.79)**

In a similar way it can be demonstrated equality of coefficients describing the direct and inverse piezoelectric effect and the equality of coefficient of thermal expansion and the coefficient describing piezocaloric effect:

$$d_{ijk} = \frac{\partial P_i}{\partial \sigma_{ij}} = \frac{\partial \eta_{jk}}{\partial E_i} \text{ and } \alpha_{ij} = \frac{\partial \eta ij}{\partial T} = -\frac{\partial S}{\partial \sigma_{ij}}. \quad \textbf{(1.80)}$$

Thermodynamic identity plays a very important role in experimental research and technical applications of dielectrics. When setting the piezoelectric coefficients in the direct of a piezoelectric effect or pyroelectric coefficient we can calculate the deformation of material under the influence of an electric field or the value of the electrocaloric effect.

References

[1] J.F. Nye, Physical Properties of Crystals, Their Representation by Tensors and Matrics, (1957) Oxford, Claredon Press.

[2] Zagadnienia Fizyki Dielektryków, pod red. T. Krajewskiego, Wydawnictwa Komunikacji i Łączności, (1970) Warszawa.

[3] Przemiany Fazowe (red A. Graja i A.R, Ferchmin) (2003) Ośrodek Wydawnictw Naukowych w Poznaniu roku (rozdział 5 opracowany przez Antoniego Pawłowskiego).

[4] Physics of Superionics Conductors, Edited by M.B. Salamon, Springer-Verlag Berlin Heidelberg New York (1979).

[5] Physics of Solids, C.A. Wert, R.M. Thomson, McGrow–Hill Inc.(1970).

[6] A. Chełkowski, Fizyka Dielektryków, PWN (1972).

[7] Ćwiczenia Laboratoryjne z Fizyki dla Zaawansowanych, praca zbiorowa pod red. F. Kaczmarka, PWN (1982).

PIEZOELECTRICITY

2

Chapter

CONTENT

2.1. Short history of the piezoelectric effect

The direct piezoelectric effect was first observed in 1880, and was initiated by the brothers Pierre and Jacques Curie [1,2]. By combining their knowledge of pyroelectricity with their understanding of crystal structures and behavior, the Curie brothers demonstrated the first piezoelectric effect by using crystals of tourmaline, quartz, topaz, cane sugar, and Rochelle salt. Their initial demonstration showed that quartz and Rochelle salt exhibited the most piezoelectricity ability at the time.

"*We have found a new method for the development of polar electricity, consisting in subjecting them to variations in pressure along their hemihedral axes*"

J&P Curie

Working on the piezoelectric phenomena Curie Brothers reported a series of results presenting experiments that could use this effect for measuring force and high voltages [3, 4]. The most famous device was the "quartz piezoelectrique" applied to produce known electric charges for the measurement of voltages, currents, capacitances. This piezo-quartz instrument was used by Maria Curie in her work on radioactivity. The experimental device set up by Pierre and Maria Curie is shown in Fig. 2.1. A powder to be studied is spread on the lower plate of a crude ionization chamber. The charges collected on the upper plate are compensated by opposite charges obtained by progressively applying a weight to the piezoelectric quartz. The compensation is continuously controlled by the electrometer. The absolute value of the ionization current could be calculated knowing the applied weight and the time during which the compensation could be maintained. For the radium and polonium discoveries Maria Curie was awarded the Nobel Price in Chemistry in 1911 [5, 6].

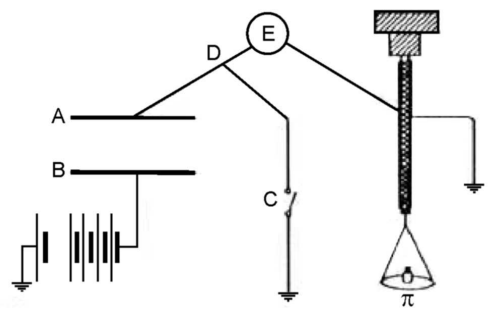

Fig. 2.1 Scheme of Pierre and Marie Curie's experimental set up (from Marie Curie's thesis) [7]. A, B ionization chamber plates, E electrometer, Q piezoelectric quartz.

The name "piezoelectric" comes from Greek (πιεζειν= *piezein* which means to squeeze or press) and means "electricity caused by pressure". This word was proposed by Wilhelm Gottlieb Hankel [8] in 1881.

A reverse piezoelectric effect is the term given to the phenomenon in which an applied electric field produces a mechanical strain in the same materials, the piezoelectric materials. The reverse piezoelectric effect was first predicted by Gabriel Lippmann, and shortly afterwards demonstrated experimentally by Jacques and Pierre Curie [9].

Just after the discovery of piezoelectricity, much more work has been done to define crystallographic principles of the effect. In 1893 Lord Kelvin made a significant contribution to piezoelectricity by presenting analogy models and laying down some of the basic framework that led to the modern theory of piezoelectricity. Examination of the impressive papers of 1892–94 of Eduard Riecke and Woldemar Voigt confirms that these scientists contributed greatly to the development of the theory of piezoelectricity. Additionally in 1910, Voigt published the first textbook on physical crystallography, in which the correct description of the piezoelectric effect in different crystallographic classes and the word 'tensor' to describe mechanical stress were given [10].

However, at that time the phenomenon of piezoelectricity was obscured because of a complicated description in crystals with low symmetry and no visible applications. Over the next few decades, piezoelectricity remained in the laboratory, something to be experimented on as more work was undertaken to explore the great potential of the piezoelectric effect. The breakout of World War I marked the introduction of the first practical application for piezoelectric devices, which was the sonar device. This initial use of piezoelectricity in sonar created intense international developmental interest in piezoelectric devices. Over the next few decades, new piezoelectric materials and new applications for those materials were explored and developed.

During World War II, research groups in the US, Russia and Japan discovered a new class of man-made materials, called ferroelectrics, which exhibited piezoelectric constants many times higher than natural piezoelectric materials. Although quartz crystals were the first commercially exploited piezoelectric material and still used in sonar detection applications, scientists kept searching for higher performance materials. This intense research resulted in the development of barium titanate and lead zirconate titanate, two materials that had very specific properties suitable for particular applications.

The reverse piezoelectric effect was used by Pound and Rebka for testing the gravitational shift predicted by Einstein [11, 12]. They used the resonant absorption without

recoil of γ quanta discovered by Mössbauer for compessation of changes in photon energy in the gravitational field of the Earth by relative movement of the radiation source γ and absorbent. For precise control of this small movement the piezoelectric transducers were used, which allowed to define changes in photon energy with an accuracy of 10^{-16}.

Another important example of scientific application of reverse piezoelectric effect is scanning tunneling microscope (STM). The operating principle of a scanning tunneling microscope (STM) is based on the so-called tunneling current, which starts to flow when a sharp tip approaches a conducting surface at a distance of approximately one nanometer. The tip is mounted on a piezoelectric tube, which allows tiny movements by applying a voltage at its electrodes. Thereby, the electronics of the STM system control the tip position in such a way that the tunneling current and, hence, the tip-surface distance is kept constant, while at the same time scanning a small area of the sample surface. This movement is recorded and can be displayed as an image of the surface topography. Gerd Binnig and Heinrich Rohrer, have been awarded the Nobel Prize in Physics 1986 for the STM construction [13, 14]. The reverse piezoelectric effect was similarly used in needle positioning in atomic force microscope (AFM) [15].

In the 20th century metal oxide-based piezoelectric ceramics and other man-made materials enabled designers to employ the piezoelectric effect and the inverse piezoelectric effect in many new applications. These materials generally are physically strong and chemically inert, and they are relatively inexpensive to manufacture. The composition, shape, and dimensions of a piezoelectric ceramic element can be tailored to meet the requirements of a specific purpose. Ceramics manufactured from formulations of lead zirconate / lead titanate exhibit greater sensitivity and higher operating temperatures, relative to ceramics of other compositions, and "PZT" materials currently are widely used piezoelectric ceramics [16].

2.2. Simple molecular model of piezoelectric effect

In Figure 2.2 simple molecular model of the piezoelectric effect is presented. It explains the generation of an electric charge as the result of a force applied on the material. Before subjecting the material to some external stress, the gravity centers of the negative and positive charges of each molecule coincide (Fig. 2.2(a)). Therefore, the external effect of the negative

and positive charges are reciprocally cancelled. As a result, an electrically neutral molecule appears. When exerting some stress on the material, its internal reticular structure can be deformed, causing the separation of the positive and negative centers of the molecules and generating little dipoles (Fig. 2.2(b)). The facing poles inside the materials are mutually cancelled and a distribution of a linked charge appear on the material's surface (Fig. 2.2(c)). That is to say, the material is polarized. This polarization generates an electric field and can be used to transform the mechanical energy used in the material's deformation into electrical energy [17].

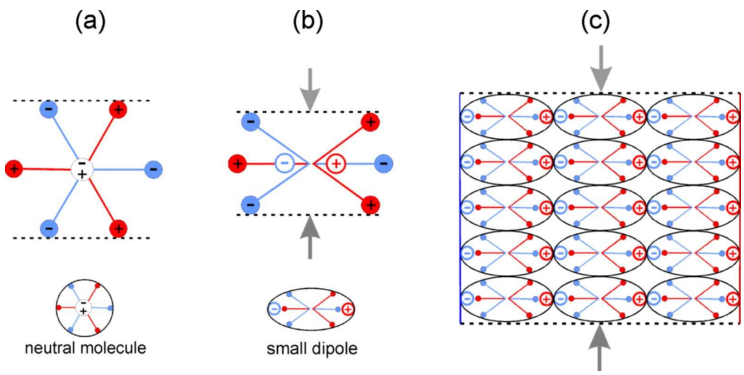

Fig. 2.2 Simple molecular model for explaining the piezoelectric effect. (a) before subjecting the material to some external stress where the centers of the negative and positive charges of each molecule coincide and the external effect of the charges are reciprocally cancelled, as a result, an electrically neutral molecule appears. (b) After exerting some pressure on the material where the internal structure is deformed and that causes the separation of the positive and negative centers of the molecules, as a result, little dipoles are generated. (c) the facing poles inside the material are mutually cancelled and the polarization generate an electric field and can be used to transform the mechanical energy of the material's deformation into electrical energy.

In Fig. 2.3 the piezoelectric material on which external stresses are applied is presented. Two electrodes are deposited on the surface where the linked charges of opposite sign appear. These electrodes are externally short circuited through a wire to galvanometer. When exerting some stresses on the piezoelectric material, a linked charge density appears on the surface of the crystal in contact with the electrodes. This polarization generates an electric field which causes the flow of the free charges existing in the conductor. Depending on their sign, the free charges will move towards the ends where the linked charges generated by the crystal's polarization is of opposite sign. This flow of free charges will remain until the free charges neutralizes the polarization effect. When the stresses on the crystal stops, the

polarization will disappear, and the flow of free charges will be reserved, coming back to the initial standstill condition.

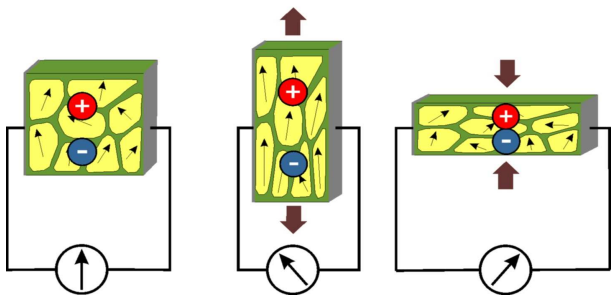

Fig. 2.3 Schematic representation of the direct piezoelectric effect.

2.3. Theory of piezoelectricity

Crystals are anisotropic materials. This means that their physical properties are different in different crystallographic directions. The exact description of the physical properties of crystals, taking into account their anisotropic character, is possible only through the vector and tensor calculi. More information considering this problem can be found in [18].

Tensor theory of piezoelectric effect

Piezoelectric properties of crystals can be described by two different linear equations defining the relationship between electrical and mechanical quantities. The direct piezoelectric phenomenon, is the ability of some materials to generate an electric field in response to applied mechanical strain. The effect is closely related to a change of polarization within the material's volume due to applied stress. The relationship between these two physical quantities, where the Einstein's summation rule for repeated indices is implied, can be represented as follows

$$P_m = d_{mij}\sigma_{ij} \qquad (m,i,j = 1,2,3) \tag{2.1}$$

where P_m means the polarization of a crystal, being a vector, is specified by three components while σ_{ij} means stress which is specified by a second-rank tensor with nine components. According to the general mathematical rule the piezoelectric modules form third-rank tensor.

In developed form, components of polarization in a direct piezoelectric phenomenon can be described as follows:

Polarization component in X_1 direction

$$P_1 = d_{111}\sigma_{11} + d_{112}\sigma_{12} + d_{113}\sigma_{13} + \\ + d_{121}\sigma_{21} + d_{122}\sigma_{22} + d_{123}\sigma_{23} + . \\ + d_{131}\sigma_{31} + d_{132}\sigma_{32} + d_{133}\sigma_{33}$$

Polarization component in X_2 direction

$$P_2 = d_{211}\sigma_{11} + d_{212}\sigma_{12} + d_{213}\sigma_{13} + \\ + d_{221}\sigma_{21} + d_{222}\sigma_{22} + d_{223}\sigma_{23} + . \\ + d_{231}\sigma_{31} + d_{232}\sigma_{32} + d_{233}\sigma_{33} \qquad \textbf{(2.2)}$$

Polarization component in X_3 direction

$$P_3 = d_{311}\sigma_{11} + d_{312}\sigma_{12} + d_{313}\sigma_{13} + \\ + d_{321}\sigma_{21} + d_{322}\sigma_{22} + d_{323}\sigma_{23} + . \\ + d_{331}\sigma_{31} + d_{332}\sigma_{32} + d_{333}\sigma_{33}$$

Stress arises from applying a force to a surface, and its units are N/m^2 (force/area). Force is a vector quantity, and hence is a first-rank tensor. But when one apply force to a surface one have to consider also the relative orientations of the force vector and the normal to the surface. This problem is illustrated in Fig. 2.4. The first index informs about the direction of the axis along which the stress is applied and the second indicates the direction of the normal of the crystal wall exposed to this stress. In the case of isotropic materials, if the force is applied normal to the surface, the result will be a compression of the crystal in the direction of the force. But if the force is applied in a direction parallel to the face of the crystal, the result is a shear of the crystal. If the direction of the force and the direction of the normal to the face the force is acting are parallel, we have a tensile stress, and if the two directions are orthogonal we have a shear stress. When a force is applied at an arbitrary direction to a surface, we have a mixture of the two types of stress, which can be obtained by separating the force vector into the components normal and parallel to the face [19].

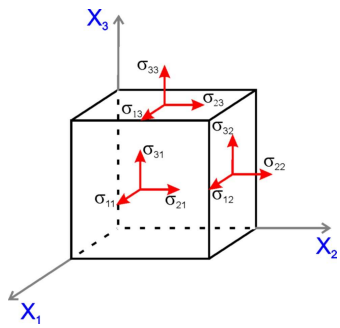

Fig. 2.4 Distribution of mechanical stress.

When mechanical stress do not cause rotations of the crystal around axis passing through its center, then the following condition $\sigma_{ij} = \sigma_{ji}$ must be fulfilled. Number of independent components of the stress tensor decrease, by 3. Therefore, for a full description of this state of stress, it is sufficient to take into consideration just six different non-zero tensor components of σ_{ij}. The symmetry of the stress tensor involves the symmetry of the piezoelectric module due to the indices *ij*. In the most general case there may be 3 components of polarization P_{m} and the 6 components of stress and therefore maximal number of independent and non-zero piezoelectric modules will be equal to 3 x 6 = 18.

Consider, for example the case where the normal stress $\sigma_{22} \neq 0$ while other tensor components $\sigma = 0$, then the direct piezoelectric effect can be described by three simple equations:

$$P_1 = d_{122}\sigma_{22}, \qquad P_2 = d_{222}\sigma_{22}, \qquad P_3 = d_{322}\sigma_{22}. \tag{3}$$

Polarization in these directions occurs only when the values of the crystal piezoelectric d_{122}, d_{222}, d_{322} modules will be different from zero. Fig. 2.5 schematically illustrates the possible directions of polarization in the crystal under non-zero mechanical stresses σ_{22}.

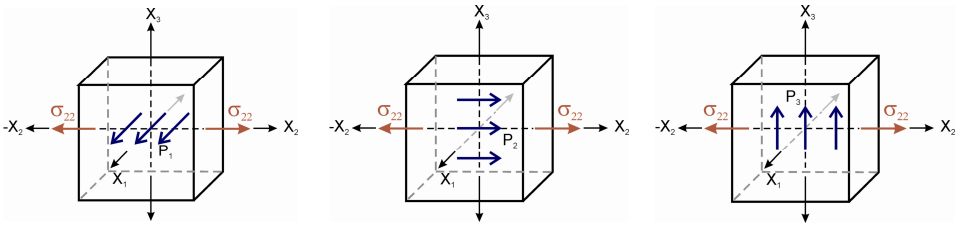

Fig. 2.5 Possible directions of polarization creation in the crystal under the mechanical stress σ_{22}.

Now consider the case when the crystal is subjected to the shear stresses $\sigma_{23} = \sigma_{32}$, and other components of stress tensor σ_{ij} are equal to zero, then following equations can be obtained:

$$\begin{aligned} P_1 &= d_{123}\sigma_{23} + d_{132}\sigma_{32} = (d_{123} + d_{132})\sigma_{23}, \\ P_2 &= d_{223}\sigma_{23} + d_{232}\sigma_{32} = (d_{223} + d_{232})\sigma_{23}, \\ P_3 &= d_{323}\sigma_{23} + d_{332}\sigma_{32} = (d_{323} + d_{332})\sigma_{23}. \end{aligned} \qquad \textbf{(2.4)}$$

In this case physical meaning can be only attributed to the sum of modules (d_{123}+d_{132}), (d_{223}+d_{232}) and (d_{323}+d_{332}). Fig. 2.6 schematically illustrates the possible direction of polarization formed in the crystal under the non-zero shear stresses $\sigma_{23} = \sigma_{32}$.

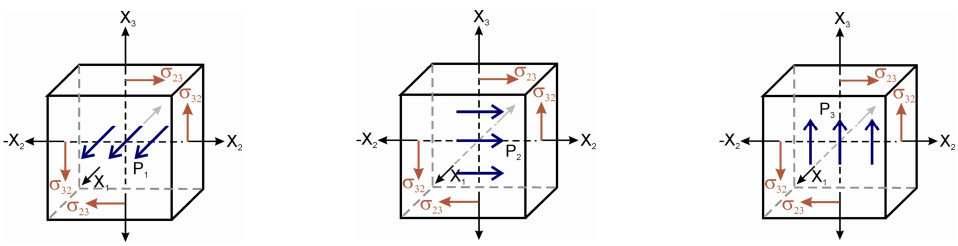

Fig. 2.6 Possible directions of polarization creation in the crystal under the shear stresses σ_{23}= σ_{32}.

Reverse piezoelectric effect relies on the change the shape of the solid by a small amount (up to a 4% change in volume) under an applied voltage:

$$\eta_{ij} = d_{mij}E_m \qquad (m,i,j = 1,2,3) \qquad \textbf{(2.5)}$$

where η_{ij} denotes the components of strain tensor, E_m – the electric field, d_{mij} – the components of piezoelectric modules. Method of determination of strain tensor components is illustrated in Fig. 2.7. Components containing the same indices determine the normal strain of the crystal in the direction of the axis of reference system. Components containing mixed

indices define the so-called proper shearing, which does not include any rotations. In this case $\eta_{ij} = \eta_{ji}$. So defined components form a symmetric strain tensor η_{ij}.

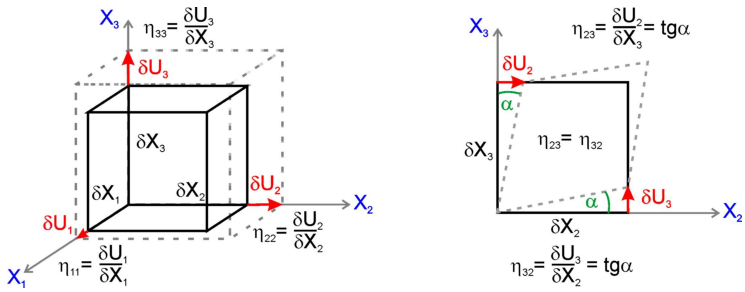

Fig. 2.7 The notation of normal and shear strains.

The developed form of reverse piezoelectric effect can be write

Direct strains

in X_1 direction $\eta_{11} = d_{111}E_1 + d_{211}E_2 + d_{311}E_3$

in X_2 direction $\eta_{22} = d_{122}E_1 + d_{222}E_2 + d_{322}E_3$

in X_3 direction $\eta_{33} = d_{133}E_1 + d_{233}E_2 + d_{333}E_3$

Shear strains

in X_1 direction $\eta_{23} = \eta_{32} = d_{123}E_1 + d_{223}E_2 + d_{323}E_3$

in X_2 direction $\eta_{13} = \eta_{31} = d_{113}E_1 + d_{213}E_2 + d_{313}E_3$

in X_3 direction $\eta_{12} = \eta_{21} = d_{112}E_1 + d_{212}E_2 + d_{312}E_3$

Matrix notation of piezoelectric effect

A general second-rank tensor used to describe the stress σ_{ij} and strain η_{ij} has $3^2 = 9$ independent components. When the components are written out explicetely they form square array where the first suffix refers to the row and second to the column. The fact that second-rank tensor is symmetrical in *i* and *j* allows to use more concise notation known as the matrix notation.

$$\begin{vmatrix} \sigma_{11} & \sigma_{12} & \sigma_{13} \\ \sigma_{21} & \sigma_{22} & \sigma_{23} \\ \sigma_{31} & \sigma_{32} & \sigma_{33} \end{vmatrix} = \begin{vmatrix} \sigma_1 & \sigma_6 & \sigma_5 \\ \sigma_6 & \sigma_2 & \sigma_4 \\ \sigma_5 & \sigma_4 & \sigma_3 \end{vmatrix} \qquad \begin{vmatrix} \eta_{11} & \eta_{12} & \eta_{13} \\ \eta_{21} & \eta_{22} & \eta_{23} \\ \eta_{31} & \eta_{32} & \eta_{33} \end{vmatrix} = \begin{vmatrix} \eta_1 & \frac{1}{2}\eta_6 & \frac{1}{2}\eta_5 \\ \frac{1}{2}\eta_6 & \eta_2 & \frac{1}{2}\eta_4 \\ \frac{1}{2}\eta_5 & \frac{1}{2}\eta_4 & \eta_3 \end{vmatrix}$$

Up to this point all the equations described piezoelectric effect have been used in full tensor notation, because only in this way their true character be displayed. But when calculating in particular problems it is advantageous to reduce the number of suffixes as much as possible. This is done by defining new symbols d_{11}, d_{12} etc. In terms of these new symbols the piezoelectric modules can be rewritten as:

$$\begin{array}{lll} d_{11} = d_{111} & d_{12} = d_{122} & d_{13} = d_{133} \\ d_{21} = d_{211} & d_{22} = d_{222} & d_{23} = d_{233} \\ d_{31} = d_{311} & d_{32} = d_{322} & d_{33} = d_{333} \end{array}$$

$$\begin{array}{lll} \frac{1}{2}d_{14} = d_{123} = d_{132} & \frac{1}{2}d_{15} = d_{113} = d_{131} & \frac{1}{2}d_{16} = d_{112} = d_{121} \\ \frac{1}{2}d_{24} = d_{223} = d_{232} & \frac{1}{2}d_{25} = d_{213} = d_{231} & \frac{1}{2}d_{26} = d_{212} = d_{221} \\ \frac{1}{2}d_{34} = d_{323} = d_{332} & \frac{1}{2}d_{35} = d_{313} = d_{331} & \frac{1}{2}d_{36} = d_{312} = d_{321} \end{array}$$

In the matrix notation the equations describe the direct and reverse piezoelectric effects take the following form:

$$P_i = d_{ij}\sigma_j \qquad \text{and} \qquad \eta_j = d_{ij}E_i \qquad (i = 1,2,3;\ \ j = 1,\ldots 6) \qquad \textbf{(2.6)}$$

The following scheme summarizes the piezoelectric equations in the matrix notation. Read horizontally by rows it gives the direct effect and read vertically by columns it gives the reverse effect.

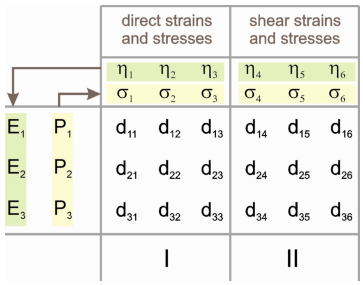

Thermodynamic description of piezoelectricity

From the thermodynamic considerations, assuming thermodynamic equilibrium in which all described physical phenomena are reversible, it follows a uniform description of all the physical properties of crystals. Properties of piezoelectric crystals in a constant temperature T = const., can easily be represented by a simple diagram shown in Fig. 2.8.

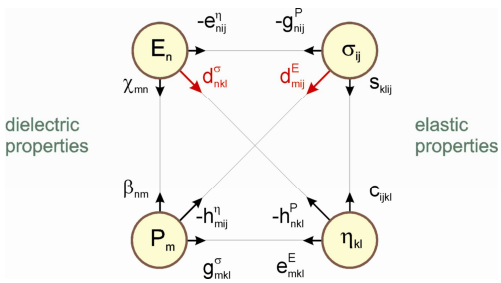

Fig. 2.8 Auxiliary diagram for the thermodynamic description of the dielectric, elastic and piezoelectric properties of the crystals.

Physical quantities appearing on the right side of this diagram describe the elastic properties of a crystal, while on the left side the dielectric one. Change of the crystal deformation causes, according to the Hook's law, changes of the stress $d\sigma_{ij} = c_{ijkl} d\eta_{kl}$, where c_{ijkl} denotes elasticity tensor. Similarly, the change of the electric field dE_n causes changes of the crystal polarization $dP_m = \varepsilon_0 \chi_{mn} dE_n$ where χ_{mn} states from a component of the electric susceptibility tensor and ε_0 is the vacuum electric permittivity. Both of these equations describe the principal phenomena occurring also in crystals, which do not exhibit piezoelectric effect. In piezoelectric crystals, with no center of symmetry, there is a mutual

coupling between all physical quantities which are located in different corners of the quadrangle shown on the diagram. Assuming that for small electric field and small mechanical stress, polarization P_m and deformation η_{kl} are linear functions of all other physical quantities E_n and σ_{ij} we obtain $P_m = P_m\left(E_n, \sigma_{ij}\right)$ and $\eta_{kl} = \eta_{kl}\left(E_n, \sigma_{ij}\right)$. Any small change of P_m and η_{kl} can be written as

$$dP_m = \left(\frac{\partial P_m}{\partial E_n}\right)_{\sigma,T} dE_n + \left(\frac{\partial P_m}{\partial \sigma_{ij}}\right)_{E,T} d\sigma_{ij} = \varepsilon_0 \chi_{mn}^{\sigma,T} dE_n + d_{mij}^{E,T} d\sigma_{ij} \tag{2.7}$$

$$d\eta_{kl} = \left(\frac{\partial \eta_{kl}}{\partial E_n}\right)_{\sigma,T} dE_n + \left(\frac{\partial \eta_{kl}}{\partial \sigma_{ij}}\right)_{E,T} d\sigma_{ij} = d_{nkl}^{\sigma,T} dE_n + s_{klij}^{E,T} d\sigma_{ij} \tag{2.8}$$

where:

$\chi_{mn}^{\sigma,T}$ - the electric susceptibility (where mechanical stress is constant),

$s_{klij}^{E,T}$ - the elastic coefficient (where electric field is constant),

$d_{mij}^{E,T}$ - the piezoelectric constant in direct effect,

$d_{nkl}^{\sigma,T}$ - the piezoelectric constant in reverse effect.

When $E = 0$ and $\sigma = 0$ it is said that the crystal is electrically and mechanically free. All coefficients should be fixed at a constant temperature T. Assuming that the initial value of electric field and stress are equal to zero, after integration of the equations (2.7) and (2.8), we obtain:

$$P_m = \varepsilon_0 \chi_{mn}^{\sigma,T} E_n + d_{mij}^{E,T} \sigma_{ij} \tag{2.9}$$

$$\eta_{kl} = d_{nkl}^{\sigma,T} E_n + s_{klij}^{E,T} \sigma_{ij} \tag{2.10}$$

The first of these equations defines a complete change of crystal polarization P_m caused by an external electric field E_n and stress σ_{ij}. The second equation determines the total deformation of the crystal η_{kl} caused by an external electric field E_n and by a stress σ_{ij}. When in the first equation $E_n = 0$ and in the second one $\sigma_{ij} = 0$ - these equations adequately describe the simple and reverse piezoelectric effects.

According to the First Thermodynamic Law the change of internal energy U per unit volume of a crystal is determined by the equation:

$$dU = \sigma_{ij} d\eta_{ij} + E_n dP_n + TdS \tag{2.11}$$

where σ_{ij}, η_{kl}, $E_n dP_n$ and TdS denote total changes of mechanical, electric and thermal energies respectively. Defining the thermodynamic potential Φ in the form

$$\Phi = U - \sigma_{ij}\eta_{ij} - E_n P_n - ST \tag{2.12}$$

after differentiating and taking into account the equations (2.11) the following formula can be obtained

$$d\Phi = -\eta_{ij} d\sigma_{ij} - P_n dE_n - SdT \tag{2.13}$$

Assuming that the thermodynamic potential is a function only of independent variables $\Phi = \Phi(\sigma_{ij}, E_n, T)$ we may write:

$$\left(\frac{\partial^2 \Phi}{\partial \sigma_{ij} \partial E_n}\right)_T = -\left(\frac{\partial \eta_{ij}}{\partial E_n}\right)_{\sigma,T} = -d_{nij}^{\sigma,T} = \left(\frac{\partial^2 \Phi}{\partial E_n \partial \sigma_{ij}}\right)_T = -\left(\frac{\partial P_n}{\partial \sigma_{ij}}\right)_{E,T} = -d_{nij}^{E,T} \tag{2.14}$$

This equation shows the mutual equivalence of the relevant modules defining the simple and reverse piezoelectric phenomena occurring in the mechanically and electrically free crystals.

2.4. Crystal symmetry and piezoelectricity

It is well known from the very beginning that the crystallographic symmetry of materials plays an important role in the piezoelectric phenomena. According to the definition of the piezoelectric effect, in crystals possessing the center of symmetry all components of the piezoelectric tensor should vanish.

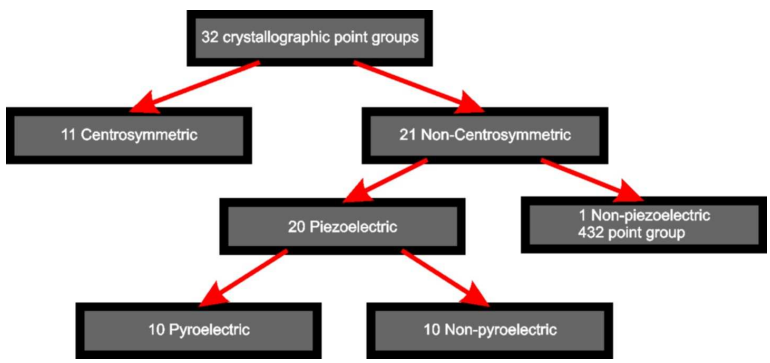

Fig. 2.9 Symmetry hierarchy for piezoelectricity.

As illustrated in Fig. 2.9 of the 32 crystallographic point groups, only 21 are noncentrosymmetric. Odd-rank tensor properties are symmetry forbidden in centrosymmetric structures. In the remaining 21 point groups, the piezoelectricity may exist, except for the cubic class 432, where the piezoelectric charges developed along the <111> polar axes cancel each other. However, the absence of piezoelectricity in this particular case does not play any significant role, because there are only few crystals that belong to this class. In this context, it should be mentioned that statistically about 30% of all materials (from about several millions known by now) are non-centrosymmetric. However, the piezoelectric properties are revealed in only few thousands of them, with about several hundreds having piezoelectric activity valuable for the applications. Therefore, it can be concluded that the absence of the center of symmetry represents the necessary but not sufficient requirement for a material to exhibit any sizeable piezoelectric effect. In Table. 2.1 the point groups that permit piezoelectricity for all crystallographic systems are listed [20].

Table. 2.1 Centrosymmetric and noncentrosymmetric point groups in crystals with different symmetries

Crystal system	Symmetry elements	Noncentro-symmetric	Centro-symmetric
Cubic	center, axis, plane	$23, \bar{4}3m, 432$	m3, m3m
Hexagonal	center, axis, plane	$6, \bar{6}, 622, 6mm, \bar{6}m2$	$6/m, 6/mmm$
Trigonal	center, axis, plane	$3, 32, 3m$	$\bar{3}, \bar{3}m$
Tetragonal	center, axis, plane	$4, \bar{4}, 422, 4mm, \bar{4}2m$	$4/m, 4/mmm$
Orthorhombic	center, axis, plane	$222, mm2$	mmm
Monoclinic	center, axis, plane	$2, m$	$2/m$
Triclinic	center	1	$\bar{1}$

The number N of independent components of a third-rank tensor, in principle, may be as large as $3^3 = 27$. The piezoelectric tensor, however, can have maximum of 18 independent components because $d_{ijk} = d_{jik}$ owing to the symmetry of the stress and strain tensors ($\sigma_{ij} = \sigma_{ji}$; $S_{ij} = S_{ji}$). The case of $N = 18$ corresponds to triclinic crystals of class 1. In crystals with higher symmetry, the number N reduces further. This feature follows from the Neumann's principle:

The symmetry elements of any physical property of a crystal must include the symmetry elements of the point group of this crystal.

Symmetry of the crystals significantly reduces the number of independent piezoelectric modules. As an example, consider the effect of the symmetry center. Suppose that we stress the crystal which possesses the symmetry center, and as a result of this we induce polarization. Then, the whole system - crystal plus stress - is transformed with the respect to the symmetry center. Stress remains unchanged, because symmetrical with the respect to the symmetry center and also the crystal will not change, while the direction of polarization will reverse. So we have to deal with the same crystal, with the same stress, but opposite polarization. Such a situation is possible only if the polarization is zero. Therefore, the crystal, which has a symmetry center, can not have piezoelectric properties [21].

Transforming the axis of the coordinate system of the piezoelectric tensor with the respect to the one of an symmetry elements, it is easy to show how the piezoelectric modules vanishes for different symmetry. Consider two simple cases:

(a) Symmetry center

Transformation matrix can be written as

$$a_{ij} = -\delta_{ij}$$
$$\delta_{ij} = \begin{cases} 1 & i = j \\ 0 & i \neq j \end{cases} \qquad \textbf{(2.15)}$$

After the transformation the piezoelectric modules will be equal to:

$$d'_{ijk} = a_{il}a_{jm}a_{kn}d_{lmn} = -\delta_{il}\delta_{jm}\delta_{kn}d_{lmn} = -d_{ijk}\,. \qquad \textbf{(2.16)}$$

But since the crystal has center of symmetry

$$d'_{ijk} = d_{ijk}\,, \qquad \textbf{(2.17)}$$

and therefore

$$d_{ijk} = 0\,. \qquad \textbf{(2.18)}$$

(b) Two-fold axis ***2***

Let us suppose that the two-fold axis is parallel to the OX_3, then the transformation leads to the following expressions

$$x_1 \to -x_1, \quad x_2 \to -x_2, \quad x_3 \to x_3, \tag{2.19}$$

or simply

$$1 \to -1, \quad 2 \to -2, \quad 3 \to 3. \tag{2.20}$$

Then each piezoelectric module is transformed according to equation (2.20). If the sign changes, the modulus must be equal to zero, if remains unchanged, the modulus does not vanish. Thus, for example, $d_{133} \to -d_{133}$ so $d_{133} = 0$, but $d_{123} \to d_{123}$ so d_{123} remaining non zero. It is easy to show that only those moduli which have a single 3 or three 3's suffixes will remain. So the non-vanishing d_{ijk} are those marked below

$$\begin{array}{ccc} d_{111} & d_{112} & \boxed{d_{113}} \\ & d_{122} & \boxed{d_{123}} \\ & & d_{133} \end{array} \qquad \begin{array}{ccc} d_{211} & d_{212} & \boxed{d_{213}} \\ & d_{222} & \boxed{d_{223}} \\ & & d_{233} \end{array} \qquad \begin{array}{ccc} \boxed{d_{311}} & \boxed{d_{312}} & d_{313} \\ & \boxed{d_{322}} & d_{323} \\ & & \boxed{d_{333}} \end{array} \tag{2.21}$$

In the matrix notation (with two indices) the corresponding moduli will take a following form

$$\begin{pmatrix} 0 & 0 & 0 & d_{14} & d_{15} & 0 \\ 0 & 0 & 0 & d_{24} & d_{25} & 0 \\ d_{31} & d_{32} & d_{33} & 0 & 0 & d_{36} \end{pmatrix} \tag{2.22}$$

In Table. 2.2 the comparison for all crystallographic classes is presented. According to the legend shown at the end of the table, small dots denote modules which are equal to zero. Bold dots indicate non-zero modules. Two lines connecting bold dots indicate that these two modules have equal numerical values. When the bold line is connected with an empty circle, it means that these two modules have the same value but an opposite signs.

Table. 2.2 Piezoelectric modules for 21 class symmetry.

CRYSTAL STRUCTURE	POINT GROUP	PIEZOELECTRIC MODULES d_{ij}	POINT GROUP	PIEZOELECTRIC MODULES d_{ij}
CUBIC	$\bar{4}3m$ 23	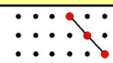		
TRIGONAL	3	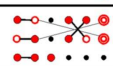	32	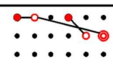
	3m	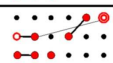		
HEXAGONAL	6	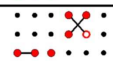	6mm	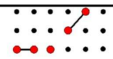
	622	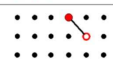	$\bar{6}$	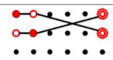
	$\bar{6}$m2	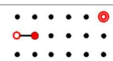		
TRICLINIC	1	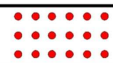		
MONOCLINIC	2	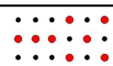	m	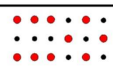
ORTHORHOMBIC	222	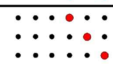	mm2	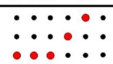
TETRAGONAL	4	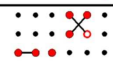	$\bar{4}$	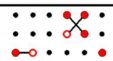
	422	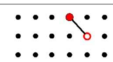	4mm	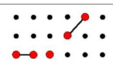
	$\bar{4}$2m	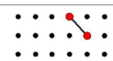		
$d_{ij}=0$ $d_{ij}\neq 0$		$d_{ij}=d_{kl}$ $d_{ij}=-d_{kl}$		$d_{ij}=-2d_{kl}$

2.5. Piezoelectric materials

Many materials exhibit the piezoelectric effect:

Naturally-occurring crystals:

- Rochelle salt ($NaKC_4H_4O_6$). Ferroelectric having a large piezoelectric effect, making it useful in sensitive acoustical and vibrational devices. The Rochelle salt crystal exhibits ferroelectricity in the temperature region between -18 and 24^oC in which the

crystal is monoclinic and outside this temperature range, the crystal presents a paraelectric phase, for which the space group is orthorhombic [22,23,24].

- Quartz. The chemical composition of quartz corresponds to nearly pure silica (~100% SiO_2). Still, the crystal structure of quartz incorporates some amount of trace elements. Al, Fe, Ga, Ge, Ti, and P in natural quartz occupy the Si position [25]. Quartz exhibits a strong piezoelectric effect perpendicularly to the prism axis [26].
- Tourmaline is a group name applied to the natural silicate minerals of the general formula $XY_3Z_6(BO_3)_3Si_6O_{18}(OH)_4$ where X can be Na or Ca; Y can be substitutions of monovalent, divalent, trivalent or quadrivalent cations (Li, Mg, Mn, Fe, Al etc.); and Z can be occupied by Al, Mg, Cr, Fe_{3+}, Fe_{2+}. Tourmaline crystal shows parallel grouping (or growth), and has a rhombohedral (trigonal) crystal structure with a space group of $R3m$ [27,28].
- Berlinite ($AlPO_4$). Aluminum orthophosphate is a rhombic crystal made of sodium phosphate and aluminum salt. In this chemical configuration, aluminum is present as three-way positively charged cation (Al_{3+}) reciprocal electrostaticaly to the phosphate anion (PO_4) [29].
- Topaz. The crystal structure is based on monolayers of oxygen anions alternating with monolayers of iron. One-third of the available octahedral sites are filled with Al and one-twelfth of the tetrahedral sites with Si. The oxygens are coordinated by one Si and two Al atoms, and the fluorine by two Al atoms [30].
- Bone: Dry bone exhibits some piezoelectric properties due to the apatite crystals, and the piezoelectric effect is generally thought to act as a biological force sensor [31, 32].

Synthesized crystals

- Gallium orthophosphate ($GaPO_4$, GP). GP is colorless crystal crystallizing in a trigonal crystal system which is similar to quartz due to the fact that the silicon atoms are alternating replaced by gallium and phosphor. The material is purely piezoelectric (no pyroelectric discharge) and has excellent high temperature properties up to 970° C, with excellent stability of many physical constants [33].

- Langasite ($La_3Ga_5SiO_{14}$, LGS). LGS is a piezoelectric material which is similar to quartz, LN ($LiNbO_3$) and LT ($LiTaO_3$) in its acoustic behavior [34].

Ceramics

An important group of piezoelectric materials are the piezoelectric ceramics. These are polycrystalline materials with the perovskite crystal structure – a tetragonal / rhombohedral structure very close to cubic. They have the general formula $A^{2+}B^{1}+O^{2-}{}_3$, in which A denotes a large divalent metal ion such as for example barium, lead or strontium, and B denotes a tetravalent metal ion such as titanium or zirconium etc. When a temperature exceeds certain value known as the Curie temperature, these crystallites exhibit simple cubic symmetry, the elementary cell of which is shown FIG. 2.10(a). This structure is centrosymmetric with positive and negative charge site coinciding, so there are no dipoles present in the materials. Below the Curie point, however, the crystallites take on tetragonal symmetry changes to one in which the positive and negative charge sites no longer coincide (FIG. 2.10(b)), so each elementary cell then has a built-in electric dipole which may be reversed, and also switched to certain allowed directions by the application of an electric field.

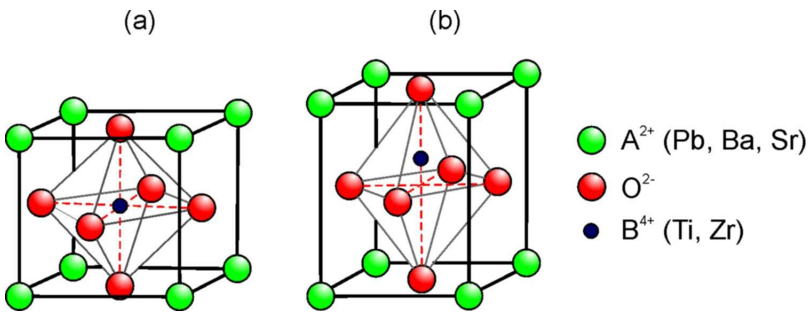

FIG. 2.10 PZT elementary cell. (a) cubic lattice (above Curie temperature); (b) tetragonal lattice (below Curie temperature).

- Lead Zirconate Titanate ($(Pb[Zr_xTi_{1-x}]O_3$ $0<x<1)$)-more commonly known as "PZT", is the most common piezoelectric ceramic in use today [35]. PZT is a binary solid solution of $PbZrO_3$ an antiferroelectric (orthorhombic structure) and $PbTiO_3$ a ferroelectric (tetragonal perovskite structure). PZT has a perovskite type structure with the Ti^{4+} and Zr^{4+} ions occupying the B site at random. At high temperatures PZT has the cubic perovskite structure which is paraelectric. On cooling below the Curie

temperature, the structure undergoes a phase transition to form a ferroelectric tetragonal or rhombohedral phase. In the tetragonal phase, the spontaneous polarization is along the <100> set of directions while in the rhombohedral phase the polarization is along the <111> set of directions [36].

- Lead Lanthanum Zirconate Titanate ($(Pb_{1-x}La_x)(Zr_{1-y}Ti_y)_{1-x/4}\ O_3\ V^B_{0.25x}\ O_3$, PLZT). This long formula assumes that La^{3+} ions go to the A site and vacancies (V^B) are created on the B site to maintain charge balance. PLZT is a transparent ferroelectric ceramic formed by doping La^{3+} ions on the A sites of lead zirconate titanate (PZT). The PLZT ceramics have the same perovskite structure as $BaTiO_3$ and PZT. The transparent nature of PLZT has led to its use in electro-optic applications. Before the development of PLZT, the electro-optic effect was seen only for single crystals [37].
- Barium Titanate ($BaTiO_3$, BT). BT was the first discovered piezoelectric ceramic. It has five phases as a solid, listing from high temperature to low temperature: hexagonal, cubic, tetragonal, orthorhombic, and rhombohedral crystal structure. All of the structures exhibit the ferroelectric effect except cubic [38]. BT has a paraelectric cubic phase above its Curie point of about 130° C. In the temperature range of 130° C to 0° C it exhibit the ferroelectric tetragonal phase. The spontaneous polarization is along one of the [001] directions in the original cubic structure. Between 0° C and -90° C, the ferroelectric orthorhombic phase occurs. On decreasing the temperature below -90° C the phase transition from the orthorhombic to ferroelectric rhombohedral phase leads to polarization along one of the [111] cubic directions [39].
- Lead Titanate ($PbTiO_3$, PT) is a well-known ferroelectric material with a perovskite structure with a high Curie temperature (490° C). On decreasing the temperature through the Curie point a phase transition from the paraelectric cubic phase to the ferroelectric tetragonal phase takes place [40].
- Lithium Niobate ($LiNbO_3$) and Tantalate ($LiTaO_3$). They have similar structure which is actually a variant of the perovskite structure with a much more restrictive arrangement. The $LiNbO_3$ and $LiTaO_3$ are ferroelectrics which are stable with very high Curie points of 1210° C and 620° C for $LiNbO_3$ and $LiTaO_3$ respectively [41].

Polymers

- Polyvinylidene fluoride (PVDF): PVDF exhibits piezoelectricity several times greater than quartz. Unlike ceramics, where the crystal structure of the material creates the piezoelectric effect, in polymers the intertwined long-chain molecules attract and repel each other when an electric field is applied [42,43].

Lead-free piezoceramics

More recently, there is growing concern regarding the toxicity in lead-containing devices driven by the result of restriction of hazardous substances directive regulations. To address this concern, there has been a resurgence in the compositional development of lead-free piezoelectric materials.

- Sodium Potassium Niobate (KNN). In 2004, Saito el al. [44] have found for the composition close to MPB, the material's properties are close to PZT ceramics, and its Curie temperature is also high. For an grain-orientated ceramics can be match to those optimum modified PZT compositions.
- Bismuth Ferrite ($BiFeO_3$ also commonly referred to as BFO). It is one of the most promising lead-free piezoelectric materials by exhibiting multiferroic properties at room temperature [45].

2.6. Equivalent circuit of piezoelectrics

The electromechanical behavior of a piezoelectric material in oscillation can be represented by an electrical equivalent circuit. The equation describing the elastic vibrations of crystal of mass m, friction coefficient $r = 2\beta$ and force constant g, occurring under the action of periodic force $F\sin(\omega t)$ in the x-axis direction has the following form

$$m\frac{d^2x}{dt^2} + 2\beta\frac{dx}{dt} + \gamma x = F_0 \sin(\omega \cdot t) \qquad \textbf{(2.23)}$$

From above equation in the case of a piezoelectric crystal, mechanical quantities may be expressed by electrical ones. Employing equation describing direct piezoelectric effect of a charge Q induced on the crystal surface during the vibration, the $Q = \alpha x$ relation may be obtain, where α is a constant dependent on elastic and piezoelectric properties of the crystal.

On the other hand equation describing the reverse piezoelectric effect yields $F = \alpha U$ relationship, where U is the voltage applied to the crystal electrodes. Substituting these results into above equation and differentiating with respect to time t the following equation can be obtained

$$\frac{m}{\alpha}\frac{d^2Q}{dt^2}+\frac{2\beta}{\alpha}\frac{dQ}{dt}+\frac{\gamma}{\alpha}Q=2U_0\sin(\omega\cdot t)\left|\frac{d}{dt}\right.,$$

$$\frac{m}{\alpha^2}\frac{d^2I}{dt^2}+\frac{2\beta}{\alpha^2}\frac{dI}{dt}+\frac{\gamma}{\alpha^2}I=\omega U_0\cos(\omega\cdot t), \qquad \textbf{(2.24)}$$

where I means current intensity. Substituting $\frac{m}{\alpha^2}=L$, $\frac{2\beta}{\alpha^2}=R$, $\frac{\gamma}{\alpha^2}=\frac{1}{C}$ we get

$$L\frac{d^2I}{dt^2}+R\frac{dI}{dt}+\frac{I}{C}=\omega U_0\cos\omega t\ . \qquad \textbf{(2.25)}$$

From the above consideration follows that the piezoelectric crystal placed in alternating electric field behaves the same way as an electrical circuit connected in series with inductance L, capacitance C and resistance R. Generally the piezoelectric crystal in alternating electric field acts behaves not only as an electromechanical transducer, but also as a capacitor of a given capacity C_0 (Fig. 2.11)

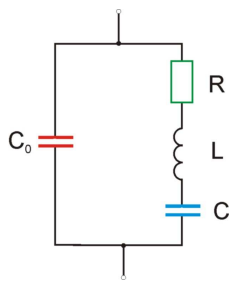

Fig. 2.11 The alternate electric circuit of oscillating piezoelectric crystal.

Left branch impedance of the equivalent circuit containing capacity C_0 of a crystal has the following form:

$$Z_L=\frac{1}{i\omega C_0} \qquad \textbf{(2.26)}$$

Right branch impedance of the equivalent circuit, containing the inductance L, the capacity C and the resistance R can be written as:

$$Z_R = R + i\omega L + \frac{1}{i\omega C}. \tag{2.27}$$

Resultant impedance of the entire circuit is equal to

$$Z_C = R_C + iX_C \tag{2.28}$$

where R_C and X_C denote resultant resistance and reactance of the entire circuit, respectively [46]. The resultant resistance has the form

$$R_C = \frac{R}{\omega^2 C_0^2 \left[R^2 + \left(\omega L - \frac{1}{\omega C} - \frac{1}{\omega C_0} \right)^2 \right]} \tag{2.29}$$

and the resultant reactance

$$X_C = -\frac{R^2 + \left(\omega L - \frac{1}{\omega C} \right)\left(\omega L - \frac{1}{\omega C} - \frac{1}{\omega C_0} \right)}{\omega C_0 \left[R^2 + \left(\omega L - \frac{1}{\omega C} - \frac{1}{\omega C_0} \right)^2 \right]} \tag{2.30}$$

For R = 0, the dependence of the reactance X_C and the admittance $Y_C = 1/X_C$ on the frequency of alternating field ω are illustrated on curves given in Fig. 2.12. From this relationship one may conclude that the equivalent circuit of the piezoelectric crystal has two different resonant frequencies at which the reactance and admittance of the circuit take their values equal to zero. These frequencies can be expressed as follows

$$X_C = 0 \quad \Rightarrow \quad \omega_r = 2\pi f_r = \sqrt{\frac{1}{LC}},$$

$$Y_C = \frac{1}{X_C} = 0 \quad \Rightarrow \quad \omega_a = 2\pi f_a = \sqrt{\frac{1}{L\frac{CC_0}{C + C_0}}}. \tag{31}$$

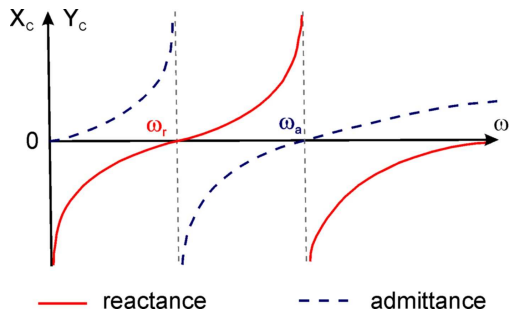

Fig. 2.12 The reactance X_c and the admittance Y_c of the equivalent circuit of piezoelectric as a function of probing frequency.

Experimentally, when piezoelectric element is exposed to an AC electric field, it will change its dimensions cyclically, with a frequency of the field. The frequency at which the ceramic element vibrates most readily, and most efficiently converts the electrical energy input into mechanical energy, is the resonance frequency. As the probing frequency is increased, the piezoelectric's oscillations first approach a frequency at which admittance is maximum (minimum impedance). This maximum admittance frequency approximates the series resonance frequency, ω_r, the frequency at which reactance in an electrical circuit describing the piezoelectric is zero, if resistance caused by mechanical losses is ignored. The minimum admittance frequency also corresponds is the resonance frequency ω_r. As the probing frequency is further increased, admittance increases and reaches zero (maximum impedance). The maximum impedance frequency approximates the parallel resonance frequency ω_a, the frequency at which reactance in the equivalent electrical circuit is infinite if resistance caused by mechanical losses is ignored. The maximum reactance frequency is called the anti-resonance frequency. The composition of the ceramic material and the shape and volume of the element determine the resonance frequency - generally, a thicker element has a lower resonance frequency than a thinner element of the same shape.

2.7. Experimental investigations of piezoelectric effects

Methods for measurements of the piezoelectric properties of materials can be divided into static, quasistatic and dynamic.

Static methods rely on direct measurement of the charges induced on the surfaces of piezoelectric crystals under the influence of external mechanical stress or on the measurement of the crystal strains under the influence of external electric field.

Quasistatic methods rely on measurement of deformation of the crystal under the influence of periodically alternating electric field (reverse piezoelectric phenomenon), or on the measurement of the charges generated on the crystal surface under the influence of variable mechanical stress (direct piezoelectric effect) of much smaller frequency than the resonant frequency.

Dynamic methods rely on measurement of the resonance frequency and antiresonance eigenvibrations of plates cut out of piezoelectric materials (crystals, ceramics or film) and setting the parameters of alternative electrical circuits of the samples.

The idea of measurements of direct piezoelectric phenomena is presented in Fig. 2.13. The methods rely on a placement of the piezoelectric crystal between two electrodes which are connected with the electrometer. A reference capacitor with known capacity C_0 is connected parallel to the crystal. All elements of the system, including the sample, have capacity C_u. In case of the reference capacitor absence under an influence of the external force, the electric charges q_1 are induced on the crystal surface (with area of S). This results that the system capacitance C_u is charged to potential U_1. In the case of the parallel connection of capacity C_0, to potential U_2. So it can be written as:

$$q_1 = C_u \cdot U_1 = (C_u + C_0) \cdot U_2 = d_{11} \cdot F_1 . \tag{2.32}$$

It follows that a capacity of the measured system C_u is

$$C_u = \frac{C_0 U_2}{U_1 - U_2} . \tag{2.33}$$

Then piezoelectric module d_{11} equals to

$$d_{11} = \frac{q_1}{F_1} = \frac{\frac{q_1}{S}}{\frac{F_1}{S}} = \frac{P_1}{\sigma_1} = \frac{C_0}{F_1} \cdot \frac{U_1 \cdot U_1}{U_1 - U_2} . \tag{2.34}$$

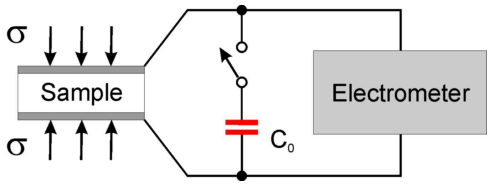

Fig. 2.13 Measurement scheme of the direct piezoelectric phenomena

Simple setup based on this method is presented in Fig. 2.14. The weight is placed on the lever arm in a known unilateral distance from the axis of rotation. Shoulder through the rod presses on a sample and generates electric charges on its surface Q. These charges are accumulated on the capacitance C_p of the sample. By measuring the voltage U on the sample and knowing its capacity, we may calculate the electric charge Q generated by applying known stress σ to the sample.

The charge Q induced on the surfaces of the sample is determined by the equation:

$$Q = Sd\sigma \,. \tag{2.35}$$

This charge may be calculated from the formula:

$$Q = UC_p \tag{2.36}$$

where C_p means electric capacity of the sample.

Mechanical stress σ applied to the sample can be determined from the formula:

$$\sigma = \frac{F}{S'} \tag{2.37}$$

F is the force with which the rod is pushing for the sample while S' is its area subjected to the action of this force. It should be noted that the surface S and S' are equal only when we examine the longitudinal piezoelectric effect (electrodes are put down on the surface exposed to stress). The force in gravitational field can be expressed

$$F = \frac{Mgr}{R} \tag{2.38}$$

where M denotes the mass of the weight, g – gravity constant, r – distance between weight and the axis of rotation, R – distance between pressing pin and the axis of rotations. Using the above equations it can be easily shown that for longitudinal piezoelectric phenomenon:

$$U = \frac{d}{C_p}F = \frac{dMg}{C_pR}r \tag{2.39}$$

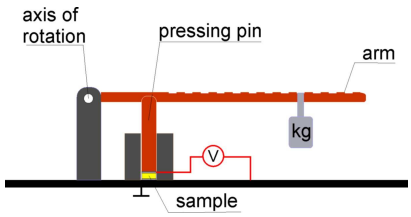

Fig. 2.14 Setup for measurement of direct piezoelectric effect.

It is worth noticing that using the formula (2.36), we disregard the losses of a charge and the input resistance of the voltmeter (assuming that the time constant of the system is much greater than the time of measurement). To increase the time constant of the sample an additional capacitor with a known capacity C_d in parallel should be added. In this case the capacity C_p in equation (2.30) should be replaced by the sum of the capacity of a sample C_p and additional capacity C_d.

Simple setup of reverse piezoelectric effect investigations is presented in Fig. 2.15. The experimental method is based on Caspari and Merz method [47] and rely on a capacity measurements of a parallel capacitor. On the measured sample stays a "finger" to which the bottom of air capacitor is attached. The second plate of this capacitor is mounted to the micrometric screw allowing to precisely control a distance between their plates and this way a sensitivity of the deformation measurements.

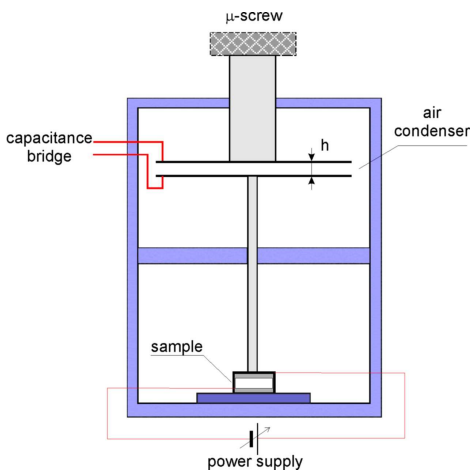

Fig. 2.15 Simple setup for reverse piezoelectric effect measurements.

The density of surface charge in this capacitor is given by:

$$\sigma = \frac{Q}{S} = \frac{dQ}{dS}. \tag{2.40}$$

The capacity of parallel capacitor obtained from the Gauss law can be written as:

$$C = \iint_S \frac{\varepsilon_0}{d} dS = \frac{\varepsilon_0 S}{d}. \tag{2.41}$$

Relative deformation of reverse piezoelectric effect is given by

$$\eta = \frac{\Delta h}{L} = d \cdot E = d \cdot \frac{U}{L'} \tag{2.42}$$

where L – the length of sample, U – the applied voltage, and L' – the distance between the electrodes of the sample.

For longitudinal piezoelectric effect $L=L$' and equation can be written down as follows

$$\Delta h = d \cdot U. \tag{2.43}$$

By applying electric field we cause change in dimensions Δh. This will in turn cause change in capacity given by equation

$$\Delta C = \frac{\varepsilon_0 \cdot S}{h_0} - \frac{\varepsilon_0 \cdot S}{h_1} \tag{2.44}$$

where ε_0 is the permittivity of a vacuum, S is the area of electrodes and h_0 and h_1 are distance between capacitor electrodes before and after we apply the electric field.

Thus the piezoelectric module d and the deformation Δh of the sample can be calculated from the following equation

$$\Delta h = \eta \cdot h = d \cdot E \cdot h = \varepsilon_0 S \left(\frac{1}{C_2} - \frac{1}{C_1} \right). \tag{2.45}$$

Knowing the area of electrodes S and capacities C_0 and C_1 we may obtain h_1 , h_0 and Δh (Fig. 2.16). Now if we consider Δh vs. U we can use a linker regression method to obtain the piezoelectric modulus d. During measurements it is necessary to take into account the capacity of wires and dispersed capacities. Sum of these capacities can be obtained through measuring capacity of system in the function of electrode separation. To change distance between electrodes we use a micrometer screw. High precision of manufacturing slides and high parallelism of plates is crucial for correct functioning of this setup. It is worth pointing out that if the distance between electrodes is few tenths of millimeter and we use cheap and

simple capacitance meter we can obtain resolution of order 10^{-6} 10^{-8} m. And if we use precise dilatometer and high resolution bridge we can obtain even higher precisions up to 10^{-12} m – which is less than diameter of an atom.

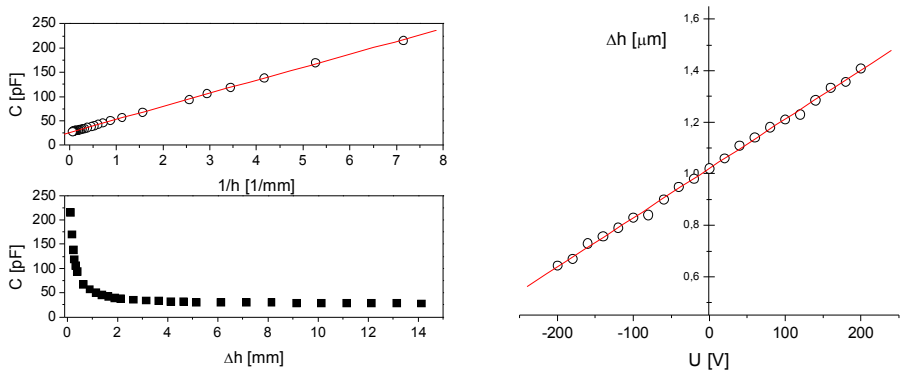

Fig. 2.16 The results of reverse piezoelectric effect measurements using capacitance method.

2.8. Applications

The first application of piezoelectric power was a piezoelectric transducer. The piezoelectric transducer uses a piezoelectric ceramics to convert vibration to electrical signals and vice versa. Other uses of piezoelectric power is your everyday electric cigarette lighter. This same mechanical construction can also be found in gas grill lighter or stove sparkler which uses built in igniters incorporating piezoelectric materials. Another useful everyday example is your car's air bag. The piezoelectric sensors detect the amount of shock and sends an electrical signal to activate the air bag. The application of piezoelectric power to ultrasonic scaler allows for a more effective cost and efficiency. Piezoelectric transducers are capable of extended use without overheating and have a higher temperature of the Curie point than magnetostrictive transducers. The piezoelectric transducer converts the ultrasonic electrical signal into ultrasonic vibration and then applied to the scaler. There are dozens of application for piezoelectricity. The piezoelectric pick-up in your acoustic guitar is one of them, your microphones, in medical imaging devices, loudspeakers, diesel engines. Ink jet printers use piezoelectric power to push the ink to paper from the ink jet print head. The quartz clock was one of the first application of piezoelectricity with a quartz tuning fork create a series of

electrical pulses. Radio transmitters uses the same exact technique as with radio receivers. Auto focus cameras uses piezoelectric motors. Piezoelectricity is being researched and in continued development finding new and better ways to improve and discover many more new and exciting application.

[1] J. Curie, P. Curie, *Développement, par pression, de l'électricité polaire dans les cristaux hémièdres à faces inclinées*, Comptes Rendus de l'Académie des Sciences, 91 (1880) 294–5.

[2] J. Curie, P. Curie, *Sur l'électricité polaire dans les cristaux hémièdres à faces inclinées*, C. R. Acad. Sci. Gen., 91 (1880) 383–6.

[3] J. Curie and P. Curie, *Lois de degagement d'èlectricitè dans la turmaline*, C. R. Acad. Sc. Paris, **92** (1881) 186.

[4] J. Curie and P. Curie, Sur les phenomenes *èlectriques de la tourmaline et des critaux hèmièdres a faces inclinèes*, C. R. Acad. Sci. Gen., **92** (1881) 350.

[5] P. Curie, M. Curie, *Sur une substance nouvelle radio-active, contenue dans la pechblende*, C. R. Acad. Sci. **127** (1898) 175-178.

[6] P. Curie, M. Curie, G. Bemont, *Sur une nouvelle substance fortement radio-active contenue dans la pechblende (manuscrit de cette note)*, C. R. Acad. Sci. 127 (1898) 1215-1217.

[7] M. Sklodowska - Curie (doctoral thesis), *Recherches sur les substances radioactives*, Paris 1903.

[8] W. G. Hankel, Abh. Sächs., **12** (1881) 457.

[9] M. G. Lippmann, *Principe de la conservation de l'électricité*, Ann. Chimie et Phys., **24** (1881) 145.

[10] M. Trainer, *Kelvin and piezoelectricity*, Eur. J. Phys. 24 (2003) 535.

[11] R. V. Pound, G. A. Rebka Jr., *Gravitational Red-Shift in Nuclear Resonance*, Phys. Rev. Lett., **3** (1959) 439–441.

[12] R. V. Pound and G. A. Rebka, Jr., *Apparent Weight of Photons*, Phys. Rev. Lett. 4, (1960) 337–341.

[13] G. Binnig, H. Rohrer, *Scanning tunneling microscopy*, IBM J. Research and Development, **30** (1986) 355-369.

[14] G. Binnig, H. Rohrer, *In touch with atoms*, Rev. Mod. Phys. 71, (1999) S324–S330.

[15] G. Binning, C. F. Quate, Ch. Gerber, *Atomic force microscope,* Phys. Rev. Lett., 56 (1986) 930.

[16] J. N. Lalena, *From quartz to quasicrystals: probing nature's geometric patterns in crystalline substances*, Cryst. Rev. 12 (2006) 125 — 180.

[17] A. Arnau, *Piezoelectric transducers and applications*, Springer-Verlag, (2008) Berlin-Heidelberg.

[18] J. F. Nye, *Physical Properties of Crystals- their representation by tensors and matrices* – (1985) Oxford.

[19] M. T. Dove, *Structure and dynamics: an atomic view of materials*, (2003) Oxford University Press.

[20] A. Safari and E. K. Akdogan, *Piezoelectric and acoustic materials for transducer applications*, Springer Science+Business Media, (2008) New York.

[21] A. von Hippel, *Piezoelectricity, Ferroelectricity and Crystal Structure*, Z. Physik, 133 (1952) 158.

[22] J. Valasek, *Properties of Rochelle Salt Related to the Piezo-electric Effect*, Phys. Rev. **20** (1922) 639–664.

[23] C. I. Vigness, *Inverse Piezoelectric Properties of Rochelle Salt*, Phys. Rev. **46** (1934) 255–257.

[24] A. O. dos Santos, L. P. Cardoso, J. M. Sasaki, M. A. R. Miranda, F. E.A. Melo, *X-ray multiple diffraction as a probe to determine all the piezoelectric coefficients of a crystal: Rochelle salt case*, J. Phys.: Condens. Matter **15** (2003) 7835–7842.

[25] L. W. McKeehan, *The Crystal Structure of Quartz*, Phys. Rev. 21, (1923) 503–508.

[26] L. H. Dawson, *Piezoelectricity of Crystal Quartz*, Phys. Rev. **29** (1927) 532–541.

[27] G. W. Fox, G. A. Fink, *The Piezoelectric Properties of Quartz and Tourmaline*, Physics **5**, (1934) 302-307.

[28] W. A. Deer, R. A. Howie, J. Zussman, "*Rock-Forming Minerals*." Vol. 1B: Disilicates and Ring Silicates. 2nd edition. London, (1986) Longman Group Ltd.

[29] D. Schwarzenbach, *Verfeinerung der Struktur der Tiefquarz-Modifikation von $AlPO_4$*, Zeitschrift fur Kristallographie, **123** (1966) 161-185.

[30] P. H. Ribbe, G. V. Gibbs, *The crystal structure of topaz and its relation to physical properties*, The American Mineralogist, **56** (1971) 24-30.

[31] E. Fukada and I. Yasuda, *On the piezoelectric effect of bone*, J. Phys. Soc. Japan, **12 (**1957**)** 1158-1162.

[32] S. R. Pollack,E. Korostoff, W. Starkebaum, W. Lannicone*, Micro-electrical studies of stress-generated potentials in bone. in Electrical Properties of Bone and Cartilage*, (Edit. Brighton, C.T., Black, J. & Pollack, S.R.), Grune & Stratton, Inc., (1979) New York.

[33] P. Krempl, G. Schleinzer, W. Wallno¨fer, *Gallium phosphate, $GaPO_4$: a new piezoelectric crystal material for high-temperature sensorics*, Sensors and Actuators A: Physical, **61** (1997) 361-363.

[34] Il Hyoung Jung, Keun Ho Auh, *Crystal growth and piezoelectric properties of langasite ($La_3Ga_5SiO_{14}$) crystals*, Materials Letters, **41** (1999) 241-246.

[35] A. E. Crawford, *Lead zirconate-titanate piezoelectric ceramics*, Br. J. Appl. Phys. **12** (1961) 529-534.

[36] D. Berlincourt, *Piezoelectric Ceramics: Characteristics and Applications*, J. Acoust. Soc. Am., **70** (1981) 1586–1595.

[37] H. Shigeki, A. Takayuki, H. Masaya, N. Hiroshi, K. Ichizo, O. Masaru, *Effect of Substrate Temperature on Electrical Characteristics of (Pb, La)(Zr, Ti)O_3 Ultrathin Films Deposited by Metalorganic Chemical Vapor Deposition*, Jpn. J. Appl. Phys. **34** (1995) 5086-5090.

[38] S. Roberts, *Dielectric and Piezoelectric Properties of Barium Titanate*, Phys. Rev. **71** (1947) 890-895.

[39] Y. Xu, *Ferroelectric Materials and their Applications*, North Holland, (1991) Amsterdam.

[40] Sandford S. Cole, H. Espenschied, *Lead Titanate: Crystal Structure, Temperature of Formation, and Specific Gravity Data*, J. Phys. Chem., **41** (1937) pp 445–451.

[41] T. Volk, M. Wohlecke, *Lithium Niobate: Defects, Photorefraction and Ferroelectric Switching*. (2008) Springer pp. 1–9.

[42] H. Kawai, *The piezoelectricity of Poly (vinylidene Fluoride)*, Jpn. J. Appl. Phys. **8** (1969) 975-976.

[43] A. Vinogradov, M. Schwartz, "*Piezoelectricity in Polymers*", Encyclopedia of Smart Materials, Volumes 1-2, John Wiley & Sons (2002) 780-792.

[44] Y. Saito, H. Takao, T. Tani, T. Nonoyama, K. Takatori, T. Homma, T. Nagaya and M. Nakamura, *Lead-free piezoceramics***,** Nature **432** (2004) 81-87.

[45] J. Wang, J. B. Neaton, H. Zheng, V. Nagarajan, S. B. Ogale, B. Liu, D. Viehland, V. Vaithyanathan, D. G. Schlom, U. V. Waghmare, N. A. Spaldin, K. M. Rabe, M. Wuttig, R. Ramesh, *Epitaxial $BiFeO_3$ Multiferroic Thin Film Heterostructures*, *Science* **299**, (2003) 1719 – 1722.

[46] T. Krajewski (red), *Zagadnienia fizyki dielektryków*, WKiŁ, (1970) Warszawa.

[47] M. E. Caspari and W. J. Merz, *The Electromechanical Behavior of $BaTiO_3$ Single-Domain Crystals*, Phys. Rev., 80 (1950) 1082-1089.

PYROELECTRICITY

Chapter 3

CONTENT

3.1. Brief history of the pyroelectric effect

Pyroelectricity as a phenomenon has been known for 24 centuries - the Greek philosopher Theophrastus probably wrote the earliest known account. He described a stone, called *lyngourion* in Greek or *lyncurium* in Latin, that had the property of attracting straws and bits of wood. Those attractions were no doubt the effects of electrostatic charges produced by temperature changes most probably in the mineral tourmaline. Theophrastus and other writers of the two millennia that followed were far more interested in the origin of the stone and its possible therapeutic properties than they were in physical explanations. Theophrastus proposed that lyngourion was formed from the urine of a wild animal [1].

Two thousand years after Theophrastus, tourmaline's unusual physical properties were reintroduced to Europe through the book entitled "Curious Speculations During Sleepless Nights. It author Johann Georg Schmidt wrote a series of 48 dialogs, one of which contained a section describing hard and glassy bodies that were not magnetic. He described the experiences of Dutch gem cutters when they tested the durability of tourmaline in a fire:

> "*The ingenious Dr. Daumius, chief physician to the Polish and Saxon troops on the Rhine, told me that, in the year 1703, the Dutch first brought from Ceylon in the East Indies a precious stone called tourmaline, turmale, or trip, which had the property of not only attracting the ashes from the warm or burning coals, as the magnet does iron, but also repelling them again*."

In 1717 chemist and physician Louis Lemery wrote the first scientific paper of pyroelectricity in a journal. The naturalist Carl von Linné (Linnaeus) was the first to relate the pyroelectric property of tourmaline to electricity; he called the mineral *lapis electricus* – an electric stone [2]. Experiments on tourmaline during the 18th century performed by Franz Ulrich Theodor Aepinus, Johann Karl Wilcke, Benjamin Wilson, Joseph Priestley, John Canton, and Torben Bergman made major contributions to the rapidly developing field of electrostatics [3]. In 1824 David Brewster, was the first author to use the term "pyroelectricity" [4]. One of the materials he studied was a "tartrate of soda and potash" - Rochelle salt. John Mothée Gaugain made the first precise measurements of pyroelectric charges in 1859 [5]. He reached some important conclusions: The total quantity of electricity produced by a crystal of tourmaline depends uniquely upon the limits within which its temperature is varied; within those limits, the amount of electricity produced during heating is the same as that produced during cooling, but with the signs of the charges reversed; and the amount of charge produced is proportional to the crosssectional area of the crystal and is independent of its length. William Thomson (Lord Kelvin) published the first major theoretical treatment of pyroelectricity in 1878; his paper included the electrocaloric effect prediction [6]. Jacques and Pierre Curie proposed that the electrical effects due to nonuniform heating of quartz crystals might have been caused by pressure, a speculation that led to their 1880 discovery of piezoelectricity. W. Voigt established an outstanding school of crystallography, thermodynamics and crystal physics [7]. During the latter part of the 19th century and the early decades of the 20th century, seven Nobel laureates - Wilhelm Röntgen,

Pierre Curie, Gabriel Lippman, Heike Kammerlingh Onnes, Erwin Schrödinger, Archer J. P. Martin, and Max Born - published papers on pyroelectricity. In 1938 Yeou Ta published a paper that initiated the great growth that continues in the field today [8]. In the paper for the first time it was proposed that tourmaline crystals could be used as IR sensors in spectroscopy. Some research was conducted on pyroelectric IR detectors during and immediately after World War II in the UK, US, and Germany, but the results appeared only in classified documents. In 1962 J. Cooper made the first detailed analysis of the behavior of fast IR detector using $BaTiO_3$ [9]. In the same year, he proposed the use of pyroelectric devices for measuring temperature changes as small as 0.2μK [10]. In 1969, Le Carvennec proposed the use of pyroelectric elements for thermal imaging [11]. Pyroelectric devices have been also used for applications in space for example in Net-flux Radiometer contained in the Galileo Probe [12].

3.2. Definitions

Pyroelectricity is the property presented by certain materials that exhibit an electric polarization ΔP when a temperature variation ΔT is applied uniformly:

$$\Delta P = \gamma \cdot \Delta T \tag{3.1}$$

where γ is the pyroelectric coefficient at constant stress. Pyroelectric crystals actually have a spontaneous polarization, but the pyroelectric effect can only be observed during a temperature change.

Pyroelectric coefficient can be expressed as:

$$\gamma = \frac{\partial P_S}{\partial T} \tag{3.2}$$

where: P_S – the spontaneous polarization.

The unit of pyroelectric coefficient is $\left[\frac{C}{m^2 \cdot K}\right]$.

If a pyroelectric crystal with an intrinsic dipole moment (top) is fashioned into a circuit with electrodes attached on each surface (Fig. 3.1), an increase in the temperature T prompts the spontaneous polarization P_S to decrease as the dipole moments, on average, diminish in magnitude. The horizontal tilting of the dipoles, (pictured at bottom of Fig. 3.1),

signifies the effect. A current flows to compensate for the change in bound charge that accumulates on the crystal edges.

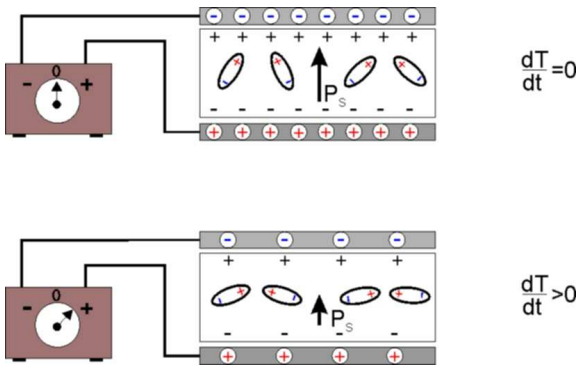

Fig. 3.1 Schematic drawing showing the origin of the pyroelectric current.

Another definition of pyroelectricity is an ability to generate induced charges on the crystal surface when they are heated or cooled. It is explained as a migration of positive and negative charges (and therefore establishment of electric polarization) to opposite ends of a crystal's polar axis as a result of a change in the temperature. This can be expressed as follows:

$$\Delta Q = \gamma \cdot S \Delta T \tag{3.3}$$

where:

ΔQ – the charges generated on the crystal surface,

S – the surface of the crystal.

The relation between generated charges and polarization is:

$$Q = \Delta P \cdot S\,. \tag{3.4}$$

The unit of the polarization is $\left[\frac{C}{m^2}\right]$.

For detailed description of pyroelectric effect the dimensional analysis of used physical quantities is required. So, if there is a small temperature change ΔT (scalar), uniform over the crystal, the change in the polarization in the vector ΔP_i is given by

$$\Delta P_i = \gamma_i \cdot \Delta T \tag{3.5}$$

where the γ_i are the three pyroelectric coefficients (i = 1, 2, 3). The pyroelectric effect in a crystals is thus specified by the vector $\vec{\gamma}$.

Pyroelectricity can be visualized as one side of a triangle, where each corner represents kinetic, electrical, and thermal energy states in the crystal (Fig. 3.2). The lines joining pairs of circles signify that a small change in one of the variables produces a corresponding change in the other. The three short bold lines that connect pairs of thermal, elastic, and electric variables define the physical properties of a heat capacity, elasticity, and electrical permittivity, respectively. As an example, a small increase in the temperature T produces an increase in an entropy S proportional to the heat capacity divided by temperature. The diagram also illustrates coupled effects, denoted by lines joining pairs of circles at different corners of the diagram. The diagram's colored lines indicate that the two contributions make up pyroelectric effect. In the first, the crystal is rigidly clamped under constant strain S, to prevent expansion or contraction. A change in the temperature causes a change in electric displacement as shown by the green line, which signifies the primary pyroelectric effect. The second contribution - the secondary pyroelectric effect - is a result of crystal deformation: Thermal expansion causes a strain that alters the electric displacement via a piezoelectric process, as shown by the dashed red lines. Measuring the primary effect directly is extremely difficult. But the secondary effect can be readily calculated from the values of the thermal expansion coefficient, the elastic stiffness, and the piezoelectric strain constant. So experimentally, the pyroelectric effect under the constraint of constant stress-the so-called total effect, the sum of red and green lines is what is usually measured [3].

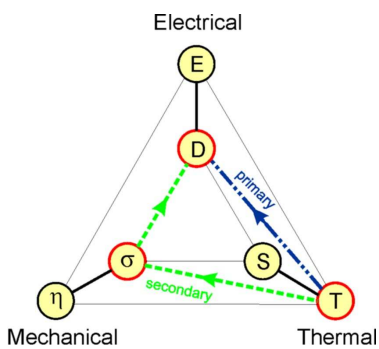

Fig. 3.2 The triangular diagram illustrating the thermodynamically reversible interactions that may occur among the thermal, mechanical, and electrical properties of a crystal.

3.3. Simple model of the pyroelectric effect

In the microscopic scale, the pyroelectric effect occurs because of the asymmetric interaction potential caused by electrically charged atoms within the crystal structure of the material. Schematically it may be presented as in Fig. 3.3. In the two-dimensional lattice of cations and anions, the cations are displaced relative to the unit cells "centre" to giving rise to an electrical dipole moment (or spontaneous polarization P_S) along the ($x_1 - x_2$) line.

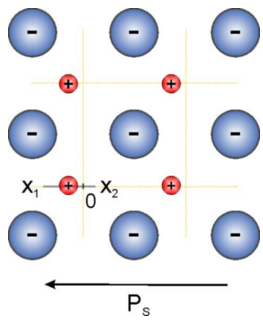

Fig. 3.3 Schematic two-dimensional presentation of pyroelectricity.

The potential energy of any cation along this line will have an asymmetric form as illustrated in Fig. 3.4. Any excitation caused by an increase in lattice temperature, will change its quantised energy level (E_1 to E_n) within the well leading to a change in its mean equilibrium position in the lattice (along the line A-B in Fig. 3.4). This gives a change in the overall electrical dipole moment, which appears as the macroscopic pyroelectric effect [13].

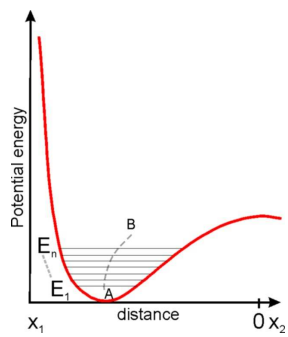

Fig. 3.4 Potential energy of cation in lattice of Fig. 3.3 along the line x_1-x_2, E_1 to E_n represent the quantised energy levels for the cation and the locus A-B is the change in its equilibrium position with change in energy [13].

In dielectrics exhibiting pyroelectricity the dipole moment can arise as a consequence of the packing in an ionic crystal, because of the alignment of polarized covalent bonds in molecular crystals or crystalline polymers or because of atomic displacements controlled by the position of hydrogen ions in a hydrogen bonded crystal [13].

3.4. Thermodynamic description of pyroelectricity

Polarization of the crystal is a function of the temperature, the deformation η_{ij} and the electric field E_i:

$$P_k = P_k\left(T, \eta_{ij}, E_i\right) \tag{3.6}$$

On the other hand deformation depends on the temperature, the mechanical stresses and the electric field

$$\eta_{ij} = \eta_{ij}\left(T, \sigma_{lm}, E_i\right) \tag{3.7}$$

If the intensity of electric field equals to zero $E_i = 0$, then changes of the polarization and the deformation can be written as follows:

$$dP_k = \left(\frac{\partial P_k}{\partial T}\right)_{\eta_{ij}} dT + \left(\frac{\partial P_k}{\partial \eta_{ij}}\right)_T d\eta_{ij}, \tag{3.8}$$

$$d\eta_{ij} = \left(\frac{\partial \eta_{ij}}{\partial T}\right)_{\sigma_{lm}} dT + \left(\frac{\partial \eta_{ij}}{\partial \sigma_{lm}}\right)_T d\sigma_{lm}. \tag{3.9}$$

Assuming that in whole crystal the stresses are uniform $\sigma_{lm} = \text{const}$, from equations (8) and (9) the total pyroelectric effect can be written as:

$$\left(\frac{\partial P_k}{\partial T}\right)_{\sigma_{lm}} = \left(\frac{\partial P_k}{\partial T}\right)_{\eta_{ij}} + \left(\frac{\partial P_k}{\partial \sigma_{lm}}\right)_{\eta_{ij}} \cdot \left(\frac{\partial \sigma_{lm}}{\partial \eta_{ij}}\right)_T \cdot \left(\frac{\partial \eta_{ij}}{\partial T}\right)_{\sigma_{lm}} \tag{3.10}$$

where:

$\left(\frac{\partial P_k}{\partial T}\right)_{\sigma_{lm}} = \gamma_k^{\sigma}$ - the total pyroelectric coefficient,

$\left(\frac{\partial P_k}{\partial T}\right)_{\eta_{ij}} = \gamma_k^{\eta}$ - the primary pyroelectric coefficient,

$\left(\frac{\partial P_k}{\partial \sigma_{lm}}\right)_{\eta_{ij}} = d^{\eta}_{klm}$ - the piezoelectric moduli,

$\left(\frac{\partial \sigma_{lm}}{\partial \eta_{ij}}\right)_{T} = C^{T}_{lmij}$ - the elastic compliance coefficients,

$\left(\frac{\partial \eta_{ij}}{\partial T}\right)_{\sigma_{lm}} = \alpha^{\sigma}_{ij}$ - the coefficients of thermal expansion.

Hence for a free crystal the total pyroelectric effect in equation (10) can be rewritten as:

$$\gamma^{\sigma}_{k} = \gamma^{\eta}_{k} + d^{\eta}_{klm} \cdot C^{T}_{lmij} \cdot \alpha^{\sigma}_{ij} \qquad \textbf{(3.11)}$$

Distinctly the secondary pyroelectric coefficient is given by the product of d^{η}_{klm}, C^{T}_{lmij} and α^{σ}_{ij}. Though secondary pyroelectricity is due to piezoelectricity, only those piezoelectric crystals which belong to the ten polar classes are permitted by crystal symmetry to exhibit secondary pyroelectricity.

3.5. Theory of pyroelectricity

The first quantum theory of primary pyroelectric effect for the case of ionic crystals was formulated by Max Born in the year 1945 [14]. In his paper, Born had indicated that primary pyroelectric coefficient would be proportional to the temperature *T*. However in his later treatise on lattice dynamics he predicted the T^3 law for the pyroelectric coefficient [15]. Successively the physicists in their papers have proved clearly many interesting features of the theory, especially the role of mechanical and electrical anharmonicity in primary pyroelectricity which in fact was not noticed by Born [16, 17, 18].

In principle, in order to understand pyroelectricity in any material, one has to consider the various mechanisms of the spontaneous polarization (such as ionic, electronic, orientational or surface charge) and study their variation with temperature. Generally in dielectrics, both the electronic polarization and the ionic polarization are mainly due to the elastic displacement of electron clouds and lattice vibrations within the atoms or molecules. Their interaction is an intramolecular phenomenon, and restoring force against the displacement is relatively insensitive to temperature, so electronic and ionic polarization processes are only slightly dependent on temperature. However, orientational polarization is a rotational process, which

includes not only the thermal stimulation, but also mechanical friction processes. The rotation of a dipole in a material is like a small ball rotating in a viscous fluid. Under an external force, it tends to change from its original equilibrium state to a new, dynamic equilibrium state. When the force is removed, it relaxes back to its original equilibrium state. This polarization involves the inelastic movement of particles, and its interaction is an intermolecular phenomenon and so orientational polarization is strongly temperature-dependent [19].

In the case of ionic crystals, there are two important mechanisms of polarization. One being responsible for an absorption in the infrared i.e. the lattice or ionic polarization and the other in the ultraviolet i.e. the electronic polarization. In the very simplest and crude model known as the rigid ion model, the electron cloud around the ion is assumed to be rigid and consequently there is no contribution from electronic polarization. For such a model, the total dipole moment of the crystal is given by:

$$M = \sum_a \alpha_a Q_a \tag{3.12}$$

where Q_a are the active normal coordinates i.e. those which produce uniform polarization in the direction of M. α_a are suitable normalizing constants. Following Szigeti's procedure the macroscopic dipole moment M is normalized with respect to the number of moles N_m as $p = M / N_\mathrm{m}$ [16]. This normalization to a mole is better than to a unit volume, because changing of density one should compare the dipole moment produced by the same amount of material.

In reality the electrons are deformed during the lattice vibrations as they experience short range forces and also the dipolar field due to ions. The electron deformation is not just linearly proportional to lattice displacements but also involves higher terms. Hence when one takes into consideration the electronic polarization, the normalized macroscopic dipole moment of the crystal is given by:

$$p = p_0 + \sum_a \alpha_a \langle Q_a \rangle + \sum_{j\,j'} \beta_{j\,j'} \langle Q_j Q_{j'} \rangle \tag{3.13}$$

where p_0 is the moment in the undisplaced configuration and α_a and $\beta_{jj'}$ are the expansion coefficients. An important point to note is that α_a includes both the effects due to lattice displacements and also the first order effects due to electron deformation. The Q_a are the active normal coordinates, those which produce uniform polarization in the direction of p [16].

The above expression for the dipole moment clearly implies the presence of electrical anharmonicity in the crystal.

For the ease of harmonic crystal, the potential energy is proportional to the square of the normal coordinates. In reality crystals are not harmonic and the mechanical anharmonicity has to be taken into account. For such a crystal the potential energy involves the cubic and higher powers of the normal coordinates:

$$W = \frac{1}{2}\sum_{j}\omega_j^2 Q_j^2 + \sum_{j\,j'\,j''} b_{j\,j'\,j''} Q_j Q_{j'} Q_{j''} + \ldots \,. \tag{3.14}$$

The primary pyroelectric coefficients γ^{η} could be expressed in terms of coefficients which appear in the expansion of dipole moment and potential energy

$$\gamma^{\eta} = \sum_{j}\left(\beta_{jj} - \sum_{a}\frac{\alpha_a b_{ajj}}{\omega_a^2}\right)\frac{C_j}{\omega_j^2} \tag{3.15}$$

Here C_j is the contribution of the j^{th} mode to the specific heat and is given by $\hbar\omega_j\left(\partial\overline{n}_j/\partial T\right)$, $\overline{n}_j$ being the average occupation number of the phonons with energy $\hbar\omega_j$ [20].

3.6. Pyroelectricity and a crystal symmetry

From a Neumann's Principle polarization *P* must conform to the point-group symmetry of the crystal. It follows immediately that a pyroelectric effect cannot exist in a crystal possessing a centre of symmetry, a fact which provides a practical method of testing for the absence of the centre. A little thought allows to realize that a pyroelectric effect can only proceed along a direction in a crystal which is unique, in the sense that it is not repeated by any symmetry element. If there should exist in the point group a unique direction which is an axis of symmetry (2-, 3-, 4- or 6-fold), this will necessarily be the direction of *P*. But the presence of such a unique symmetry axis is not essential for the existence of a pyroelectric effect. It may be noted, in passing, that a unique direction as defined above is not synonymous with a polar direction. A polar direction is any direction of which the two ends are not related by any symmetry element of the point group. Thus, a diad axis in class 32 is a polar direction, but it is not a unique direction. All unique direction are polar, but only some polar directions are unique.

The direction of the polarization vector ***P*** and the form of it components in the 21 non-centrosymmetrical classes are depicted in Table 3.1.

Table 3.1. Crystal symmetry and the direction of polarization P.

System	Symmetry class	Polarization components			Direction of polarization
Triclinic	1	$\mathbf{P_1}$	$\mathbf{P_2}$	$\mathbf{P_3}$	no symmetry restricted on the direction of **P**
Monoclinic	2	**0**	$\mathbf{P_2}$	**0**	x_2 parallel to the diad axis, rotation or inverse
	m	$\mathbf{P_1}$	**0**	$\mathbf{P_3}$	**P** has any direction in the symmetry plane
Orthorhombic	mm2	**0**	**0**	$\mathbf{P_3}$	**P** parallel to the diad axis
	222	**0**	**0**	**0**	
Tetragonal, trigonal, hexagonal	4, 4mm, 3, 3m, 6, 6mm	**0**	**0**	$\mathbf{P_3}$	**P** parallel to the 4, 3 or 6 axis
Tetragonal, trigonal, hexagonal	$\bar{4}$, $\bar{4}$2m, 422, 32, $\bar{6}$, $\bar{6}$m2, 622	**0**	**0**	**0**	
Cubic	432, $\bar{4}$3m, 23	**0**	**0**	**0**	

Thus, the following 10 classes may theoretically show pyroelectricity under uniform heating or cooling:

1 2 3 4 6

m mm2 3m 4mm 6mm

They are called the polar classes.

3.7. Measurements

Qualitative methods

For the first time the quantity study of electrical distribution in pyroelectric effect was done by a experimental method invented by Kundt that display the electric effect clearly [21]. Kundt spread a mixture of sulphur and minium (red lead oxide) that was sifted through a cotton sieve, a process that electrifield the sulphur with negative and the minimum with positive electric charges. Dusting an electrified object like a pyroelectric crystal with this

powder provides a picture of its surface electric tension in red and yellow - the red minium colors the areas of negative voltage and the yellow sulphur colors the positive parts [22].

Another qualitative method for observing the pyroelectric effect was proposed by Bleekrode [23]. In this case, the pyroelectric crystal is cooled by vapours of liquid air, and then it hangs freely in the atmospheric air. Crystal cooled to a low temperature causes to condensate of water vapor in the air and the formation of tiny ice crystals. Crystals settle and grow on the surface towards the direction of the force lines of the electric field produced by pyroelectric charges, reaching a size finally several millimeters. This method can be used only in case of "strong" pyroelectric effect.

The qualitative method for observing the "weak" pyroelectric effect was developed by Martin [24]. A small piece of a crystal was hung on a very fine glass capillary near a flat metal electrode. The temperature of the crystal and the electrodes is reduced by the vapours of liquid air. If on the crystal surface the pyroelectric charges appears due to the change of its temperature, the crystal will be attracted to the metal electrodes due to the normal electrostatic interaction.

Static method

Direct measurement of pyroelectric charges caused by temperature changes is difficult because each of a tested crystal has a non-zero conductivity. Thus, each measuring method used in investigations of pyroelectric properties should be design so that during the measurement of pyroelectric charges, voltage between the electrodes of the test crystal is practically equal to zero. The first system fulfilling all above conditions was first developed by the Curie brothers [25]. Diagram of this test method is illustrated in Fig. 3.5.

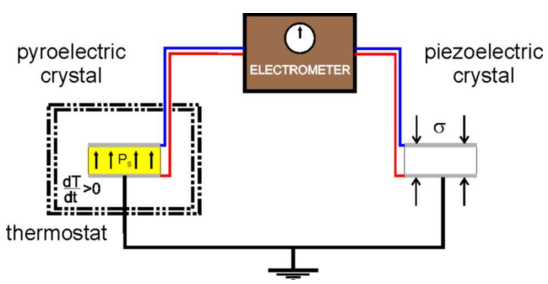

Fig. 3.5 Simplified diagram of the system using static method to study the pyroelectric properties.

The tested crystal with metal electrodes, is in parallel connected to the quartz plate through an electrometer which plays the role of the zero device. Pyroelectric charges formed on the crystal surface is compensated by the piezoelectric charges induced on the surface of a quartz plate under the influence of known external mechanical stress. From the values of the piezoelectric modulus of quartz and applied mechanical stresses needed for mutual compensation of piezoelectric and pyroelectric charges, the magnitude of these charges q can be specified. Knowing the pyroelectric charge q and the surface S of the crystal electrodes, the change of spontaneous polarization ΔP_S crystal can be determined. By measuring the temperature changes ΔT which alters the polarization of the crystal, the pyroelectric coefficient can be calculated from the following equation:

$$\gamma^{\sigma} = \frac{q}{S\,\Delta T} = \frac{\Delta P^{S}}{\Delta T}. \tag{3.16}$$

Quasistatic method

The simple quasistatic method of straightforward measurement of pyroelectric coefficient was developed by Byer and Roundy [26] in which the current produced by an constant temperature changes is measured. In this method thermally induced pyroelectric charges produces a flow of current parallel to the polar axis described by

$$I = \frac{dQ}{dt} = S\frac{dP}{dt} = S\frac{\partial P}{\partial T}\frac{\partial T}{\partial t} = S\gamma\frac{dT}{dt} \tag{3.17}$$

where $\gamma = dP/dT$ is the pyroelectric coefficient evaluated at temperature T and S is the surface area normal to the polar axis. It is easy to see that when dT/dt is held constant over a wide temperature range, a measurement of the current I gives a direct plot of $\gamma(T)$ over that temperature range. The measurement apparatus and its equivalent circuit is shown in Fig. 3.6 where R, is the crystal leakage resistance and R, is the meter input resistance. For this circuit the pyroelectric current is given by:

$$I_M = I\frac{R_C}{R_C + R_M}. \tag{3.18}$$

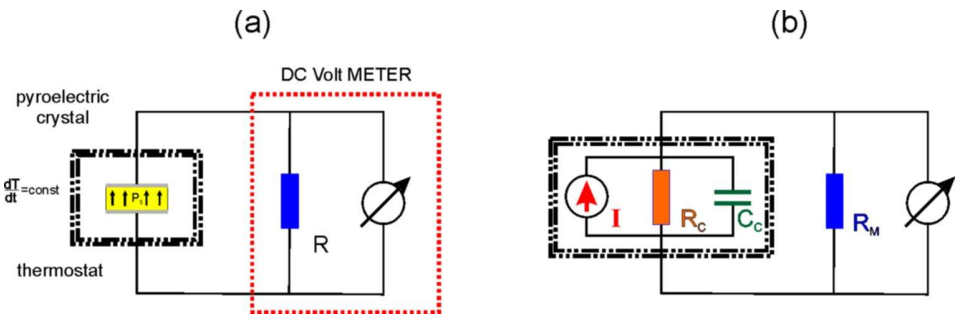

Fig. 3.6 (a) Scheme of the experimental setup for pyroelectric measurements by quasidynamic method. (b) The equivalent electrical circuit of measurement apparatus.

To use this method the resistance condition $R_C >> R_M$ should be fulfilled, because than the measured current I_M equals I to within 1%. This is easily arranged experimentally since typically R_M =105 Ω and $R_C > 10^{10}$ Ω.

The second quasistatic method widely used is the charge integration method. The measurement under short-circuit (constant E) conditions developed by Glass [27]. The apparatus of this method is presented in Fig. 3.7. A calibrated capacitor C_F is connected in the feedback loop and the pyroelectric charge developed across the crystal is instantaneously transferred to the feedback capacitor in order to maintain zero-field conditions across the amplifier input. Since the field across the crystal is zero the current through the crystal is zero and the change of measurement is not affected by the crystal resistance. The change of spontaneous polarization as a function of temperature can be easily obtained by integration of the pyroelectric charge [28].

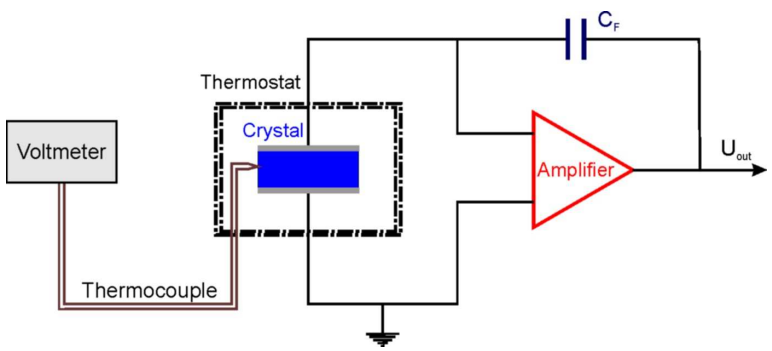

Fig. 3.7 Scheme of apparatus for pyroelectric measurements by charge integration method.

Dynamic method

Substantial progress in the development of methods testing pyroelectric properties arisen through Chynoweth research [29], who proposed a simple dynamic method (Fig. 3.8). This method is based on the pulse heating pyroelectric crystal with electroded surfaces. The plate is heated by a modulated light beam intensity. In an external circuit the flow of electric current induced by pyroelectric charges induced on the surface can be detected.

Specifically, it can be described as follows: Light radiation with power *W(t)* periodically modulated at a frequency ω

$$W(t) = W_0 S e^{i\omega t} = S h \rho C \frac{dT}{dt} \tag{3.19}$$

is incident on the surface of the pyroelectric crystal plate (area *S* and thickness *d*), which has emissivity η.

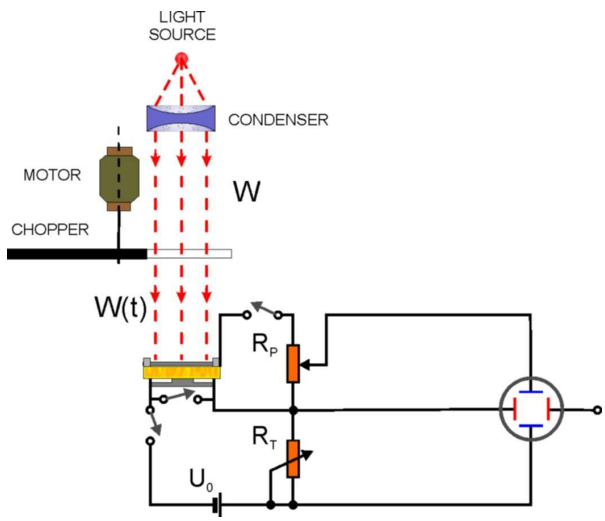

Fig. 3.8 Schematic diagram of dynamic method for pyroelectric measurements.

A square-wave radiation input, for example, will tend to give a current response of the form shown in Fig. 3.9. The element has a thermal capacity C_T and a thermal conductance to the surroundings *G*. Then the formed electrical signal is amplified. The temperature difference between the element and its surroundings, θ, is described by the following equation:

$$C_T \frac{d\theta}{dt} + G\theta = S\varepsilon_1 W_0 e^{i\omega t} \tag{3.20}$$

which has the solution

$$\theta(t) = \frac{S\varepsilon_1 W_0}{G + i\omega C_T} e^{i\omega t} \tag{3.21}$$

On the other hand the generated pyroelectric current is

$$I = S\frac{dP_m^S}{dt} = S\frac{dP_m^S}{dT}\frac{dT}{dt} = S \cdot p_m^\sigma \cdot \frac{dT}{dt} \tag{3.22}$$

and thus the pyroelectric current per input power is

$$\frac{I(t)}{W(t)} = \frac{\frac{dP_s}{dt} S \frac{dT}{dt}}{S\,h\,\rho\,C_T \frac{dT}{dt}} = \frac{p_m^\sigma}{h\,\rho\,C_T} \tag{3.23}$$

and hence the pyroelectric coefficient is

$$p_m^\sigma = \frac{W(t)}{I(t) \cdot h\,\rho\,C} \tag{3.24}$$

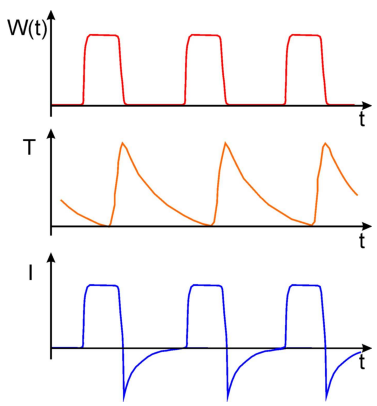

Fig. 3.9 Schematic presentation of measured quantities: *W(t)* - square-wave shape of radiation input; *T(t)* – shape of temperature changes; *I(t)* – typical current response for square-wave radiation modulation.

The dynamic method used in low temperatures allows to measure the specific heat. From the third law of thermodynamics because the coefficient is negative and the specific heat is proportional to T^3 it is easy to show that the primary pyroelectric coefficient when temperature goes to zero cannot have a linear temperature dependence [30].

3.8. Pyroelectric materials

The highest pyroelectric figures of merit have been observed in ferroelectric materials. The transition from the paraelectric to ferroelectric states in most of these (the 'proper' ferroelectrics) can be modeled in terms of an expansion of the free energy in a power series of the spontaneous polarization. It is possible to derive expressions for γ and ε from this in terms of the coefficients of the expansion. Liu and Long [31] have done this and concluded that $\gamma/\sqrt{\varepsilon}$ does not vary widely from one ferroelectric to another and that, therefore, improvements in material performance must be sought in the dielectric loss. To a large extent, this is borne out by the discussion which follows.

A second important point about the proper ferroelectrics is that both their dielectric properties and the pyroelectric coefficient tend to diverge as T_C is approached. This means that the ratio $\gamma/\sqrt{\varepsilon}$ and hence the pyroelectric responsivity, stay reasonably constant over a wide temperature range below T_C. This is important from a technological point of view as it means that the devices require no thermal stabilization. The following discussion reviews the present state of the art in pyroelectric materials and assesses their relative merits for different applications.

Table 3.2 summarizes the selected pyroelectric materials studied so far along with their figures of merit for voltage responsivity and detectivity.

The choice of the pyroelectric material is mainly determined by (a) its figure of merit, (b) the detector size, (c) availability and durability of the pyroelectric material, (d) environment in which the material has to operate, (e) the radiation levels to be detected, (f) the purpose for which the detector is employed, (g) the maximum ambient temperature of operation and the range over which stable operation is desired. The importance of factors (b) and (c) in the choice of pyroelectric material does not need much of an explanation. It should be possible to grow large crystals of pyroelectric material and fabricate them into thin slices. The durability is also an important factor [20].

Table 3.2 Figure of merit for various pyroelectric materials.

Material	T_C (^oC)	T (^oC)	ε	γ (^{x} 10^{-8})	Reference
TGS	**49**	**-25** **0** **25** **40**	**20** **20** **35** **100**	**0.44** **1.3** **4.0** **12.0**	**[32]**
$BaTiO_3$	**135**	**25** **60** **100**	**135** **200** **400**	**1.9** **7.0** **20.0**	**[32]**
$PbTiO_3$	**492**	**25**	**142**	**2.7**	**[32]**
$LiNbO_3$	**1210**	**-25** **25** **100**	**51** **30** **31**	**2.1** **0.4** **0.5**	**[32]**
$LiTaO_3$	**618**	**0** **25** **50** **100**	**52** **54** **56** **60**	**2.2** **2.3** **2.5** **2.7**	**[32]**
$NaNO_2$	**163**	**25**	**7.4**	**0.5**	**[34]**
KNO_3 (thin layer 8.9μm)	**135** **125**	**180**	**-**	**6000**	**[33]**
PZT4 (clevite)	**328**	**-25**	**1410**	**4.6**	**[32]**
PLZT (0/65/35)	**380**	**-**	**515**	**3.5**	**[34]**

T_C (^oC) - Curie temperature; T (^oC) - temperature in °C at which measurements were made; ε - dielectric permittivity; γ - pyroelectric coefficient in C/cm^2K.

3.9. Applications

Pyroelectric detectors possess a number of characteristics which are of significance when considering their use in a given application. Their 'AC coupled' nature makes them insensitive to unvarying fluxes of radiation so that they are ideally suited to detecting small changes in a relatively large background level of incident energy. They can be used over a large spectral bandwidth, the only requirement being that the energy be absorbed. However they can be used over a wide range of temperatures without recourse to cooling systems. Furthermore they have low power requirements and can operate for long periods on battery power, and last, but not least, they are generally low-cost devices [35].

Movement detector

This is an ideal application for pyroelectric detectors. In the absence of an intruder, the interior of an unoccupied building present a fairly constant thermal scene. An intruder moving into the area surveyed by the detector provides a varying flux of IR radiation, which can be detected and used to trigger an alarm. Most commercial detectors use a series of faceted mirrors designed to concentrate the radiation and improve the detection efficiency. Signals are generated as the intruder moves into and out of the areas covered by the mirrors. These signals are usually in the range 0.1-10 Hz, where the detectors work very well. The alarms usually operate in the 8 to 14 pm wavelength range, around the emission peak at 10 pm for bodies at 300 K. Using a filter which blocks all radiation at wavelengths shorter than 6 or 7 pm makes the detector insensitive to visible radiation and prevents false signals from, for example, sun glint. It is usual to use compensated detectors in this application to prevent false alarm signals due to environmental temperature changes.

Pollution monitoring and gas analysis

The concentrations of gases in the atmosphere can be measured from the strength of particular lines in their absorption spectra. For example, CO_2 has a strong absorption at 4.3pm. The analysis systems generally employ a modulated broad-band source of IR illuminating two pyroelectric detectors equipped with filters at the chosen wavelength. The radiation falling on one detector is allowed to pass through the gas being analyzed, while that falling on the other passes through a reference cell. By taking the ratio of the outputs from the detectors, the concentration of the pollutant can be measured.

Fire alarms

To detect fires, it is normal to operate at shorter wavelengths than for intruder alarms, typically around 4 pm. The systems usually sense the flicker frequency of the flames, at 5-40Hz to avoid false alarms.

Pyroelectric thermal imaging

Thermal imaging utilizes the different powers radiated in the far-infrared by objects in the scene which are at different temperatures [36]. There are two useful atmospheric windows in the far-IR; 3-5 pm and 8-14 pm. For objects near 300 K, the power radiated at 3-5 pm is about 6 Wm^{-2}, compared with 150 Wm^{-2} in the 8-14 pm band. This difference in radiance, coupled with the better penetration of haze and smoke by the longer wavelengths, has made operation in the 8 to 14pm band the preferred choice for general-purpose pyroelectric imaging systems. Nevertheless, the broad-band operation of pyroelectric targets means that, for specialist applications, similar devices (usually with just a change of window) can be used at the shorter wavelengths. Such techniques can be used for 'multi-color' IR imaging where absolute temperatures in the scene can be measured remotely by their radiances in the different bands. This has application to, for example, industrial process control or, in the military field, target/decoy discrimination.

[1] S. B. Lang, *Sourcebook of Pyroelectricity*, Gordon & Breach Science, London (1974).

[2] S. B. Lang, *The history of pyroelectricity: From ancient greece to space missions*, Ferroelectrics, **230** (1999) 99 -108.

[3] S. B. Lang, *Pyroelectricity: From Ancient Curiosity to Modern Imaging Tool*, Physics Today, (2005) 31-36.

[4] B. Brewster, *Observations on the pyroelectricity of minerals*, Edinburgh. J. Sci., **1** (1824), 208-215.

[5] J. M. Gaugain**,** *Mémoire sur l'électricité des tourmalines*, Annales de Chimie et de Physique, **57** (1859) 5–39.

[6] W. Thomson (Lord Kelvin), *On the thermoelastic, thermomagnetic and pyroelectric properties of matter*, Phil. Mag., **5** (1878) 427-442.

[7] W. Voigt. *Lehrbuch der Krirtalphysik* (1928), reprint by Johnson Reprint Corp.. New York (1966).

[8] Y. Ta**,** *Actions of radiations on pyroelectric crystals*, Compt. Rend., 207, (1938) 1042-1044.

[9] J. Cooper, *A Fast Response Total-Radiation Detector***,** *Nature* **194**, (1962) 269 – 271.

[10] J. Cooper, A fast-response pyroelectric thermal detector, J. Sci. Instrum., **39** (1962) 467-472.

[11] F. Le Carvennec, *Advances in Electronics and Electron Physics,* **28A,** ed. J. D. McGee, D. McMullen and E. Kahan (London and New York: Academic Press) 265-72, (1969).

[12] L. A. Sromovsky, F. A. Best, H. E. Revercomb and J. Hayden, *Galileo Net Flux Radiometer experiment*, Space Science, Reviews*,* **60** (1992) 233-262.

[13] R. W. Whatmore, *Pyroelectric devices and materials*, Rep. Prog. Phys. **49** (1986) 1335-1386.

[14] M. Born, *On the quantum theory of pyroelectricity*, Rev. Mod. Phys. **17** (1945) 245-251.

[15] M. Born and K. Huang, *Dynamical Theory of Crystal Lattices,* Clarendon Press, (1954) Oxford, England.

[16] B. Szigeti, *Temperature dependence of pyroelectricity*, Phys. Rev. Lett. **35** (1975) 1532-1534.

[17] P. J. Grout and N. H. March, *Low-Temperature behavior of Pyroelectricity*, Phys. Rev. Lett. **37** (1976) 791-792.

[18] B. Szigeti, *Low-Temperature behavior of Pyroelectricity – A reply*, Phys. Rev. Lett. **37** (1976) 792-793.

[19] K. C. Kao, *Dielectric phenomena in solids*, Elsevier Academic Press, (2004) San Diego, USA.

[20] M. R. Srinivasan, *Pyroelectric materials*, Bull. Mater. Sci., **6** (1984) 317-325.

[21] A. Kundt, *Uebereine einfache Methode zur Untersuchung der Thermo-, Actino-, und Piezoelectricitat der Krystalle*, Ann. Phy., **20** (1883) 592-601.

[22] S. Katzir, *The beginning of piezoelectricity*, Springer, Netherlands, 2006.

[23] L. Bleekrode, *Über einige Versuche mit flüssiger Luft*, Ann. Phys. **317** (1903) 218-223.

[24] A. J. P. Martin, *On a new method of detecting pyro-electricity*, Min. Mag., **22**, (1931) 519-523.

[25] P. Curie and J. Curie, *Les cristaux hémièdres à faces inclinées, comme sources constantes d'électricité*, Comptes Rendus des Séances de l'Académie des Sciences, **93** (1881) 204-207.

[26] R. L. Byer and C. B. Roundy, *Pyroelectric coefficient direct measurement technique and application to a nsec response time detector*, Ferroelectrics, **3** (1972) 333-338.

[27] A. M. Glass, *Investigation of the electrical properties of $Sr_{1-x}Ba_xNb_2O_6$ with special reference to pyroelectric detection*, J. App. Phys., **40** (1969) 4699-4713.

[28] M. E. Lines and A. M. Glass, *Principles and applications of ferroelectrics and related materials*, Clarendon Press, (1977) Oxford.

[29] A. G. Chynoweth, *Dynamic method for measuring the pyroelectric effect with special reference to Barium Titanate*, J. Appl. Phys., **27** (1956) 78-84.

[30] R. Radebaugh, *Behavior of the Pyroelectric Coefficient at Low Temperatures*, Phys. Rev. Lett., **40** (1978) 572–574.

[31] S. T. Liu and D. Long, *Pyroelectric detectors and materials*, Proc. IEEE **66** (1978) 14.

[32] H. P. Beerman, *Investigation of pyroelectric material characteristics for improved infrared detector performance*, Infrared Phys. **15** (1975) 225-231.

[33] F. El-Kabbany, W. Badawy, E. H. El-Khwas and N. H. Tahr, *Dielectric and pyroelectric properties of KNO_3 thin-layers*, J. Mater. Science 23, (1988) 776-781.

[34] L. E. Garn, E. J. Sharp, *Pyroelectric vidicon target materials*, IEEE Transactions on Parts, Hybrids, and Packaging, vol. PHP-10, (1974) p. 208-221.

[35]A. Hadni, *Applications of the pyroelectric effect*, J. Phys. E: Sci. Instrum., **14** (1981) 1233-1240.

[36] P. F. T. C. Stillwell, *Thermal imaging*, J. Phys. E: Sci. Instrum., **14** (1981) 1113-1138.

INTRODUCTION TO PHASE TRANSITIONS

Chapter 4

CONTENT

4.1 The Gibbs Law

The thermodynamic phase of a system is a phase of uniform physical and chemical properties. Under some conditions two (or more) phases can coexist at equilibrium when their thermodynamic potentials are equal [1]:

$$\Phi_A(T,x) = \Phi_B(T,x). \qquad (4.1)$$

The conditions for the equilibrium in the system of c components and φ phases, and the number of independent variables necessary to specify the state of each phase was determined by Josiah Willard Gibbs in 1875 [2, 3]. This condition is known as the Gibbs phase rule and can be written as

$$d = c - \varphi + 2 \qquad \textbf{(4. 2)}$$

where

c – the number of components,

φ – the number of phases in the thermodynamic equilibrium,

d – the number of independent variables.

Let's consider the simple phase diagram for water with pressure (p) and temperature (T) as axes (Fig.4. 1)

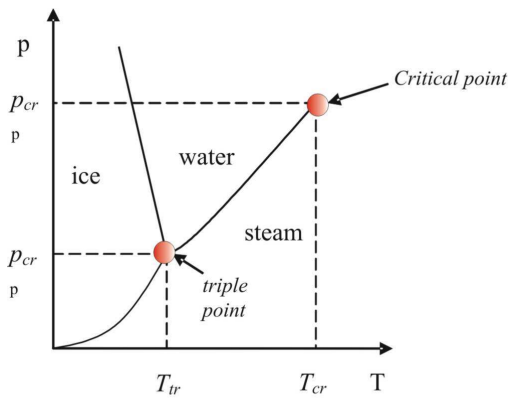

Fig.4. 1. The phase diagram for water

The phase diagram shows lines corresponding to the phase boundaries between three possible phases: solid, liquid and gas.

It is easy to identify regions where a single phase remains in equilibrium.

According the Phase Rule Eq.(4.1)

$$\Phi_A(T,x) = \Phi_B(T,x) \qquad (4.1)$$

we have

$d = 1 - 1 + 2 = 2$.

This implies that two variables (p and T) can be varied independently in the region when one phase only (liquid, gas or solid) can exist in an equilibrium state.

The curves in the phase diagram represent points where the free energy of two phases are existing at the same time. In this case, the Phase Rule Eq. (4.2) states that

$d = 1 - 2 + 2 = 1$.

Therefore, as long as there are two phases in equilibrium, there is only ne degree of freedom corresponding to the position along the phase boundaries. Now, lets consider the situation in the phase diagram where the three lines meet together. Three phases can exist in the same time, so the phase rule gives:

$d = 1 - 3 + 2 = 0$.

Zero corresponds to none of the independent variables. This means that there is only one temperature and pressure at which three phases (liquid, water and gas) coexist in thermodynamic equilibrium, called the *triple point*. The triple point of pure water is at 0.01 degrees Celsius and 0.00603 atm and is used to calibrate thermometers.

The point at which the critical temperature and the critical pressure meet is marked in Fig.4. 1. This point is called the *critical point* of the substance. The critical point for water exists at 374 ^{o}C and 218 atm. Above this point, the liquid and gas phases cannot be distinguished and become a single phase.

A phase transition is the transformation from one phase to another. Phases are different states of matter. During a phase transition the main properties of a given medium change, continuously or discontinuously, under some external conditions such as pressure or temperature. For example, water becomes gas in a high temperature. Examples of phase transitions contain freezing or sublimation of solids, polarization of ferroelectrics, condensation and the superfluid transition in liquid helium. Typical examples of the phase transitions are presented in Fig. 4. 2.

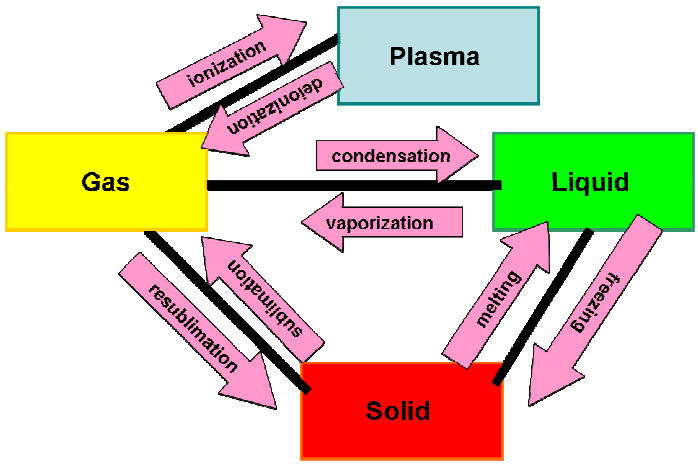

Fig. 4. 2 Diagram of different types of the phase transition

Some materials have been known for a long time to exhibit mechanisms forming permanent magnets or the magnetization direction can be changed in the external magnetic field. Materials exhibiting spontaneous magnetization are called ferromagnetics. In the 20th century it was found that for some materials known as ferroelectrics [4] the external electric field can change the direction of the spontaneous electric polarization. In paraelectrics the dipole alignment is small, whereas in ferroelectric crystals the alignment is almost absolutely over same region. In such crystals the dipole moments of the unit cells differs depending on the crystal region. Such regions are called a "domain", and a cross section through a crystal is illustrated below.

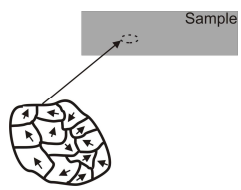

Fig. 4. 3 Schematic representation of the "domains"

Materials are polarized along one of crystallographic axes when a dipole moment appears on this axis. Depending on the crystal structure, there are a few or more possible ferroelectric axes. Ferroic materials exhibit a history-dependent behavior called hysteresis [5 - 12]. An example of the hysteresis loop is shown below (Fig. 4. 4). The hysteresis loop illustrates the relationship between the polarization (***P***) and the electric field **(*E*).**

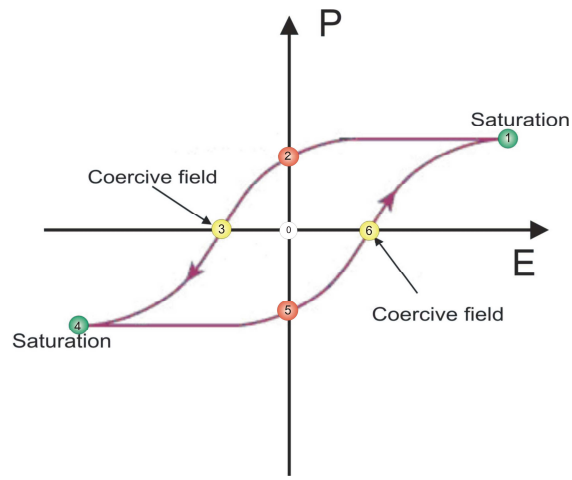

Fig. 4. 4 Ferroelectric hysteresis loop.

When a ferroelectric was not polarized before, its primary polarization line would go from “0” point to “1” under increasing of the electric field (Fig. 4. 4). At point "1" almost all of the domains are aligned and during the further increasing of the electric field very little changes in the polarization. The material reached the limit-point of the electric saturation. When the electric field is reduced to zero, the curve will move from point "1" to point "2". It can be seen that in this point some part of the polarization remains in the material even when the electric field is equal to zero. It can be concluded that some of the domains still remain aligned, and some have lost their alignment. When the electric field

is reversed, the curve moves to point "3", where the polarization is reduced to zero. This point is called the coercive field or coercive force. The classical coercive field $\boldsymbol{E_c}$ is defined as the external electric field necessary to reduce the total polarization to zero after being previously saturated. When the electric field is increasing in the negative direction the saturation can be observed again (see point “4”). When the electric filed is reduced back to zero the curve goes to point "5" In this point material have a residual polarization equal to that achieved in the point “2”. When the electric field is increasing once more in the positive direction the polarization will reached zero. It is worth to notice that the curve did not return to the point “0” any more (Fig. 4. 4) because the certain field is necessary to remove the residual electricity.

4.2. The Ehrenfest classification of the phase transition

The first attempt to classify *phase transitions* was a model introduced by the Dutch physicist Paul Ehrenfest (1880-1933) [13]. Based on this classification the phase transitions are grouped with respect to the behavior of the thermodynamic free energy as a function of other thermodynamic variables. Following Ehrenfests, the type of the phase transitions are related with the derivative discontinuity of the thermodynamic potential [14,15]. In general the criterion of the phase transition classification according to the Ehrenfest rule can be formulated as follows:

the phase transition is called n^{th} *-order if both the thermodynamic potential* $\Phi(x_1, x_2 .... x_2)$ *and its* $(n\text{-}1)^{th}$ *derivative are continuous functions, while n-th derivative is discontinuous.*

4.2.1 First order phase transition

For the first order phase transition the first derivative of the thermodynamic potential is discontinuous so

$$\Phi_A(X_1, X_2 ... X_n) = \Phi_B(X_1, X_2 ... X_n) \quad \textbf{(4. 3)}$$

and

$$\frac{\partial \Phi_A(T = T_P)}{\partial X_i} \neq \frac{\partial \Phi_B(T = T_P)}{\partial X_i} \quad \textbf{(4. 4)}$$

In the first-order phase transition there is a nonzero change in the value of the entropy $\boldsymbol{S}$, the polarization $\boldsymbol{P}$ (for ferroelectrics) and the deformation $\boldsymbol{\eta}$ at the transition temperature

$$\begin{aligned}
&\frac{\partial \Phi(A)}{\partial T} \neq \frac{\partial \Phi(B)}{\partial T} && S_A \neq S_B , \\
&\frac{\partial \Phi(A)}{\partial \sigma} \neq \frac{\partial \Phi(B)}{\partial \sigma} && \eta_A \neq \eta_B , \\
&\frac{\partial \Phi(A)}{\partial E} \neq \frac{\partial \Phi(B)}{\partial E} && P_{sA} \neq P_{sB} , \\
&\frac{\partial \Phi(A)}{\partial P} \neq \frac{\partial \Phi(B)}{\partial P} && V_A \neq V_B .
\end{aligned} \quad \textbf{(4. 5)}$$

The examples of anomalies in physical properties described by the first derivative of the thermodynamic potential during the 1st order phase transition are shown in Fig.4. 5.

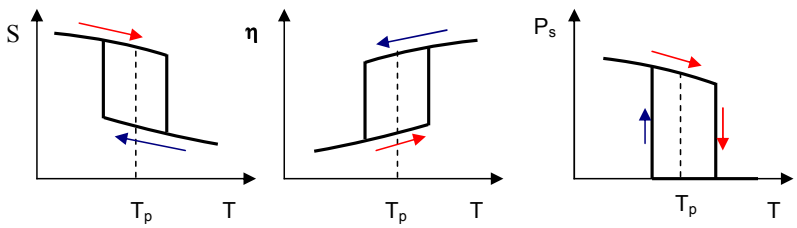

Fig.4. 5. Anomaly of physical properties described by the first derivative of thermodynamic potential during the ferroelectric first order phase transition

It is worth noting that during the phase transition the volume jump can be positive or negative whereas the entropy jump can only be positive. The negative volume jump can be observed during the phase transition in water. During the melting process a water volume decreases by about 10%.

The thermal (pressure) hysteresis and the latent heat are characteristic for the phase transitions. The latent heat is the energy required (released or absorbed) to change the phase of a substance. When the phase change is from solid to liquid the latent heat of fusion must be used, while the latent heat of vaporization is used to change the phase from liquid to gas. The specific latent heats of fusion and of evaporation is equal to $334\frac{kJ}{kg}$ and $2258\frac{kJ}{kg}$, respectively. The entropy jump, defined as $\Delta S = \frac{Q_p}{T_P}$, where T_p is the phase transition temperature, during the melting is equal to $\Delta S = \frac{334}{273} = 1.22\frac{kJ}{K \cdot kg}$.

4.2.2 Second order phase transition

In the **second-order phase transition**, the first derivative of the thermodynamic potential is continuous while its second derivative is not.

$$\frac{\partial \Phi(A)}{\partial T} = \frac{\partial \Phi(B)}{\partial T} \qquad S_A = S_B ,$$
$$\frac{\partial \Phi(A)}{\partial \sigma} = \frac{\partial \Phi(B)}{\partial \sigma} \qquad \eta_A = \eta_B ,$$
$$\frac{\partial \Phi(A)}{\partial E} = \frac{\partial \Phi(B)}{\partial E} \qquad P_{sA} = P_{sB} , \qquad \textbf{(4. 6)}$$

$$\Phi_A(T_p, x) = \Phi_B(T_p, x),$$

and for example

$$\frac{\partial^2 \Phi(A)}{\partial \sigma \partial T} \neq \frac{\partial^2 \Phi(B)}{\partial \sigma \partial T} \qquad \alpha_A(T_P) \neq \alpha_B(T_P),$$
$$\frac{\partial^2 \Phi(A)}{\partial E^2} \neq \frac{\partial^2 \Phi(B)}{\partial E^2} \qquad \chi_A \neq \chi_B ,$$
$$\frac{\partial^2 \Phi(A)}{\partial E \partial T} \neq \frac{\partial^2 \Phi(B)}{\partial E \partial T} \qquad \gamma_A \neq \gamma_B ,$$
$$\frac{\partial^2 \Phi(A)}{\partial T^2} \neq \frac{\partial^2 \Phi(B)}{\partial T^2} \qquad C_{pA} \neq C_{pB} .$$

In the second-order phase transition there is a zero change in the enthalpy, the entropy, and the volume at the transition temperature while there is an jump of the piezoelectric module (α), elastic coefficient (χ), pyroelectric coefficient (γ), specific heat (C_P),(see Fig. 4. 6) .

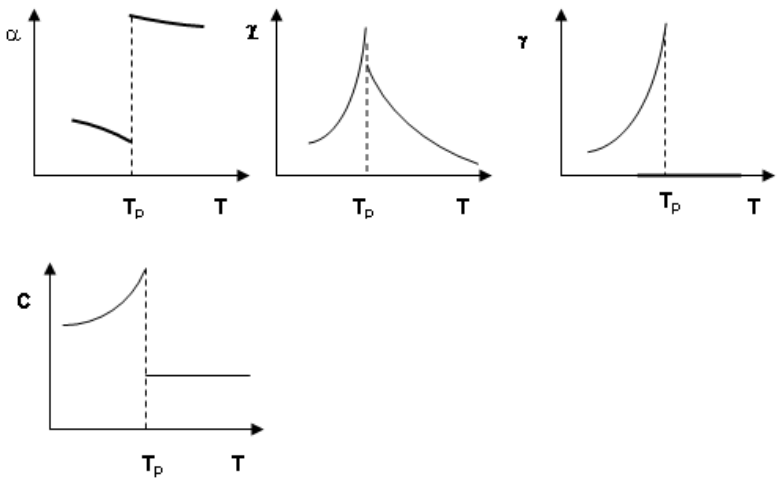

Fig. 4. 6. Examples of anomaly of the thermal expansion coefficient (α), the susceptibility (χ), the pyroelectric coefficient (γ) and the specific heat (C) during the 2nd order phase transition

The Ehrenfest approach provides information on stability relations between different phases of a chemical compound and on the direction of the phase transitions.

There are few more classifications of the phase transitions, e.g. [11]:

- by Münster – the phase transition are classified according to the temperature dependence of the specific heat and theenthalpy;
- by Buerger - the classification of the structural phase transition|: reconstructive, displactive and order/disorder phase transition[16,17],
- by Landau.

According to Buerger approach the phase transitions, not involving the strong bond breaking are called displacive. In general, the crystal structures of two

phases involved in a displacive phase transition show subgroup – supergroup symmetry relations [18].

Basing on changes in the symmetry the phase transitions can be divided into structural and isostructural ones. During the isostructural phase transition the system symmetry is not changed. The difference betweens the structural and isostructural phase transitions is presented in Fig. 4. 7.

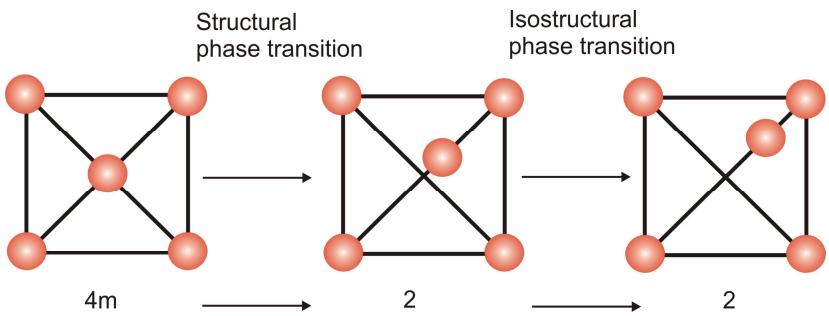

Fig. 4. 7. Schematic illustration of the structural and isostructural phase transitions

[1]. A. Strukov, A.P.Levanyuk, Ferroelectric phenomenta in crystals, Springer, (1998).

[2]. Z. Wahrscheinlichkeitstheorie verw. Gebiete 67 (1984) 121-138.

[3].B. M. Mladek, P.Charbonneau and D. Frenkel, Phys. Rev. Lett. 99 (2007) 235702.

[4]. J. Valasek, Phys. Rev. 17 (1920) 537.

[5].J.Klamut, K.Kurczewski, J.Sznajd, Wstęp do fizyki przejść fazowych, Ossolineum, (1979) Wrocław.

[6]. K. Aizu, J. Phys. Soc. Japan 27 (1969) 387.

[7]. K. Aizu, J. Phys. Soc. Japan 28 (1970) 706.

[8]. A. Devonshire, Phil. Mag. 40 (1949) 1040.

[9].A. Devonshire, Phil. Mag. 42 (1951) 1065.

[10]. Lines, A. M. Glass, *Principles and Applications of Ferroelectric and Related Materials*, Clarendon Press, (1977) Oxford.

[11]. A. Graja Red., A.R. Ferchmin, *Przemiany fazowe*, Ośrodek Wydawnictw Naukowych (2003)Poznań.

[12]. L. Landau, E. M. Lifszyc, *Statisticzeskaja Fizika*, Izd. Nauka, (1976) Moskwa

[13]. P. Ehrenfest, Proc. Kon. Amsterdam Acad., 36 Suppl. 75 b (1933) 153.

[14]. P. Ehrenfest, *The Conceptual Foundations of the Statistical Approach in Mechanics* (1990) (English translation by J. Moravcsik).

[15]. J.Klamut, K.Kurczewski, J.Sznajd, Wstęp do fizyki przejść fazowych, Ossolineum, (1979) Wrocław .

[16] . M. J. Buerger, Fortschr. Mineral., 39 (1961) 39.

[17]. M.J. Buerger, Trans. Amer- Crystattogr. Assoc., 7 (1971) 1.

[18]. F. Liebau, J. Thermal Anal, Vol. 33 (1988) 107.

Chapter 5

THEORY OF PHASE TRANSITION- LANDAU THEORY

CONTENT

5.1 Introduction

In introductory physics a phase transition is described by phenomenological theories, considering the phenomena on a macroscopic scale containing many atoms. The first equation of the state representing a phase transition was proposed by van der Waals in 1873 [1].

The fundamental idea of the phenomenological treatment of the phase transition for the first time was given by Landau in 1937 [1]. The thermodynamic theory of ferroelectrics based on Landau theory was formed by Ginzburg [2] and Devonshire [3],[4].

The great majority of physical properties of crystalline solids near the phase transition can be described by Landau theory. The theory is based on the assumption that there exists the thermodynamic parameter characteristic of the order degree called the *order parameter*, denoted as η. The magnetization for ferromagnetic-paramagnetic transitions, the polarization for ferroelectric-paraelectric transitions, or the spontaneous deformation for ferroelastic-paraelastic transitions are examples of such order parameters.

The order parameter which described the system symmetry changes has a following properties:

- in the phase with the highest symmetry (a symmetric, disordered phase) the order parameter disappears $\eta \to 0$ and in a nonsymmetric phase the order parameter $\eta \neq 0$;
- for the continuous phase transition $\eta \to 0$ when $T \to T_C$;
- below the critical point the order parameter can have more than one value.

In principle, the order parameter can be a scalar, vector or some other quantity [5]. The ferroelectric equation of state can be derived from the Gibbs free energy density Φ, which is appropriate when the independent thermodynamic variables are: a stress, an electric field, and a temperature.

$$\Phi = \Phi(p, T, \eta). \qquad \textbf{(5. 1)}$$

It is worth noting that the thermodynamic potential describes both nonsymmetrical and symmetrical phases as a consequence of:

$$\Phi(\eta) = \Phi(\eta^*) \qquad \textbf{(5. 2)}$$

where η^* - is the order parameter transformed by symmetry operations[6 - 10].

The order parameter can be found by minimizing of the thermodynamic potential. At all temperatures the following condition must be fulfilled:

$$\left(\frac{\partial \Phi}{\partial \eta}\right)_T = 0,$$
$$\left(\frac{\partial^2 \Phi}{\partial \eta^2}\right)_T \rangle 0. \qquad \textbf{(5. 3)}$$

Assuming that the order parameter η is small near the phase transition temperature, the Gibbs free energy can be expand in a Taylor series with respect to η

$$\Phi(T,\eta) = \Phi_0 + \frac{1}{2}\alpha\eta^2 + \frac{1}{4}\beta\eta^4 + \frac{1}{6}\gamma\eta^6 + ..., \qquad \textbf{(5. 4)}$$

where

Φ_0 - is the free energy density of the paraelectric phase at zero electric field,
α - the coefficient in the Landau expansion dependent of p and T,
β, γ - the coefficient in the Landau expansion.

The various types of phase transitions which can be described within the Landau-, Devonshire- and Ginzburg-Landau theories are depicted in a table below.

phase transition type	Order parameter	Theory
ferromagnetic	*magnetization*	*Landau Ginzburg-Landau*
antiferromagnetic	*differece of magnetization*	*Ginzburg-Landau*
ferroelectric	*polarization*	*Landau Ginzburg-Landau Devonshire*
ferroelastic	*strain*	*Ginzburg-Landau*
liquid-vapour	*density*	*Ginzburg-Landau*
structural	*displacement rotation*	*Landau Devonshire*

The ferromagnetic phase transition, with the magnetization as an order parameter, is a typical problem for the Landau theory. In antiferromagnetic

crystals the magnetic moments of adjacent atoms located on different sublattices are antiparallel. The difference between the magnetizations of both neighbourig sublattices is the order parameter of antifermomagnetics. Ferroelectric phase transitions with the polarization as an order parameter were described by Devnshire [3,4].

5.2 Second order phase transition

In order to describe the second order phase transition the expansion of the free energy up to 4th power is needed

$$\Phi(T,\eta) = \Phi_0 + \frac{1}{2}\alpha\eta^2 + \frac{1}{4}\beta\eta^4. \qquad \textbf{(5. 5)}$$

In such a model it is assumed that α coefficient depends on temperature $\alpha' = \alpha(T - T_c)$, whereas $\beta > 0$ and does not depend on temperature.

Based on the condition for a stable state Eq.(5.3) the behavior of the order parameter can be found from

$$\left(\frac{\partial\Phi}{\partial\eta}\right)_T = \eta\cdot(\alpha + \beta\eta^2) = 0,$$
$$\left(\frac{\partial^2\Phi}{\partial\eta^2}\right)_T = \alpha + 3\cdot\beta\cdot\eta^2 \rangle 0. \qquad \textbf{(5. 6)}$$

It can be noticed that for $T > T_c$ one minimum (one phase) exists only which corresponds to $\eta = 0$ (see Fig. 5. 1.-curve 1). For $T < T_c$ the order parameter corresponding to the stability of phase II is shown in Fig. 5. 1.curve 3.

$$\eta = \pm\sqrt{\frac{\alpha(T - T_c)}{\beta}} \qquad \textbf{(5. 7)}$$

The curve 2 presents free energy as a function of order parameter at $T \approx T_c$.

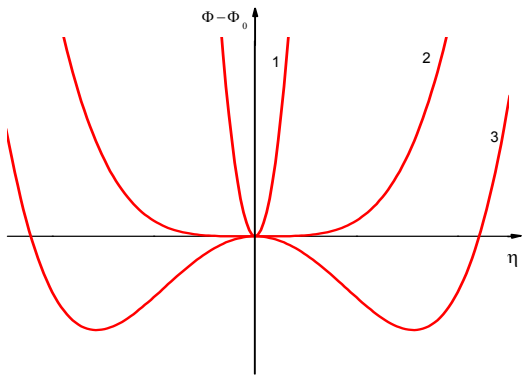

Fig. 5. 1 The order parameter dependence on thermodynamic potential for the case m = 4 [5].

In Fig.5. 2 the temperature dependence on the order parameter for the thermodynamic potential expanded to 4^{th} power. Such a transition is called the continuous phase transition, because of continuous changes of the order parameter. It is also the second-order phase transition in the Ehrenfest classification (see Chapter 4).

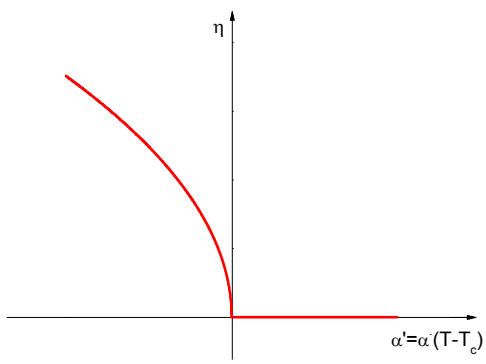

Fig.5. 2 Temperature dependence on order parameter for continuous phase transition.

5.2.1. Anomaly of electrical properties

Now let us consider the dependence of the thermodynamic potential of a ferroelectric crystal on the temperature, the order parameter and the electric field. If we insert the electric field into equation (5.3) the expansion of the thermodynamic potential can be written as follows:

$$\Phi(T,\eta,E) = \Phi_0 + \frac{1}{2}\alpha(T - T_C)\eta^2 + \frac{1}{4}\beta\eta^4 - a\eta E \qquad \textbf{(5. 8)}$$

where E – is the vector component of the electric field.

One can easily show from Eq (5.5) that the polarization (the order parameter for ferroelectrics) and the susceptibility are given as

$$P = \frac{\partial\Phi}{\partial E} = a\eta, \qquad \textbf{(5. 9)}$$

$$\chi = \frac{\partial P}{\partial E} = a\frac{\partial\eta}{\partial E}, \qquad \textbf{(5. 10)}$$

The order parameter in equilibrium states can be determined from a condition of minimizing of the energy Eq. (5.3)

$$\frac{\partial\Phi}{\partial\eta} = \alpha(T - Tc) + \beta\eta^3 - aE = 0. \qquad \textbf{(5. 11)}$$

At the absence of the external electric field (when E=0) the solution of equation (5.11) is given by:

$$\eta = \begin{cases} 0 & for \quad T > T_c, \\ \pm\left(-\dfrac{\alpha(T - T_c)}{\beta}\right)^{1/2} & for \quad T < T_c. \end{cases} \qquad \textbf{(5. 12)}$$

Using equation (5.9) the spontaneous polarization in the case of absence of the external electric field can be determined as:

$$P_s = \begin{cases} 0 & for \quad T > T_c, \\ \pm a\left(\dfrac{\alpha(T-T_c)}{\beta}\right)^{1/2} & for \quad T < T_c. \end{cases} \qquad \textbf{(5. 13)}$$

The equation of state $E = \dfrac{\partial \Phi}{\partial P}$ defines the theoretical dependence of the polarization P versus E in a form of a hysteresis loop.

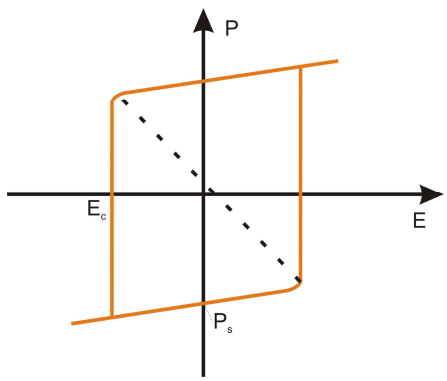

Fig. 5. 3 Polarization vs electric field –ferroelectric hysteresis loop.

The coercive field $E = E_c$ is defined as the turning point $\left(\dfrac{\partial E}{\partial P}\right)_{E=E_c} = 0$ which determines the polarization *Pc* at the coercive field as:

$$P_s = \sqrt{\frac{\alpha(T-T_c)}{\beta}}.$$

Substitution of this value back in the equation of state yields the coercive field *Ec* as

$$E_c = \pm \frac{2}{3\sqrt{3}} \sqrt{\frac{\alpha^3}{\beta}}.$$

Substitution of the solution of equation (5.11) into (5.10) we obtain

$$\frac{\partial \eta}{\partial E} = \chi = \frac{a}{\alpha(T-T_c) + 3\beta\eta^2}. \qquad \textbf{(5. 14)}$$

Now the dielectric permittivity can be found as:

$$\varepsilon = 4\pi\chi = 4\pi \frac{a^2}{\alpha(T - T_c)}, \quad \textbf{(5. 15)}$$

for a temperature region of $T > T_c$ and

$$\varepsilon = -2\pi \frac{a^2}{\alpha(T - T_c)}, \quad \textbf{(5. 16)}$$

for $T < T_c$ temperatures.

In summary, ferroelectric materials loose their spontaneous polarization at the temperature above the phase transition temperature (T_c) and become the paraelectrics. It can be shown that above and below the phase transition temperature the dielectric permittivity depends on temperature according to the Curie-Weiss law

$$\varepsilon = \frac{A}{T - T_c}, \quad \textbf{(5. 17)}$$

where A is the Curie-Weiss constant.

A plot of the real part of reciprocal of the dielectric permittivity as a function of temperature for the TGS crystals is presented in Fig. 5. 5. It can be seen that there is a difference between the both sides of phase transition temperature T_c in $\frac{1}{\varepsilon}$ slope.

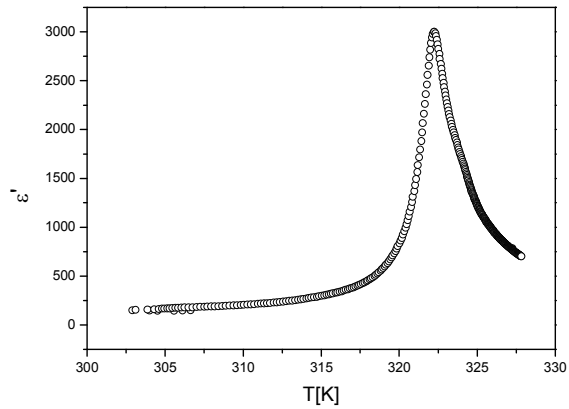

Fig. 5. 4 Plot of the dielectric permittivity versus the temperature for TGS crystals.

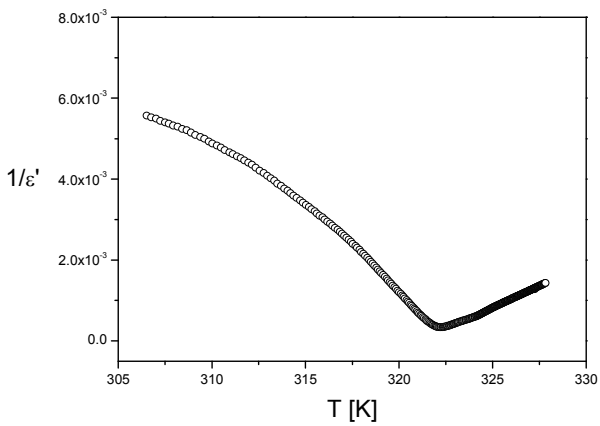

Fig. 5. 5 Temperature dependence of reciprocal of dielectric permittivity for TGS crystals.

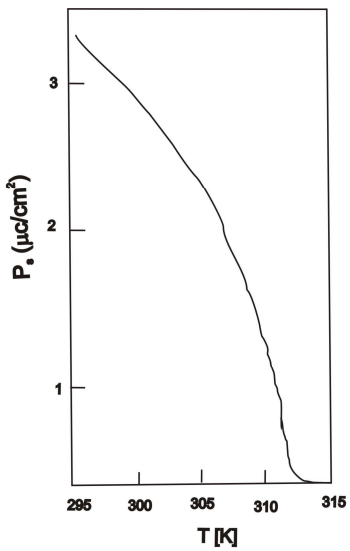

Fig. 5. 6 Temperature dependence of the spontaneous polarization for MAPBB crystals [11].

In Fig. 5. 6 the spontaneous polarization as a function of temperature is presented. Above the phase transition the continuous temperature changes of the spontaneous polarization can be observed whereas below T_c the spontaneous polarization is equal to zero.

5.2.2. Anomaly of thermal properties

Let us now study a change in the specific heat and the entropy in the second-order phase transition. In general, the entropy is defined as

$$S = -\frac{\partial \Phi}{\partial T} \qquad \textbf{(5. 18)}$$

From Eq (5.8) (with $E = 0$) and (5.18), we find the entropy

$$S = \begin{cases} \dfrac{\partial \Phi_0}{\partial T} = S_0 & for \quad T > T_c, \\ S_0 + \dfrac{\alpha^2 (T - T_c)}{2\beta} & for \quad T < T_c, \end{cases} \tag{5. 19}$$

where S_0 is the entropy in the symmetric phase.

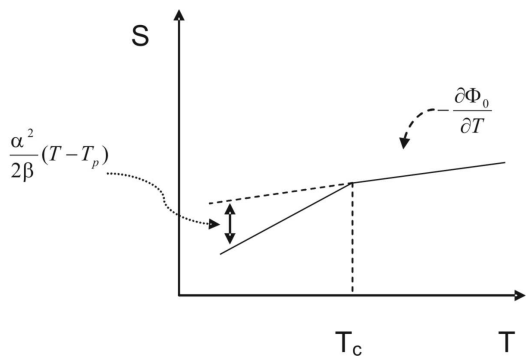

Fig.5. 7 Schematic representation of the crystal entropy changes near the second-order phase transition region.

It is worth noticing that absence of the entropy jump corresponds to the second-order phase transition.

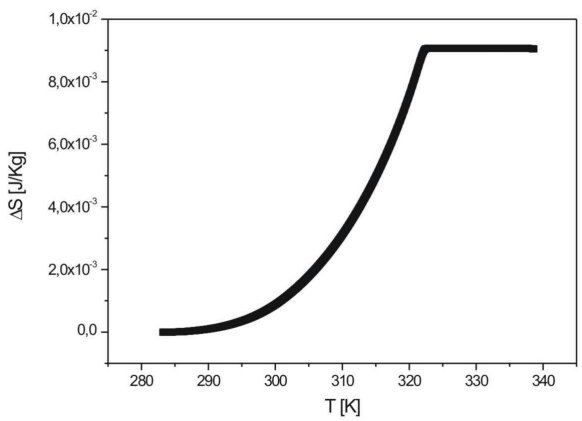

Fig.5. 8 Temperature dependence of the entropy of the TGS crystals in a wide temperature range and near the T_c.

The heat capacity of the crystals is defined as $C_p = T \cdot \left(\frac{\partial S}{\partial T} \right)$ and is equal to

$$C_p = \begin{cases} C_p^0 & for \quad T > T_c, \\ C_p^0 + \frac{\alpha^2 T}{2\beta} & for \quad T < T_c. \end{cases} \qquad \textbf{(5. 20)}$$

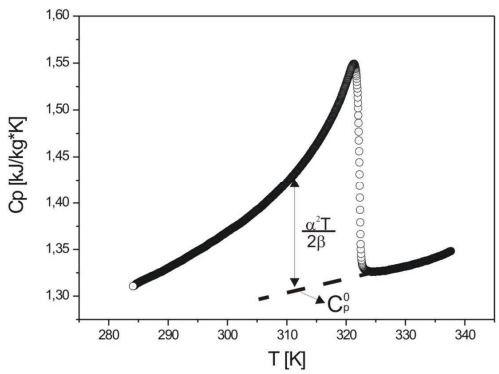

Fig.5. 9 Temperature dependence of the specific heat for the TGS crystals.

It is easy to see that at the phase transition temperature heat capacity undergoes a jumps according to $\frac{\alpha^2 T}{(2\beta)}$.

It is worth noticing that three determined parameters: the polarization (***P***), the dielectric permittivity (***ε***) and the specific heat (C_p) expressed by three coefficients in the free energy expansion α, β are related near the phase transition temperature in the following way

$$C_p - C_p^0 = \frac{\alpha^2}{2\beta} T = \frac{\alpha}{2} \frac{P_s^2}{\frac{(T - T_p)}{T}}. \qquad \textbf{(5. 21)}$$

5.3. First-order phase transition

In order to describe the first order phase transition it is necessary to take into account the coefficient at sixth order term in expression Eq. (5.4)

$$\Phi(T,\eta) = \Phi_0 + \frac{1}{2}\alpha\eta^2 + \frac{1}{4}\beta\eta^4 + \frac{1}{6}\gamma\eta^6, \qquad \textbf{(5. 22)}$$

where $\alpha, \gamma > 0$ and $\beta < 0$ [5].

As before, the order parameter can be found from condition of the minimum of the thermodynamic potential (5.3)

$$\begin{cases} \dfrac{\partial\Phi}{\partial\eta} = \eta(\alpha(T - T_c) + \beta\eta^2 + \gamma\eta^4) = 0, \\ \dfrac{\partial^2\Phi}{\partial\eta^2} = \alpha(T - T_c) + 3\beta\eta^2 + 5\gamma\eta^4 > 0, \end{cases} \qquad \textbf{(5. 23)}$$

It can be easily shown that there are following solutions of Eq. (5.23)

$$\begin{cases} \dfrac{\partial\Phi}{\partial\eta} = \eta(\alpha(T - T_c) + \beta\eta^2 + \gamma\eta^4) = 0, \\ \dfrac{\partial^2\Phi}{\partial\eta^2} = \alpha(T - T_c) + 3\beta\eta^2 + 5\gamma\eta^4 > 0, \end{cases}$$

$$\eta_0 = 0 \qquad \textbf{(5. 24)}$$

and for the high-temperature phase and

$$\eta_1^2 = \frac{-\beta \pm \sqrt{\beta^2 - 4\gamma\alpha(T - T_c)}}{2\gamma} = -\frac{\beta}{2\gamma}\left\{1 \mp \left[1 - \frac{4\alpha(T - T_c)\gamma}{\beta^2}\right]^{0.5}\right\} \qquad \textbf{(5. 25)}$$

for the low-temperature phase.

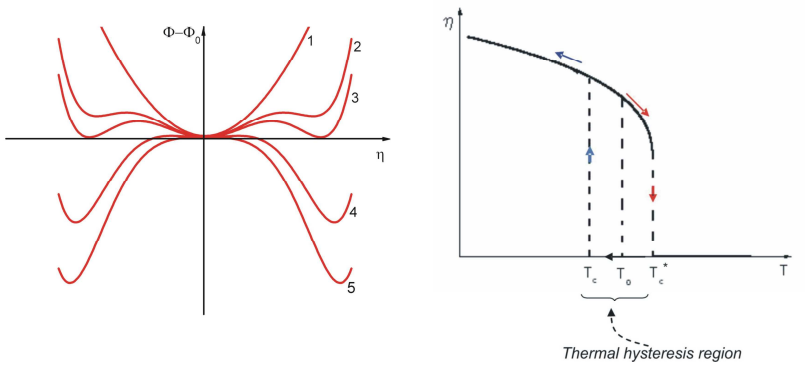

Fig. 5. 10 Dependence of the thermodynamic potential on the order parameter for several different temperatures and temperature dependence of the order parameter in the case of the first order phase transition [5, 12].

Conditions of Eq(5.23) are presented in Fig. 5. 10 which shows the order parameter dependence of the thermodynamic potential. The curve "1" in Fig. 5. 10 corresponds to the temperatures region $T > T_2 = T_c + \frac{\beta^2}{4\alpha\gamma}$, where crystals can remain in the symmetric phase with one minimum of the thermodynamic potential at $\eta = 0$. At $T = T_2$ (curve "2" in Fig. 5. 10) a dependence of the thermodynamic potential on the order parameter displays inflection points. During the cooling the minima appears (stability of the phase II increasing). The equilibrium state of the phases I and II is when the $\Phi(\eta \neq 0) = \Phi(\eta = 0)$ condition is fulfilled. It corresponds to the temperature $T_1 = T_c + \frac{3\beta^2}{16\gamma\alpha}$ (curve "3" in Fig. 5. 10). Below T_1 the phase I becomes unstable and remains metastable unless the α coefficient changes the sign at $T = T_c$.

Temperature T_c corresponds to the temperature range where the symmetric phase can exit. The temperature dependence of the spontaneous polarization in the case

of the first order phase transition for the $PbTiO_3$ crystals is presented in Fig. 5. 11.

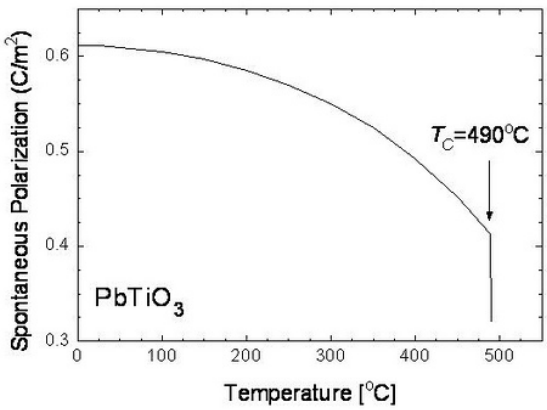

Fig. 5. 11 Temperature dependence of the spontaneous polarization of the $PbTiO_3$ [9] .

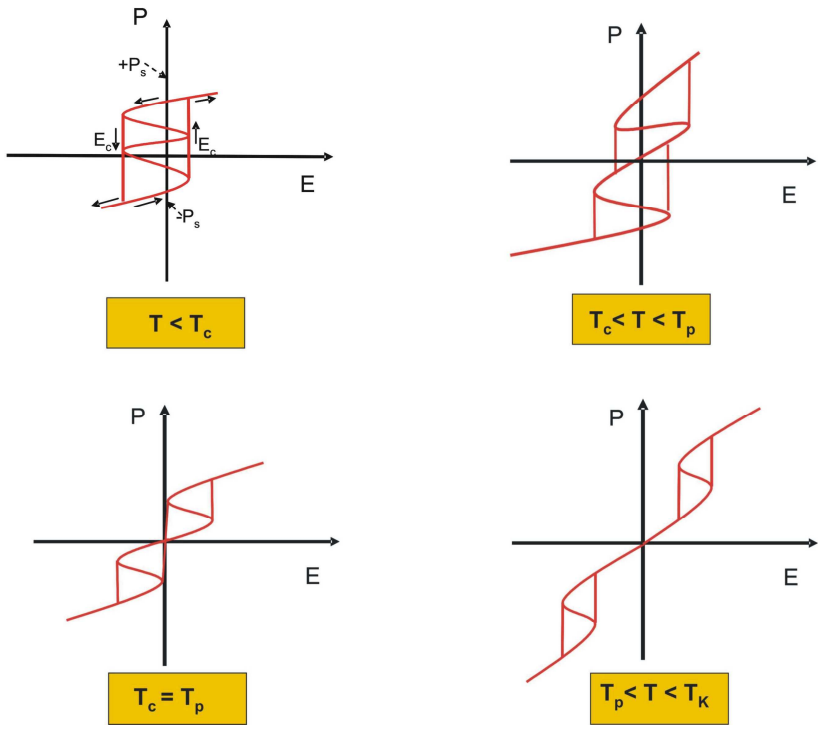

Fig. 5. 12 Plot of the polarization against the electric field for the first order phase transition for several temperatures [5, 9, 12]

5.3.1. Electrical properties

The dependence of the polarization on the electric field for the first order phase transition is shown in Fig. 5. 12. It can be seen that far from the transition temperature the dependence of the polarization on the electric field has a form of double hysteresis loop shifted to the higher electric filed. It should be mentioned that a presence of a double hysteresis loop is sometimes considered to be a property of the same special group of materials well known as antiferroelectrics.

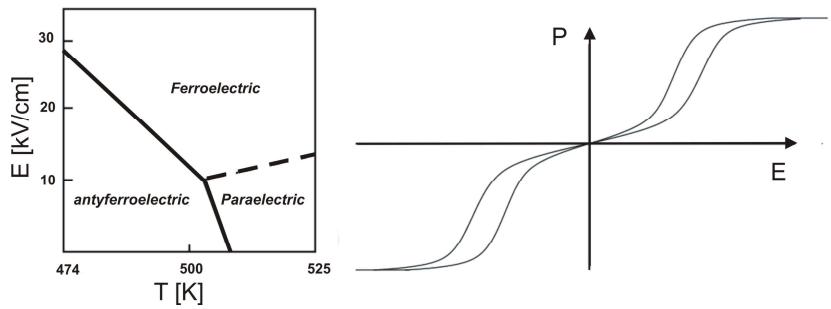

Fig. 5. 13 The polarization *P* of antiferroelectric $PbZrO_3$ versus an externally applied electric field E[12].

Lead zirconate ($PbZrO_3$) is an example of a crystal which exhibits the first order phase transition. The polarization *P* of antiferroelectric $PbZrO_3$ as a function of the applied electric filed *E* is shown in Fig. 5. 13. Strong fields "switch" the antiferroelectric phase into a ferroelectric state. The phase transition sequence in $PbZrO_3$ crystals can be explained with the aid of the schematic representation of temperature dependence of the thermodynamic potential. Below, a diagram of the thermodynamic potentials as the temperature function of a $PbZrO_3$ crystals is presented (Fig. 5. 14).

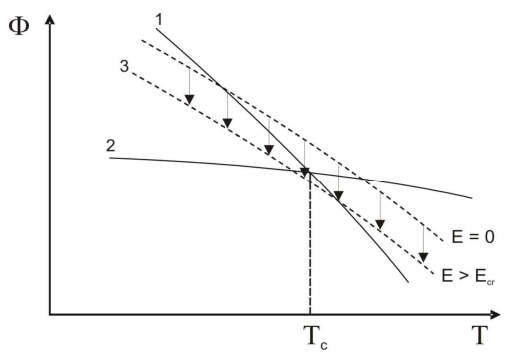

Fig. 5. 14 Diagram of the thermodynamic potentials of three phases of antiferroelectric crystals $PbZrO_3$ [5, 12].

It can be observed that when the external electric field is equal to zero (***E*** = 0) the transition from the symmetric phase to the nonpolar nonsymmetric phase (see phase sequence 1→2 in Fig. 5. 14) can be realized with a decreasing of the temperature. When the external electric field is greater than the critical electric field (***E*** > E_{cr}) in the temperature region of the phase transition the thermodynamic potential of the ferroelectric phase is found to be the lowest and therefore the ferroelectric phase appears to be stable.
(sequence 1→3 in Fig. 5. 14).

If we take into account the sixth-degree invariants into Eq.(5.4) with $\beta = 0$ and $\gamma > 0$ the condition of the thermodynamic potential minimum can be written as

$$\frac{\partial \Phi}{\partial \eta} = 0 = \alpha(T - T_c) \cdot \eta + \gamma \cdot \eta^5. \qquad \textbf{(5. 26)}$$

We can find, that the order parameter is equal to zero $\eta = 0$ for $T > T_c$ and for $T < T_c$

$$\eta^4 = -\frac{\alpha(T - T_c)}{\gamma}. \qquad \textbf{(5. 27)}$$

Finally, the dependence of the order parameter on the temperature for $T < T_c$ will take the following form

$$\eta = \pm\left(\frac{\alpha(T - T_c)}{\gamma}\right)^{1/4}. \qquad \textbf{(5. 28)}$$

It turns out that a strong decreasing of the order parameter upon approach to the phase transition temperature by the law $(T - T_c)^{\frac{1}{4}}$ results in a strong dependence of the specific heat on the temperature.

5.3.2. Anomaly of thermal properties

For the entropy we have

$$S = -\frac{\partial \Phi}{\partial T} = S_0 + \frac{\alpha^{\frac{3}{2}}(T - T_c)^{\frac{1}{2}}}{(2 \cdot \gamma^{\frac{1}{2}})} \quad . \tag{5. 29}$$

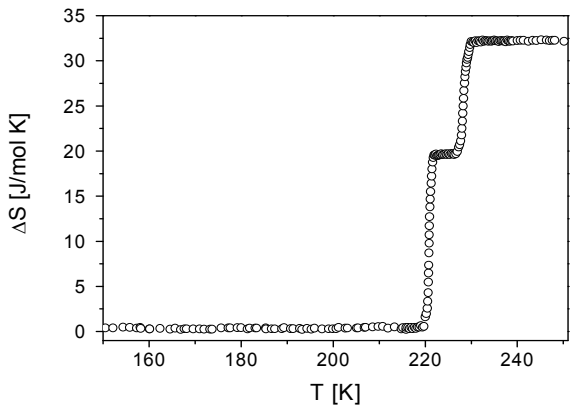

Fig. 5. 15 Temperature dependence of the entropy changes of a TEA_2MnCl_4 crystals [13].

Fig. 5. 15 presents the temperature dependence of the entropy changes in the wide temperature rage. TEA_2MnCl_4 crystals exhibit two first order phase transitions at T_1= 221 K and T_1= 228 K. The jumps of the entropy changes at the phase transition temperatures can be seen.

Then, the heat capacity of the crystal is equal to:

$$C_p = C_p^0 + \frac{\alpha^{\frac{3}{2}} \cdot T}{4\gamma^{\frac{1}{2}}}(T - T_c)^{-\frac{1}{2}}. \tag{5. 30}$$

The temperature dependence of the specific heat of the TEA_2MnCl_4 crystals measured during the heating process is presented in Fig. 5. 16. Two anomalies typical for the first-order phase transitions at T_1 = 221 K and T_2 = 228 K are clearly seen. One can see that the specific heat in the critical temperature (when $T = T_c$) approaches to infinity according to Eq.(5.30).

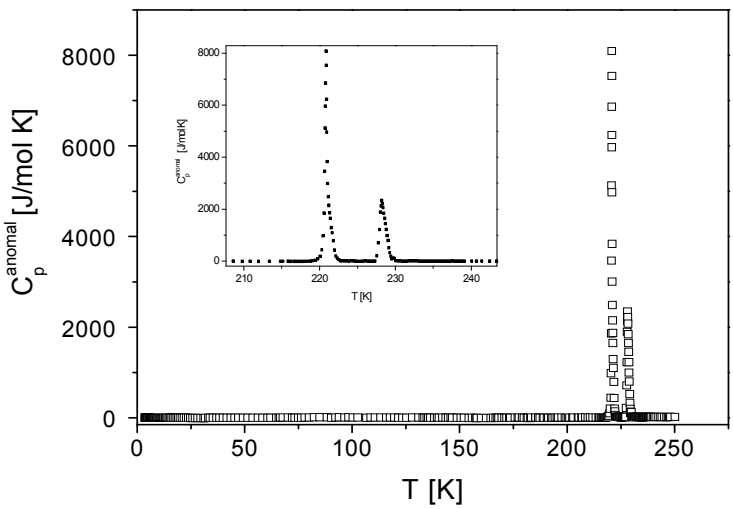

Fig. 5. 16 Temperature dependence of the anomalous part of the specific heat for TEA_2MnCl_4 crystals [13].

5.3.2. General properties of the first order phase transition

Using a model with η^6 we could describe the phase transition on (α, β) plane [5,9]. When $\beta < 0$ the phase transition is of the first order while for the positive value of β the phase transition is of the second order, likewise for η^4 model (Fig.5. 17). For the first order phase transition the coexistence region of two phases can exist only in the temperature range:

$$\Delta T = T_2 - T_c = \frac{\beta^2}{4\gamma\alpha} \quad . \tag{5. 31}$$

The two phases are interchangeable for $T > T_1$ and $T > T_2$, at each point of the range ΔT the phase transition can occur. A temperature when the energy of both phases are equal is the most probable for the phase transition.

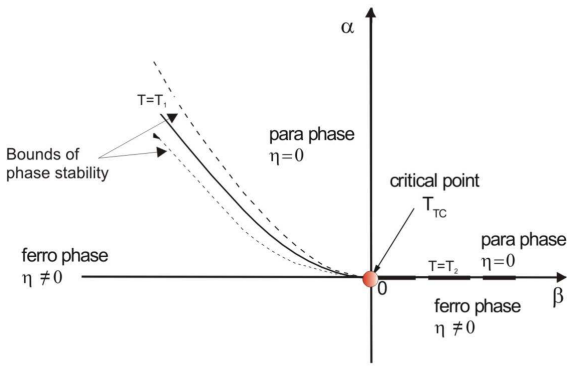

Fig.5. 17 Phase diagram ($\alpha(\beta)$) for η^6 model [8]

The thermal hysteresis phenomenon is characteristic for the first order phase transition, as a results of a metastable region existing for both phases. During the first-order phase transition a jump of the order parameter can be observed

$$\eta(T_1) = \left(-\frac{\beta}{4\gamma} \right)^{0.5} . \qquad \textbf{(5. 32)}$$

According to Eq. (5.25), below the temperature T_1 the increase of the order parameter can be observed. The emission or the absorption of latent heat of the phase transition is connected with a discontinuous character of the order parameter ($\eta(T)$).

Under some special circumstances with β=0 in equation (5.22) the phase transition becomes tricritical (see red point in Fig.5. 17).

5.3.3. Tricritical point

A thermodynamic system where the phase transition going from the continuous phase to the discontinuous one is described by the tricritical point. The critical state is characterized by regularities following from an equation of the free energy. The tricritical point is defined by following conditions

$$\begin{aligned} \alpha(p_t, T) &= 0, \\ \beta(p_t, T) &= 0. \end{aligned} \qquad \textbf{(5. 33)}$$

Using equation (5.22)[14] the properties of the tricritical point can be concluded

a) if $p = p_t \rightarrow \eta \sim (T_c - T)^{1/4}$,

b) specific heat below T_c is proportional to $(T_c - T)^{-0.5}$,

c) thermal hysteresis connected with the phase transition approaches zero when $p \rightarrow p_t$.

The tricritical point has been widely studied by Landau and Lifshits [8,15], Ginzburg (called the Curie critical point) [16] and Griffiths [17]. The tricritical point exists in the case of the liquid and gaseous phases which are similar by the symmetry (example see Chapter 4). $BaTiO_3$ is one of examples of ferroelectric materials showing tricritical point determined from dielectric measurements. Pressure dependence of the ferroelectric-paraelectric transition temperatures for $BaTiO_3$ crystals is presented in Fig. 5. 18 [18]. One can observe that the temperature hysteresis between the phase transition temperature on heating and on cooling decreases with the increasing pressure and approaches zero at pressure equal to 34 kbar.

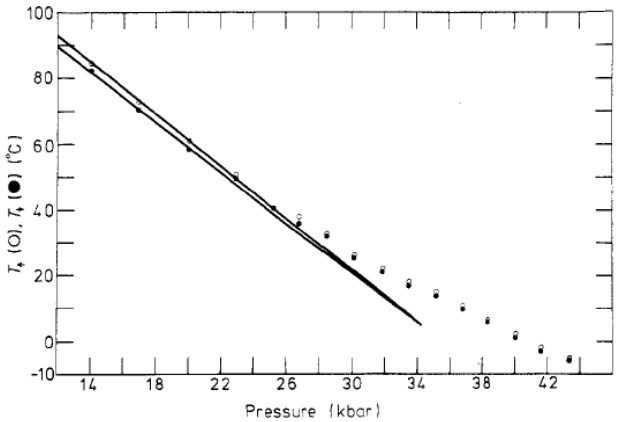

Fig. 5. 18 Phase transition temperature dependence on pressure for $BaTiO_3$ crystals [18].

For 34 kbar we can observe that the line corresponding to the first order phase transition transforms into the line corresponding to the second order phase transition.

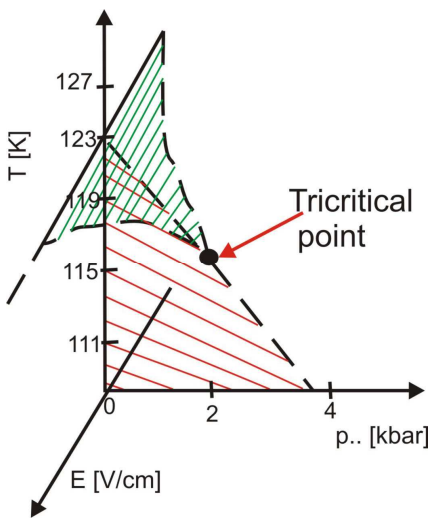

Fig. 5. 19 Phase diagram for KDP crystal [19].

A similar situation as presented above was observed for KDP crystals [19]. The tricritical point in the pressure-temperature-electric field three-dimensional space is presented in Fig. 5. 19. From dielectric measurements the tricritical point near 2 kbar is indicated.

5.4. General properties of the thermodynamic potential with the one component order parameter

The thermodynamic potential allowing one-component order parameter can be generalized to any even value of n. An expansion with $m \geq 8$ performed with respect of one component order parameter may describe the isostructural phase transition (Larin and Guffan [20]). In that case the thermodynamic potential can be presented as:

$$\Phi(\eta) = \Phi_0 + \alpha\eta^2 + \beta\eta^4 + \gamma\eta^6 + \delta\eta^8. \qquad \textbf{(5. 34)}$$

The equation of state can be written in the case of m = 8

$$\eta\left(\alpha + \beta\eta^2 + \gamma\eta^4 + \delta\eta^6\right) = 0. \qquad \textbf{(5. 35)}$$

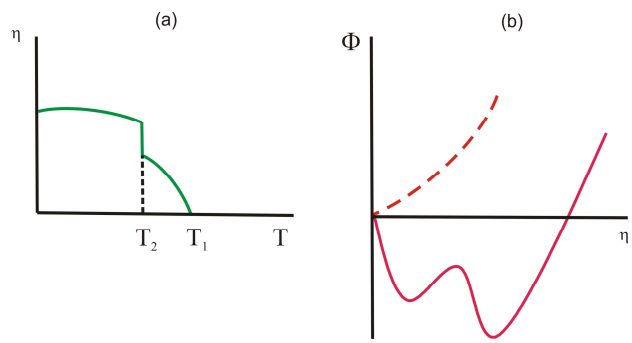

Fig. 5. 20 Temperature dependence of the order parameter (a) and the order parameter as a function of the thermodynamic potential (b) in the case of m = 8 [9].

It can be summarized that depending on a sign of γ the Eq. (5.23) may posses one solution or three positive solutions of η^2. If $\gamma > 0$, then only one low-

temperature stable phase is possible, as it was for the case of m=6. For $\gamma < 0$ (and $\delta > 0$) two low temperature stable phases with the identical symmetries can be found and it corresponds to m = 8. In Fig. 5. 20 a succession of the phase transition for the case of m = 8 is presented. One can see that the second order phase transition is followed by the first order transition. The sequences of the possible phase transitions when the thermodynamic potential can be expanded to any even value of m can be generalized as follows :

the thermodynamic potential describes a sequence of one-to-second order phase transitions and $\frac{m}{2}-1$ first order phase transitions when m is even, otherwise for odd m's all phase transitions are of the first order and the transition number is $m-\frac{1}{2}$, see Fig. 5. 21 [8, 9].

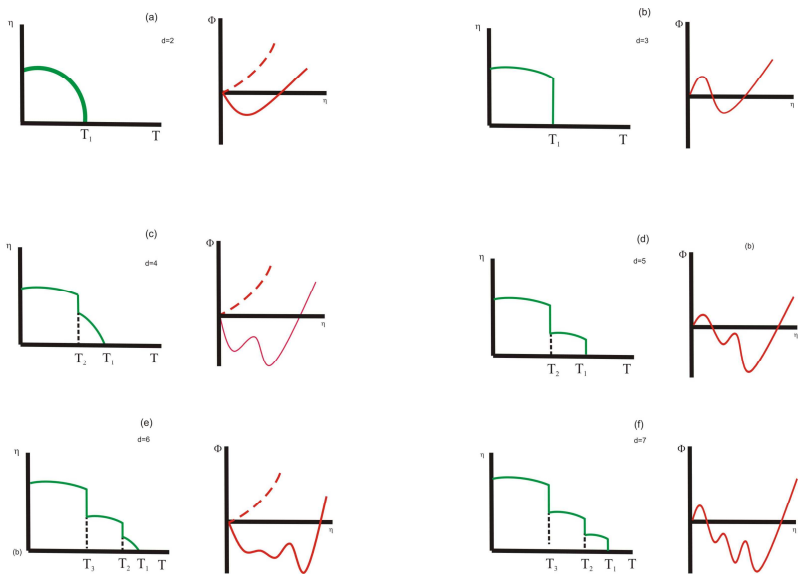

Fig. 5. 21 Temperature dependence of the order parameter and order parameter as a function of thermodynamic potential for several odd (on the right) and even (on the left) value of d [9].

5.5. Two component order parameter

In order to describe a structural phase transition from 4/mmm symmetry group to mmm symmetry with a twining unit cell two-component order parameter must be considered [8, 9].

The thermodynamic potential as a function of the order parameters and the mechanical stress can be written as

$$\Phi = \alpha_1(\eta^2+\xi^2)+\alpha_2(\eta^2+\xi^2)^2+\alpha_3(\eta\cdot\xi)^2+\alpha 4_3(\eta^2+\xi^2)^3+\alpha_5(\eta^2+\xi^2)^4 + \alpha_6(\eta^2+\xi^2)^5-\delta_1\cdot\eta\cdot\xi\cdot\sigma-\rho_1\cdot\sigma^2, \quad \textbf{(5. 36)}$$

where

η, ξ – the order parameter component,

σ – the strain tensor component,

α_1, α_2, α_3, α_4, α_5, α_6, – the expansion terms (where $\alpha_1 = \alpha_1(T)$ i $\alpha_6 > 0$),

ρ_1 – the elastic susceptibility,

δ_1 – the constant connected with the deformation and the order parameters.

In the case of crystals without any mechanical stress ($\boldsymbol{\sigma} = 0$) and any electric field ($\boldsymbol{E} = 0$) the equilibrium conditions of the thermodynamic potential minimum are given by

$$\begin{cases}\dfrac{\partial\Phi}{\partial\eta}=0\\ \dfrac{\partial\Phi}{\partial\xi}=0\end{cases}, \qquad \begin{cases}\dfrac{\partial^2\Phi}{\partial\eta^2}>\\ \dfrac{\partial^2\Phi}{\partial\xi^2}>0\end{cases}, \qquad \begin{vmatrix}\dfrac{\partial^2\Phi}{\partial\eta^2} & \dfrac{\partial\Phi}{\partial\eta}\\ \dfrac{\partial\Phi}{\partial\xi} & \dfrac{\partial^2\Phi}{\partial\xi^2}\end{vmatrix}>0. \quad \textbf{(5. 37)}$$

Using the first condition in Eq. (5.37) , we obtain

$$\begin{aligned}\eta\cdot\left[\begin{matrix}\alpha_1+2\cdot\alpha_2(\eta^2+\xi^2)+\alpha_3\xi^2+3\cdot\alpha_4(\eta^2+\xi^2)^2\\ +4\cdot\alpha_5(\eta^2+\xi^2)^3+5\cdot\alpha_6(\eta^2+\xi^2)^4\end{matrix}\right]=0,\\ \xi\cdot\left[\begin{matrix}\alpha_1+2\cdot\alpha_2(\eta^2+\xi^2)+\alpha_3\eta^2+3\cdot\alpha_4(\eta^2+\xi^2)^2\\ +4\cdot\alpha_5(\eta^2+\xi^2)^3+5\cdot\alpha_6(\eta^2+\xi^2)^4\end{matrix}\right]=0,\end{aligned} \quad \textbf{(5. 38)}$$

with a following solution :

$$\eta = 0 \quad \text{i} \quad \xi = 0, \tag{5. 39}$$

$$\eta = 0 \quad \text{i} \quad \xi \neq 0, \quad \alpha_1 + (2\cdot\alpha_2 + \alpha_3)\cdot\xi^2 + 3\cdot\alpha_4\cdot\xi^4 + 4\cdot\alpha_5\cdot\xi^6 + 5\cdot\alpha_6\cdot\xi^8 = 0, \tag{5. 40}$$

$$\xi = 0 \quad \text{i} \quad \eta \neq 0, \quad \alpha_1 + (2\cdot\alpha_2 + \alpha_3)\cdot\eta^2 + 3\cdot\alpha_4\cdot\eta^4 + 4\cdot\alpha_5\cdot\eta^6 + 5\cdot\alpha_6\cdot\eta^8 = 0, \tag{5. 41}$$

$$\xi \neq 0, \quad \eta \neq 0, \quad \xi^2 = \eta^2, \tag{5. 42}$$

$$\alpha_1 + (4\cdot\alpha_2 + \alpha_3)\cdot\eta^2 + 12\cdot\alpha_4\cdot\eta^4 + 32\cdot\alpha_5\cdot\eta^6 + 80\cdot\alpha_6\cdot\eta^8 = 0.$$

The first solution (Eq.5.39) corresponds to the improper ferroelectric (high temperature) phase, where the spontaneous deformation is equal to zero, the other solution (5.40)-(5.42) corresponds to the condition $T < T_c$. In the ferroelectric phase the crystal deformation $u = \delta_1\cdot\eta\cdot\xi + 2\cdot\rho\cdot\sigma$ has the following form

$$u = \pm\delta_1\cdot\eta^2 + 2\cdot\rho\cdot\sigma. \tag{5. 43}$$

As it follows from Eq. (5.43) the spontaneous deformation is proportional to the square of order parameter, opposite as it is in the case of the proper ferroelastic, where the spontaneous deformation is proportional to the order parameter.

In the paraelastic phase the elastic susceptibility is equal

$$\chi = 2\cdot\rho\ , \tag{5. 44}$$

whereas, in the ferroelastic phase

$$\chi = \frac{\delta_1\cdot\eta^2}{2\cdot\left[\alpha_1 + (4\cdot\alpha_2 + \alpha_3)\cdot\eta^2 + 12\cdot\eta^4 + 32\cdot\eta^6 + 80\cdot\eta^8\right]} + 2\cdot\rho. \tag{5. 45}$$

The phase diagram representing the solution in the plane of (α_1, α_2') obtained from numerical calculations $\alpha_2' = \frac{1}{2}\cdot(4\cdot\alpha_2 + \alpha_3)$, for $\alpha_3 = 1$, $\alpha_4 = 0.25$, $\alpha_5 = 0.225$, $\alpha_6 = \frac{1}{6}$ is presented in Fig.5. 22.

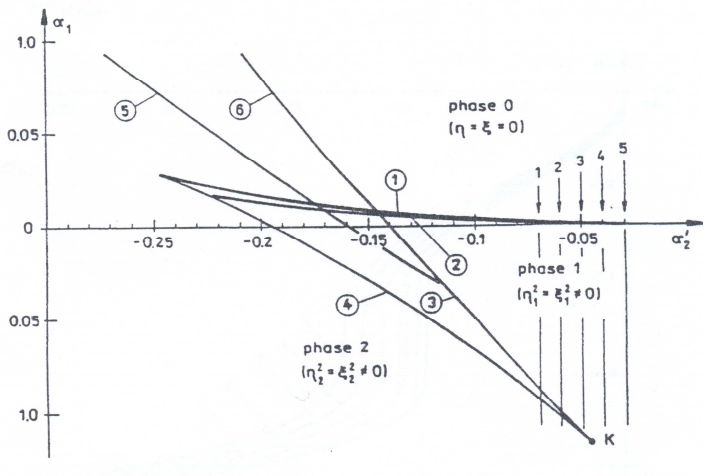

Fig.5. 22 Phase diagram in the plane of ($\alpha_1, \alpha_2^{'}$) [20, 9].

The curves "1" and "2" in Fig.5. 22 determine the limits of stability of the paraelastic phase $\eta = \xi = 0$ (phase 0) and the ferroelastic phase $\eta_1^2 = \xi_1^2 \neq 0$ (phase 1).

Transition from 0 (phase 0) to "1" phase or "2" describes the isostructural phase transitions. The limits of the stability of the improper ferroelastic phase (phase 1 and phase 2) $\eta_2^2 = \xi_2^2 \neq 0$ are represented by curves 3 and 4 in Fig.5. 22. The region between "3" and "4" curves corresponds to the region of a coexistence of two phases. Point K in Fig.5. 22 corresponds to the critical point. Curves "5" and "6" determine the limits of the stability of the paraelectric phase and the improper ferroelastic phase. A point where the ends of curves "1" and "2" are spliced is called the tricritical point and it is a point where the first order phase transition becomes a second order one.

---

[1]. Van der Walls *Z. Phys. Chem*, 13 (1897) 657.

[2].V.L. Ginzburg, *Sov.Phys.Usp*. **5** (1963) 649.

[3].A. Devonshire, *Phil. Mag*. 40 (1949) 1040.

[4]. A. Devonshire, *Phil. Mag*. 42 (1951) 1065.

[5]. A. Strukov, A.P.Levanyuk, *Ferroelectric phenomenta in crystals*, Springer, (1998).

[6]. K. Aizu, *J. Phys. Soc. Japan* 27 (1969) 387.

[7]. K. Aizu, *J. Phys. Soc. Japan* 28 (1970) 706.

[8]. L. Landau, Phys. Z. Soviet 11 (1937), 26, 545. English translation in *Collected Papers of L. D. Landau* by D. Ter Haar, Gordon and Breach, (1965) New York.

[9]. J. Toledano and P. Toledano, *The Landau Theory of Phase Transitions*, World Scientific Publishing Co., (1987) Singapore.

[10]. H. Stanley, *Introduction to Phase Transitions and Critical Phenomena*, Clarendon Press, (1971) Oxford.

[11]. M.Gaafar, S.M.Khalil, *Fizyka A*, 8 (1999) 25.

[12]. Lines, A. M. Glass, *Principles and Applications of Ferroelectric and Related Materials*, Clarendon Press, (1977) Oxford.

[13]. A.Cizman, R.Poprawski, D.Włosewicz, V.I.Nizhankovskii, *Ferroelectrics*, 369 (2008)10.

[14]. R.Blinc, B.Zaks, *Soft Modes in Ferroelectric and Antiferroelectric*, Amsterdam:north (1974), Holland.

[15]. L. Landau, E. M. Lifszyc, *Statisticzeskaja Fizika*, Izd. Nauka, (1976) Moskwa.

[16]. V.L. Ginzburg, *Sov.Phys.Usp*. **5** (1963) 649.

[17]. R.B. Griffiths, *Phys.Rev.Lett*. **24** (1970) 715.

[18]. R.Clarke, L.Benguigui, *J.Phys.C:Solid State Phys*. **10** (1977) 1963.

[19]. V.H.Schmidt, A.B. Western, A.G.Baker, *Phys.Rev.Lett*. **37** (1976) 839.

[20]. J. Gufan, *Strukturnye fazovye prechody*, Izd.Nauka, (1982) Moskwa.